Danish Meteorological Institute
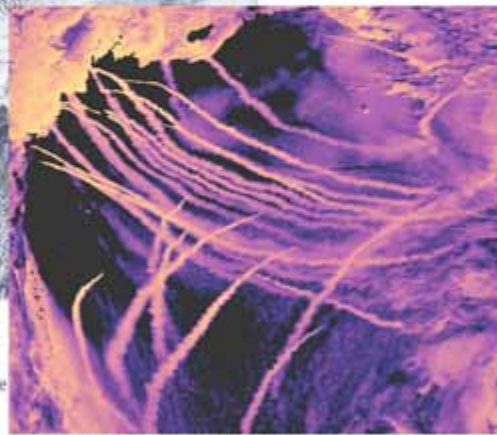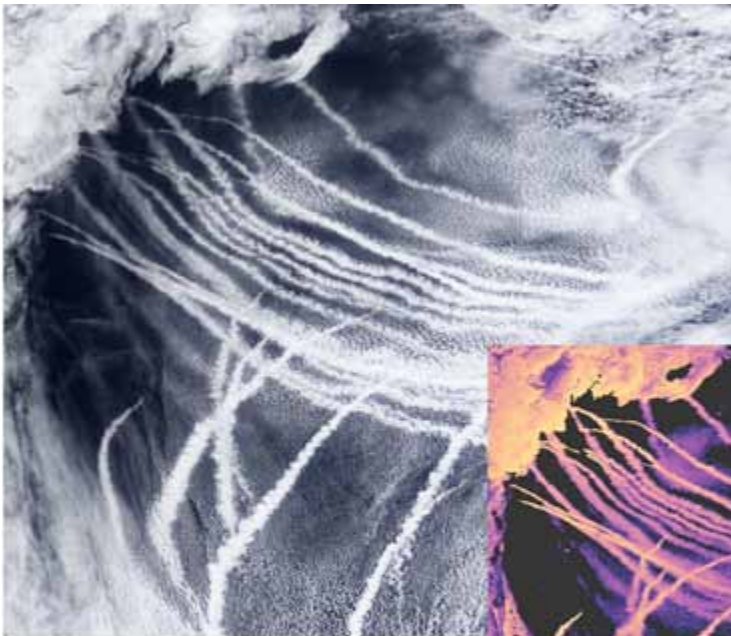
Ministry of Climate and Energy

dmi.dk

Scientific Report 09-01

PhD thesis: Integrated modeling of aerosol indirect effects

Ulrik Smith Korsholm

Ship tracks over the northeast pacific ocean on 4 march 2009.
Top picture: NASA Terra-MODIS picture in natural colors. Right:
corresponding cloud droplet size. The ship tracks are brighter
than the regular clouds because the cloud particles in them are
smaller (yellow and peach), but more numerous, than the
particles in the natural clouds (lavender to dark purple).
NASA images by Robert Simmon and Jesse Allen, based on an image by Jeff Schmaltz, MODIS Rapid Response Team. Caption by
Rebecca Lindsey.

Colophone

Contents

Preface

The work presented in this thesis was done in the Research Department at the Danish Meteorological Institute, under the supervision of professor Alexander Baklanov. Supervisor at the University of Copenhagen has been lector Aksel Walløe Hansen and Professor Eigil Kaas. The work was supported by the Copenhagen Global Change Initiative (COGCI). During the course of this study, I received the Kipp and Zonen Young Scientist Award for part of the work presented here.

Acknowledgements

Abstract

This report is based on my PhD thesis: Integrated modeling of aerosol indirect effects. Some modifications have been made mainly in the model description section in order to bring the report up to date with respect to recent model developments. The atmosphere is heavily polluted with accumulation mode aerosols which affect cloud formation and precipitation development. Consequently, continental clouds generally include two orders of magnitude more cloud droplets than marine clouds. An increased number of small droplets, in warm clouds, leads to an increase in cloud reflectance and affects cloud lifetime. Complex cloud and aerosol -microphysical and cloud dynamical feedbacks shape the response to an increased number of smaller cloud droplets and may feed back on the aerosol and trace gas distributions of the atmosphere on short time scales. The importance of such feedbacks is unknown and in this study an online coupled chemical weather model is developed, tested and employed in a case study, investigating the importance of such feedbacks on trace gas distributions. Enviro-HIRLAM is developed as an extension of the short-range weather forecast model HIRLAM and includes emission, advection, turbulent diffusion, convection and deposition of trace gases and aerosols as well as gas-phase chemistry, aerosol dynamics, gas-aerosol equilibration and aerosol activation. The activated aerosols are coupled to the cloud scheme leading to reflectance enhancement and suppression of precipitation in warm convective and stratiform clouds. In a particular case study considering convective summertime conditions it was shown that the aerosol mass concentration was satisfactory predicted and two-meter temperature predictions improved slightly when including the aerosol effects. The distribution of NO2 near the surface was affected by the feedbacks over the 24 hour period. The feedbacks induced changes in cloud cover, temperature and in local circulations by inducing convective activity which lead to a dynamical redistribution of the species rather than to changes in chemical reactions. The suppression of rain was of greater importance than reflectance enhancement and nonlinear effects acted to damp the influence of the feedbacks. Hence, in this case study the feedbacks were of great importance in determining the trace gas distributions.

Introduction

Parts of this chapter has been published as [12].

The atmosphere is a thin layer of gases and aerosols[1] enclosing the Earth. The gaseous component consists mainly of molecular nitrogen and oxygen but a range of trace gases such as water vapor, carbon dioxide, nitrogen oxides, ozone and methane are also present. The trace gases are of importance because they are radiatively and chemically active, they participate in gas-to-particle conversion processes and some are poisonous to humans and ecosystems. The distribution of trace gases is being modified by anthropogenic emissions mainly from fossil fuel combustion, transportation and industrial processes. Incomplete combustion generates nitrogen oxides and carbon monoxide as well as carbon dioxide and subsequent chemical reactions in the troposphere produce ozone. These processes also emit sulfur dioxide and aerosols.

The emission of aerosols is divided into primary and secondary as well as natural and anthropogenic components. Primary aerosols are emitted in particulate or liquid form while secondary emissions are the result of gas-to-particle conversion. In practice these distinctions are somewhat blurred, since aerosols contain complex mixtures of all components (depending of the history of the air mass containing the aerosols) and because low volatility organic gases may condense onto the aerosols in the vicinity of the source.

The size range of the aerosols extent from nanometer sized secondarily produced molecular clusters to primary particles of tens of micrometers. The main components include carbonaceous compounds, sulfates (SO_4^{2-}), nitrates (NO_3^-) and ammonium (NH_4^+). Carbonaceous compounds include organic matter and black carbon. These aerosols are mainly the by-product of incomplete combustion processes, e.g. in relation to the combustion of biomass or fossil fuel, but a substantial amount originates in secondary processes from biogenic and anthropogenic gaseous precursors. Sulfate is formed during gas-to-particle conversion processes involving precursor gases such as carbonyl sulfide, dimethyl sulfide (DMS), sulfur dioxide and hydrogen dioxide. The gases are oxidized in the presence of radicals such as hydroxyl or nitrogen, resulting in sulfate which forms particles with water and ammonium (e.g. sulfuric acid or ammonium sulfate). Another important oxidation pathway for sulfate is in cloud water, where sulfur dioxide is oxidized by hydrogen peroxide and ozone [205]. DMS is emitted in large quantities over oceanic regions, while sulfur dioxide is a combustion product mainly emitted through volcanic activity and fossil fuel burning (mainly coal). The relative abundance of sulfate and ammonium controls the secondary formation of nitrate. Ammonia acts to neutralize sulfuric acid and if an excess of ammonia is present, gaseous nitric acid and ammonia can condense and dissociate to nitrate. Ammonia is mainly emitted from animal waste, emission from soil (ammonification) and industrial processes.

The primary sources for the year 2000 was compiled by [173] and showed that wind-driven mineral dust emissions from arid regions ($1000 - 3000$ Tg yr^{-1}) account for the largest primary contribution. Wind driven emissions of sea salt, through evaporation of sea spray and the tearing of droplets from cloud tops ($20 - 106$ Tg yr^{-1}), and carbonaceous aerosols ($106 - 347$ Tg yr^{-1}) are also of importance. The secondary emissions are dominated by sulfate which is mainly anthropogenic in origin (140 Tg yr^{-1} anthropogenically produced and 102 Tg yr^{-1} naturally produced [199]). Secondary nitrate is also dominated by the anthropogenic fraction (36 Tg yr^{-1} of anthropogenically produced and 22 Tg yr^{-1} naturally produced [199]) while organic matter is dominated by the natural

---

[1]The term aerosol is here used to describe either solid or liquid particles suspended in the atmosphere.

component (10 Tg yr^{-1} anthropogenically produced and 55 Tg yr^{-1} naturally produced [199]). On a global scale the antropogenic fraction is about 10%.

Despite their low contribution to the atmospheric mass, the aerosols play a fundamental role in shaping weather through their microphysical impact on cloud and precipitation development. Hydrophilic aerosols aid droplet growth through condensation by lowering the supersaturation necessary for droplet activation[2]. Hence, the aerosols are a necessary component for cloud development. Without the presence of aerosols, clouds would only form in the presence of supersaturations in excess of 10% and, hence, be very scarce. Considering continental aerosol in the size range relevant to CCN (cloud condensation nuclei) activation (accumulation mode aerosols about 0.1 μm in diameter), it is found that the anthropogenic fraction of the aerosol is about 50% [199]. Hence, continental clouds are generally polluted and given the importance of aerosols in the development of clouds their effect should be addressed.

Atmospheric anthropogenic aerosols are mainly emitted in mega-city[3] hot-spots. The world population tend to cluster in urban areas and as a consequence the number and population of mega-cities are growing; in 2007 for the first time the world urban population exceeded its rural population [227]. The emission of anthropogenic aerosols has increased correspondingly. Until recently anthropogenic aerosol emissions were considered a local problem without any regional or global effect on weather or climate. However, a decade ago it was demonstrated that sub-micron aerosols may be transported across oceans and continents, by the wind, in about a week [90]. Since the average residence time of sub-micron sulfate aerosols is about 12 days [21], the aerosol pollutant distributions are global in nature. It is now accepted that they are of importance in the climatic radiative balance [63] and in the most recent assessment report by the Intergovemental Panel on Climate Change aerosol-cloud interactions are categorized as the largest uncertainty in current climate models [63] . However, it still remains to be shown that the anthropogenic aerosols are also of importance on shorter time-scales (in the order of days), i.e. for the regional and local weather. What is suggested here is that the global nature of the anthropogenic aerosol fields also render them important to weather and therefore to the prediction of air pollution on global, regional as well as local scales.

There are numerous physical pathways through which aerosol-meteorology interactions may feed back[4] on the aerosol and trace gas distribution and properties. As clouds form in polluted air masses the hygroscopic aerosols will compete for the available water vapor, leading to the formation of more numerous but smaller cloud droplets for the same liquid water content. Since cloud radiative properties are mainly dependent on bulk cloud properties, such as the effective radius[5] of the droplets, the effect of this is that the cloud becomes brighter than it would otherwise have been and thereby it reflects more incoming shortwave radiation during day; this effect is denoted the first indirect effect [225]. The decrease in effective radius also affects the precipitation efficiency, denoted the second indirect effect [2], and thereby cloud lifetime (these effects will be discussed in detail in chapter 5). The time scales of these effects are the same as that of the clouds, which is in the order of minutes to hours [215]. Redistribution of radiation, cloud cover and precipitation, may lead to changes in local and regional circulations and temperature and the importance for local to regional weather seems eminent. Dynamical redistributions of aerosols due to indirect effects, changes in

---

[2]The term activation is used to describe unstable droplet growth via condensation.

[3]Here the term mega-city is used to describe an urban agglomeration containing at least five million inhabitants.

[4]The term feedback is here used to describe an interaction mechanism between anthropogenic aerosols and meteorology, when a change in an initial aerosol processes affects meteorology, which in turn affects the aerosol process. If the initial process intensifies the feedbacks is positive and if it is reduced the feedback is negative.

[5]Defined as the total droplet volume to total droplet surface area ratio

chemical reaction rates due to temperature changes, and changes in photolysis rates due to variations in cloud cover are pathways through which the distribution of anthropogenic aerosol and chemical species may be affected. On a global scale about 45% of the sulfate is generated in heterogeneous chemical reactions and subsequent evaporation of cloud droplets [247]. Hence, the feedbacks mediated through the aerosol indirect effects also have the potential to modify aerosol composition on local through global scales.

Other types of aerosol-meteorology interactions, which may mediate feedbacks of importance to air pollution, also exist. Anthropogenic aerosols may directly absorb, scatter and re-emit both short and longwave radiation and thereby act as thin cloud covers, changing temperature profiles, relative humidity and surface temperature. A series of feedbacks related to the direct aerosol effect, including the daytime stability effect, the smudge-pot effect and the self-feedback effect have previously been identified [101]. Trace gases with large anthropogenic components such as ozone, nitrogen oxides and methane may also absorb incoming shortwave radiation and thereby modify heating rates, photolysis rates, etc. Hence, there are many processes through which air pollutants may affect meteorology and thereby feed back on themselves. The influence of these feedbacks are, however, quite unknown on short time-scales and it is the premise of this study that these processes shall be studied on their natural time-scales in order to establish their importance. The basic hypothesis underlining this work is as follows:

The aerosol indirect effects may give rise to important feedback processes that affect the distribution of air pollutants on short time-scales.

Models which have the ability to include feedbacks are the so-called online coupled models[6]. The first online coupled air pollution model was made in the Novosibirsk Scientific School during the 1980's [8]. During the 1990 the GATOR/MMTD model was developed in the USA [96, 97] and it still remains the most advanced online coupled model, at least with respect to the complexity of the coupling [253]. Since then, several models have been developed in Europe and the USA. The non-European models have recently been reviewed by [253]. Here a review over the models used or developed in Europe is given, excluding the so-called online access models[7].

Overview of European online coupled short-range mesoscale models

The development of traditional air pollution models, the so-called offline[8] coupled chemical transport models (CTM's), has proceeded separately from the development of NWP models. This is both due to historical reasons (before 1900, air pollution was not recognized as a science but was considered a purely regulatory issue) and because the resolution of NWP models only recently have reached the mesoscale, which is an appropriate scale for air pollution modeling. Due to a general increase in computational performance and NWP resolution, it has become feasible to couple NWP and air pollution models and start examining the effects of feedbacks. Figure 3.1 displays this view

---

[6]The usage of the term online coupled has been somewhat ambiguous in the literature. Here it is used to describe a system where all components are integrated in one model, so that the meteorological and chemical continuity equations are solved simultaneously at each time step on the same grid. Such models may include two-way interactions between chemical and meteorological fields; this issue is discussed more fully in chapter 2.

[7]In an online access model the continuity equation for the meteorological and chemical fields are solved separately in two different models, but chemical and meteorological fields are exchanged at each time step of the meteorological model. This includes models which are coupled via a coupler and it is possible to include feedbacks; this issue is discussed more fully in chapter 2.

[8]The term offline coupling is here used to describe a CTM which is executed separately from its meteorological driver, which provides meteorological input, e.g. every hour. Feedbacks are not possible to include; a more complete definition is given in chapter 2.
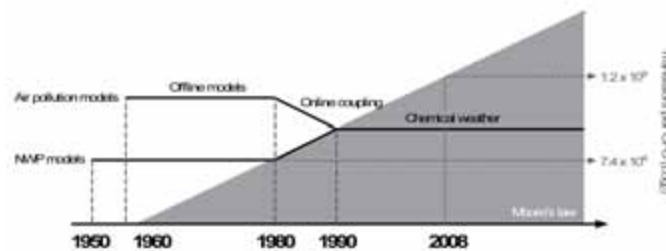
Figure 3.1: Schematic timelines showing the development of NWP and air pollution models along with the evolution of comp uter speed (the grey shaded area displays Moore's law which states that the transistor count per CPU doubles every second year. The transistor cound is a measure of computer speed). In 1950 the fi rst NWP model was executed on a computer (the ENIAC computer) and during the 1950's the fi rst air pollution box model was imlemented. Between the 1950's and 1970's three-dimensional air pollution models were developed, as computer speed increased, and in 1980 the fi rst online models appeared. The fi rst fully coupled urban through global online model (GATOR/MMTD) was developed in 1990 and several chemical weather models predicting both the chemical and meteorological weather have been developed since. Before 1990, air pollution and NWP models were developed separately but with the advent of chemical weather models, synergy between the two communities led to enhanced model development capabilities.

schematically. As the computational capabilities increased, chemistry and aerosols were implemented in an online fashion in NWP models and, as resolution increased, the models converged. In the end a common modeling system for NWP, air pollution and chemistry, for both short and long-term simulations (climate), containing the important feedbacks was conceived. Such chemical weather[9] models are able to forecast short-term variability of the order of minutes in the pollutant fields and predict weather at the same time. In fact the first global through urban fully coupled online chemical weather models (including all feedbacks between anthropogenic aerosols/gases and meteorology which may be of importance) have already been developed [95, 96, 97, 76].

It is appropriate to divide online coupled models according to their scale. A range of global online coupled models with various degrees of coupling between chemistry and meteorology (e.g. [99, 154, 141, 107, 211, 94, 135, 108]) exist; however, only the European online coupled short-range mesoscale models which include gas-phase chemistry are considered (table 3.1). Examples of non-European mesoscale online coupled models are [96, 46, 73, 76, 55]. Online coupled models which only include transport and dispersion (e.g. [159, 202, 33, 85], are not considered here since they are not of relevance to the issue of feedbacks. Only five models fit these criteria but there are other models under development and several institutes employ freely available community models such as WRF-CHEM. Of the seven models listed in table 3.1, two have not been developed in Europe. WRF-CHEM is a community model, which is mainly being developed in the USA and GEM-AQ was developed in Canada. WRF-CHEM and GEM-AQ are included in this review because they are used by European institutions for research or operational activities. Comparing with the reviews of offline air pollution models by [91] and [11] it becomes clear that the majority of air pollution models in Europe are offline coupled. As described above this is due to both historical and technical issues and in general it is assumed that online coupled models require too much computational capability to be applicable. However, the main bottleneck with respect to computer resources, in both offline CTM's and online coupled models, is the chemistry calculations. Since these are performed in both types of models and since meteorology is also needed in both types of

---

[9]The term chemical weather is here used to describe local-to-global trace gas and aerosol distributions with variability ranging from minutes to days.

Table 3.1: Online coupled models in Europe (except for GEM-AQ and WRF-CHEM) along with the main developer or user.

Model name	Institute, country
BOLCHEM[a]	CNR ISAC, Italy (www.isac.cnr.it/bolchem)[b]
GEM-AQ	York Warsaw Univ. Tech., Poland [111]
MCCM	Inst. Env. Atm. Res., FZ Karlsruhe, Germany [72]
MC2-AQ	Warsaw Univ. Tech., Poland; Multi-Scale Air Quality Network York Univ., Toronto, Canada; Environment Canada, Canada [246]
Meso-NH	CNRM, Toulouse, France; UPS, Toulouse, France (http://mesonh.aero.obs-mip.fr/mesonh)
TAPM	CSIRO, atmospheric reaearch, Australia (www.cmar.csiro.au/research/tapm)
WRF-CHEM	Community model development

[a]Abbreviations: BOLCHEM (BOlogna Limited are model for meteorology and CHEMistry), GEM-AQ (Global Environmental Multiscale-Air Quality model), MCCM (Mesoscale Climate Chemistry Model), MC2-AQ (Mesoscale Compressible community-Air quality), Meso-NH (Mesoscale Non-Hydrostatic atmospheric model), TAPM (The Air Pollution Model), WRF-CHEM (Weather Research and Forecast model coupled with Chemistry).
[b]References are given for detailed descriptions of each model.

models, it is expected that online coupled models are faster in terms of cpu-time but require more memory during simulations. In essence, in online coupled models one saves the preprocessing of the meteorological input to the CTM's.

The choice of numerical schemes for transport and dispersion reflects that the models were derived from mesoscale weather forecast models. All the models calculate transport and dispersion of chemical and aerosol species online, hence, the advective and diffusive part of the species continuity equation are solved using the same numerical solution schemes and on the same grid as for meteorological quantities. This have the advantage that inconsistencies between species and meteorological fields are eliminated. There are, however, differences between the numerical solution schemes used by the models and NWP models do usually not employ mass conservative schemes for advection. Loss of mass conservation is expected to be of importance in gas-phase chemistry where reactions are sensitive to small variations in mixing ratios (this issue is discussed more fully in chapter 2). Table 3.2 compares the relevant meteorological properties with respect to species transport and dispersion. Several of these employ semi-Lagrangian advection schemes, which are known not to conserve species mass. Vertical diffusion is of great importance to the overall transport properties of the models [36]. They typically employ TKE closure schemes in the calculation of the vertical diffusion coefficient and the species are diffused as passive scalars using the dry deposition flux as a lower boundary condition or as a loss term in the chemistry equations. Subgrid scale moist

Table 3.2: Numerical schemes used for transport and dispersion of species in European mesoscale short-range online coupled models. Details about the implementation of each scheme may be found in the references listed in table 3.1.

Model	Advection	Vertical diffusion	Convection
BOLCHEM	WAF[a]	TKE	Kain-Fritsch
GEM-AQ	SL	TKE	Tiedtke
MCCM	SS	TKE	Kain-Fritsch
MC2-AQ	SL	TKE	NONE
Meso-NH	PPM	TKE	Kain-Fritsch
TAPM	SL	GDA	NONE
WRF-CHEM	UW	YSU/MYJ	Kain-Fritsch/Grell

[a]Abbreviations: TKE (vertical diffusion schemes applying turbulent kinetic energy closure [151]), GDA (gradient diffusion approach for vertical diffusion [136]), YSU (the Yonsei University convection scheme [166]), MYJ (the Mellor-Yamada-Janjic convection scheme [152]), SL (semi-Lagrangian [189, 190]), UW (advection schemes using a third or higher order upwind scheme), SS (the advection scheme by [207]), WAF (Weighted Average Flux advection scheme [222]), PPM (the Piecewise Parabolic advection scheme [44]), Kain-Fritsch (Kain-Fritsch type scheme for moist convection [110]), Tiedtke (Tiedtke mass flux scheme for moist convection [221]), Grell (Grell moist convection scheme [74]) and KUO (Kuo-type convection scheme [125].

convection of the species, on the other hand, is not considered equally important and is not included in all models. In cases with large convective instability and for the interaction between aerosols and clouds, it is expected that moist convective redistribution of aerosol number and mass concentration is of importance. The Kain-Fritsch scheme is used by most models. All the models, except for BOLCHEM and GEM-AQ, are non-hydrostatic, reflecting the complex simulation domains which are often needed over Europe.

Chemical and aerosol schemes used in the models are displayed in table 3.3. There is great variety in the chemical schemes employed, reflecting the large number of mechanisms available. Most of the models are used for air quality purposes focusing on ozone. Hence, volatile organic compounds as well as nitrogen oxides must be well represented in the models for mesoscale usage. The complexity of the schemes is related to the number of reactions and number of advected species included. The complexity of the chemical mechanism is of great importance in online coupled models due to the cpu-time and memory requirements of the chemical mechanisms. For this reason it is important to have several mechanisms to choose from, so that an appropriate and cost-effective mechanism may be chosen for the problem at hand. Therefore, most of the models have a series of schemes which may be used. WRF-CHEM is the model which includes the widest range of mechanisms for gas-phase chemistry, reflecting the community aspect of that model. In this respect the most simplified model is TAPM. Photolysis reactions are of major importance to atmospheric chemistry. In polluted areas the oxidation capacity is largely controlled by the photolysis of the major species such as NO_x's and O_3 which produce radicals such as HO^-, NO or $O(^3P)$. Photolysis rate constants are strongly dependent on actinic fluxes which in turn depend on cloud fraction and absorption and scattering by aerosol layers and gases as well as a range of meteorological parameters. Since the temporal and spatial variability of the actinic flux is large, most online coupled models include online calculation of the photolysis rates. Here the shortwave absorption by gases is often accounted for by using radiative transfer calculations and models such as [127]. Notice that online calculation

Table 3.3: Chemistry, aerosol and deposition schemes for the European mesoscale short-range online coupled models.

Model	Chemistry	Aerosol	Deposition (dry/wet)
BOLCHEM	SAPRC90/CB-IV[a]	Pseudomodal	Resist./Cnst.
GEM-AQ	ADOM-II	Sectional	Resist./Prec.
MCCM	RADM/RACM	Modal	Resist./
	RACM-MIM		
MC2-AQ	ADOM-II	None	Resist./Cnst.
Meso-NH	RACM/ReLACS	Modal	Resist./IC.
TAPM	GRS	Passive	Resist./Prec.
WRF-CHEM	RADM2/RACM	Modal	Resist./IC., Prec.
	RACM-MIM/CBMZ/CB-V	Sectional	

[a]Abbreviations: SAPRC90 (the Statewide Air Pollution Research Center mechanism [34]), CB-IV (the Carbon Bond-IV mechanism [68]), CB-V (the Carbon Bond-V mechanism), RACM (the Regional Atmospheric Chemistry Mechanism [213]), RACM-MIM (RACM updated with the MIM Isoprene mechanism [65]) RADM (the Regional Acid Deposition Model [212]), CBMZ (the Carbon Bond Mechanism version Z [249]), ADOM-II (Acid Deposition and Oxidants Model II [138, 6]), GRS (Generic Reaction Set [229]), ReLACS (the Regional Lumped Atmospheric Chemical Scheme [47]), Resist. (Resistance formulation [236]), Cnst. (Parameterization based on constant scavenging coeffi cients), Prec. (Parameterization based on precipitation rates), IC. (In Cloud processesing of aerosols and gases).

of photolysis does not necessarily include feedbacks to meteorology, i.e. atmospheric heating rates or shortwave fluxes at the surface are not necessarily modified in the models. For the implementation in TAPM, the chemistry mode (which is the most advanced mode with respect to gas-phase chemistry) requires the use of at least 13 chemical species (10 reactions). Photolysis is based on a parameterization using solar zenith angle and temperature. The GEM-AQ and MC2-AQ models both employ ADOM-II which requires 47 species (98 chemical reactions and 16 photolysis reactions) in MC2-AQ and 50 chemical species (116 chemical reactions and 19 photolysis reactions) in GEM-AQ. In MC2-AQ photolysis rates are based on look-up tables, dependent on solar zenith angle, height and surface albedo, and with a cloud cover correction, while in GEM-AQ photolysis rates are calculated online every chemical time step using the method by [127]. The ReLACS scheme in Meso-NH uses 37 species (128 chemical reactions) and photolysis is calculated online. RADM2 is employed in both MCCM and WRF-CHEM and uses 63 species (136 chemical reactions and 21 photolysis reactions). In MCCM and WRF–CHEM photolysis is calculated online [140]. RACM which is used in WRF-CHEM and MCCM requires 77 species (214 chemical reactions and 23 photolysis reactions), RACM-MIM is used in WRF-CHEM and uses 84 species (221 chemical reactions and 23 photolysis reactions). CB-IV in BOLCHEM uses 30 species (85 chemical reactions) while SAPRC90 uses 35 species (131 chemical reactions). Photolysis is based on look-up tables in BOLCHEM.

The models also differ with respect to aerosol dynamics, composition and mixing state, depending on the specifics of the aerosol schemes. Mixing state is of great importance to the simulation of direct and indirect aerosol effects but only one model treats the transition from external to internal mixtures, and the remainder use either completely external or completely internal mixtures. The M7 aerosol model [230], used by BOLCHEM, contains descriptions of homogeneous nucleation, coagulation, thermodynamic equilibrium in aerosol-water vapor partitioning and aerosol ageing (condensation of sulfate on pre-existing aerosols). Hence, aerosols may transfer from externally mixed insoluble particles to internally mixed soluble particles. The following species are considered: SO_4^{2-}, BC (Black Carbon), OC (Organic Carbon), sea salt (ss) and dust in seven log-normal modes

represented by nucleation mode (median radius $< 0.005\ \mu m$), Aitken mode ($0.005\ \mu m <$ median radius $< 0.05\ \mu m$) for soluble species and Aitken mode for insoluble species, accumulation mode ($0.05\ \mu m <$ median radius $< 0.5\ \mu m$) for soluble species and accumulation mode for insoluble species and coarse mode ($0.5\ \mu m <$ median radius) for soluble species and coarse mode for insoluble species.

In MCCM the aerosols are considered external mixtures of NH_4^+, SO_4^{2-}, NO_3^- and secondary organic nitrate. MADE/SORGAM [201] is used to simulate homogeneous nucleation, coagulation and condensation of chemical species and water vapor using three log-normal modes. GEM-AQ contains representations of PM10[10], PM2.5, PM1, PM0.1, PPM10[11] and the aerosols consists of ss, SO_4^{2-}, BC, organic matter and dust. Following [70] aerosol mass is distributed into 12 logarithmically spaced size bins ranging from $0.005\ \mu m$ to $10.24\ \mu m$ (the number of bins may be regulated) and homogeneous nucleation, coagulation and condensation is accounted for. The MESO-NH model represents PM10, PM2.5, PM1, PM0.1, PPM10 and the aerosols are composed of SO_4^{2-}, NO_3^-, NH_4^+, dust, ss and a range of secondary organic components including nitrate. Dust and ss are considered passive. The modal aerosol model ORILAM [223] considers homogeneous nucleation, coagulation and condensation using two log-normal modes. The TAPM model considers PM10 and PM2.5 as passive tracers, i.e. only transport and dispersion are considered.

WRF-CHEM considers a wider range of aerosol schemes with options for both sectional and modal approaches. There are, currently, three aerosol schemes available: MADE/SORGAM, MOSAIC [250] and MADRID [252]. MOSAIC and MADRID are sectional models typically executed with eight size bins (can be used with any number of bins). All schemes consider internal mixtures of NH_4^+, SO_4^{2-}, NO_3^-, BC, OC and H_2O, while MOSAIC and MADRID also includes ss and CO_3^{2-}. In addition MOSAIC includes DMS chemistry. MADE/SORGAM is used with three log-normal modes and the standard deviation of the aerosol size distribution is assumed to be constant for the Aitken and accumulation modes. This assumption saves cpu-time because fewer moments of the distributions need to be advected and aerosol dynamics are simplified, but it may also induce errors in the aerosol number and mass concentrations [251].

Wet deposition is an important mechanism for removal of species from the air, and it can have great influence on species concentration fields. All models contain a representation of wet deposition, ranging from simple parameterizations with constant scavenging coefficients (BOLCHEM, MC2-AQ) to more advanced schemes based on precipitation rates and the type of precipitation (GEM-AQ, TAPM). WRF-CHEM is the most complex model regarding wet deposition. Wet aerosol may activate and contribute to the cloud droplet number concentration and cloud liquid water content in moist convective up-draughts. In-cloud removal of aerosols then follow the auto-conversion processes and collection/accretion by rain, snow or graupel. Evaporation of cloud and rain water is also included. For below-cloud scavenging, a scavenging coefficient based on precipitation rates is calculated. Meso-NH only considers wet deposition in connection with deep moist convection for selected species. The scavenging rate depends on aqueous phase reaction rates and solubility. The TAPM model considers wet deposition for particles, SO_2 and H_2O_2. Dry deposition of gases and aerosols is based on a resistance approach for all models, reflecting the lack of measurements and parameterizations in this area.

Online coupled models can, in theory, enable the full range of feedbacks but in practice only few models include any. GEMS-AQ includes ozone-radiation interactions and the effect on atmospheric heating rates. The only fully coupled model currently in use in Europe is WRF-CHEM. It includes a multitude of feedbacks including direct aerosol effects, indirect aerosol effects and gas-radiation

---

[10]PM10 refers to particulate matter (PM) with a diameter less than or equal $10\ \mu m$

[11]PPM refers to primarily emitted PM

Table 3.4: Description of feedbacks in European online coupled models.

Model name	Direct AE[a]	Indirect AE	Gas-Radiation
BOLCHEM	-	-	-
GEM-AQ	-	-	+
MCCM	-	-	-
MC2-AQ	-	-	-
Meso-NH	-	-	-
TAPM	-	-	-
WRF-CHEM	+	+	+

[a]Abbreviations: AE (Aerosol Effect), Gas-radiation (gas scattering, absorption and reflection modifying atmsospheric heating rates).

interactions (see table 3.4). Regarding the direct effect, aerosol single scattering albedo, asymmetry factor and extinction are computed as a function of wavelength and position [55]. Each chemical component is associated with a complex index of refraction and the total index is found by volume averaging. Mie theory and summation over all size bins are then used to find the optical properties. Following [55], a radiative transfer model is used to calculate the shortwave attenuation by the aerosol layer. Regarding the indirect aerosol effects, activation of wet aerosol into CCN is calculated based on Köhler-theory. Condensation of water vapor is parameterized as a function of dry-radius, relative humidity and the hygroscopicity of each component. The activated fraction is a function of supersaturation which in turn is dependent on up-draught velocity, hygroscopicity, aerosol radii and number concentration. As aerosols are caught in convective up-draughts, the CCN evolve into liquid and ice cloud droplets. Parameterizations for convective and stratiform precipitation account for evaporation and sublimation of the droplets. One drawback of this method is that non-equilibrium effects are not accounted for in the activation process, i.e. in Köhler-theory the supersaturation is assumed to be in equilibrium with the relative humidity, thereby excluding possibly important kinetic effects [163].

Online coupled models may be used to investigate the effects of feedbacks. Nevertheless, results are usually confined to climatic time scales using regional or global online coupled models [100, 102, 103, 69] whereas results for the short-range are largely missing. Examples of results for the short-range include the following investigations.

Using an online access model [232] considered the direct interaction between mineral dust and radiation in a case with high wind speed and low temperature over the Sahara. They found strong modifications of the shortwave radiation budget which was reduced by up to a factor of two over western Africa. This in turn led to changes in dynamics and cloud formation. Using the same model, and including the effects of aerosol ageing, [232] also considered the direct radiative effect of anthropogenic aerosol over a period of a week. In spite of quite low aerosol concentrations, the modification of the shortwave radiation balance resulted in strong modifications of the cloud pattern.

WRF-CHEM was used to simulate a five-day summer episode during the Texas Air Quality Study [253]. Using a 12 km horizontal grid-spacing and 57 layers from the surface to the tropopause without any aerosol-cloud interactions, meteorology, PM2.5 and chemical species were predicted with and without direct aerosol-radiation interactions. Comparison with PM2.5 measurements revealed some degree of over-prediction which was ascribed to an over estimation of the emissions

of BC and organic substances. Changes in temperature and humidity were largest in the late afternoon. Temperature was reduced up to $0.18°C$ at the surface and $0.16°C$ further up in the boundary layer, while water vapor mixing ratio was increased 3.2% near the surface and was decreased 3% further up. Large PM2.5 concentrations in the boundary layer caused a reduction in the downward radiation, thereby decreasing temperature and increasing humidity near the surface. Absorption of incoming radiation by aerosols and gases was used to explain the opposite sign of the humidity change in the upper boundary layer.

Examples of studies considering the aerosol indirect effects are given in chapter 5. From the above it is clear that WRF-CHEM is the most advanced online coupled short-range mesoscale model in use in Europe, both with respect to the number of schemes available but also the complexity of the chemical and aerosol schemes as well as the coupling between gases, aerosols and meteorology.

Main objectives of this study

As can be seen from table 3.4, no short-range online coupled mesoscale model, developed in Europe, currently contain representations of aerosol indirect effects. The primary objective of this work has been to develop an online coupled model for the mesoscale that includes representations of the first and second aerosol indirect effects. The secondary objective has been to employ the model in the study of the importance of the aerosol indirect effects in modeling the distribution of pollutants on short time scales. The strategy to achieve this has been to modify the HIRLAM (High Resolution Limited Area) model which is used for operational weather forecasting at the Danish Meteorological Institute (DMI) to include emissions, advection and dispersion of pollutant aerosols and gases, gas-phase chemistry, gas-aerosol partitioning, aerosol dynamics, dry and wet deposition of aerosols and gases and representations of the first and second aerosol indirect effects. Once implemented and evaluated, the model was applied in a case study of the importance of the aerosol indirect effects on NO_2 distributions.

Outline of this thesis

This thesis is organized in six chapters each containing parts of or full journal publications as indicated in the beginning of each sub-chapter (where reference is given to the relevant publication). For each chapter there is a short summary and conclusion. General aspects of online coupled model development and an outline of the strategy followed in order to achieve the objectives of this study is described in chapter 2. A short description of HIRLAM and a detailed description of the new model developments are given in chapter 3. This chapter is meant for documentation of the model at later stages. Model evaluation with respect to transport and dispersion, deposition, gas-phase chemistry and a comparison between online and offline simulations are given in chapter 4. Chapter 5 contains an up to date description of the aerosol indirect effects, a one-dimensional test of the model and a three-dimensional case study regarding the importance of the first and second indirect aerosol effect on the distribution of NO_2. Chapter 6 summarizes the main findings and concludes the thesis with an outlook on ongoing and future work. Chapter 7 contains a final summary. Chapters 4 and 5 contain full-length articles in order to provide a broad view of the work performed. This, however, also implies some overlaps in the text, in particular with respect to the model description in chapter 3.

Developing online coupled chemical weather models

The premise of any chemical weather model, and of any atmospheric model in general, is that the atmospheric processes, be it dynamical, physical or chemical, follow certain laws and that when expressed in mathematical form these laws, together with appropriate initial and boundary conditions, can be used to predict the evolution of the processes on a given spatial domain in a given time-span. Numerical weather prediction models and CTM's are based on such solutions and by coupling these, in a consistent manner, it is possible to obtain solutions for the evolution of the chemical weather. The governing laws are usually expressed as large sets of coupled non-linear differential equations, which, except for a few cases employing very restrictive assumptions, cannot be solved analytically. For this reason the usefulness of a chemical weather model relies not only on the choice of processes which are represented in the model, but also on the accuracy of the chosen numerical solution methods.

When developing chemical weather models a large number of decisions of both technical and scientific nature (such as numerical solution schemes, implementation strategies or choice of physical and chemical processes to include) must be taken. This chapter contains some lessons learned during the project.

Basic choice of model

The purpose of this study could in principle be achieved by developing an online coupled model based on another weather forecast model, such as WRF or ETA [155, 19] or by using a freely available online coupled model, such as WRF-Chem. This work, however, aims at developing a model for both operational and research purposes. This means that the default chemical and aerosol schemes should be computationally effective without too many species, but at the same time the model should encompass a variety of schemes for experimentation. The HIRLAM model [226] has been used for operational weather forecasting at the Danish Meteorological Institute for many years, hence, problem solving is readily at hand. Furthermore, the basic idea when simulating chemical weather is to produce both a meteorological and chemical weather forecast and hence combine several model applications. HIRLAM output is also used by a whole range of offline air pollution applications, such as pollen and ozone forecasting and emergency preparedness, hence, HIRLAM is a natural choice as baseline model.

Chemical weather is generated by interactions between dynamical, physical and chemical processes in the atmosphere. Enviro-HIRLAM is splitted into three parts covering these processes, a dry adiabatic part, also denoted the dynamical core, a diabatic part representing diabatic physical processes and a chemical part representing chemical reactions in the gas and liquid phases as well as aerosol processes. Here focus is on the dynamical core while descriptions of the physical and chemical parts and the feedbacks between them will follow in the next chapter. Enviro-HIRLAM is developed as an extension to HIRLAM and therefore the dynamical cores are identical in the two model versions while the physical parameterizations contain some changes due to the implementation of feedback mechanisms.

There are two basic choices of dynamical cores, representing two different ways of solving the dynamical equations; the Eulerian and the semi-Lagrangian cores. Each of these contain limiting assumptions which must be compared in relation to the requirements of a chemical weather model, before a choice of dynamical core can be made. Consider the Eulerian form of the continuity

equation for a chemical species of mass concentration ψ:

$$\frac{\partial \psi}{\partial t} + \nabla \cdot (\vec{v}\psi) = \mathcal{L}\psi \tag{4.1}$$

where $\vec{v} = (u, v, w)$ is the wind velocity, t represent time and $\mathcal{L}$ is a non-linear differential operator representing the effects of emission, turbulent diffusion, convection, deposition and chemical transformations on ψ. Consider the evolution of ψ(x,y,x,t) on some spatial domain $\mathcal{D}$ with (x,y,z) $\in \mathcal{D} \subset \mathcal{R}^3$ and t $\in [0, T]$ for some T > 0.

In the Eulerian approach $\mathcal{D}$ is divided into grid boxes and the spatial derivatives in 4.1 are discretized on this grid. The Eulerian core uses a central finite difference scheme (on an Arakawa C-grid), for spatial derivatives, with a three time level Leapfrog scheme for representing time derivatives. Hence, the schemes are second order accurate in space and time. This approach is locally mass conserving, however, it is dispersive and not positive definit. Therefore, unphysical negative concentration values may develop in the vicinity of sharp gradients. The Eulerian core is not unconditionally stable and the Courant-Friedrichs-Levy (CFL) condition must be fulfilled in each coordinate direction in order to assure computational stability, introducing strong limitations on the length of the time step and thereby on the computational performance of the model as a whole (note that advection is generally not the main bottleneck in computational performance, see section on computational performance in chapter 3).

In the semi-Lagrangian core the air parcels are tracked backwards from their arrival points to their departure points and ψ is found through interpolation from the previous time step [209]. The semi-Lagrangian approach does not suffer from high numerical dispersion and is not limited by the CFL time step criterion. Hereby, the semi-Lagrangian approach (typically used with semi-Implicit treatment of gravity and sound waves) is several times faster (computationally) than the Eulerian counterpart (considering pure advection), for the same accuracy (Richie, 1995). The semi-Lagrangian approach is, however, based on non-conservative discretizations and is not positive definit.

In both the Eulerian and semi-Lagrangian approaches unphysical negative tracer concentrations may develop in the vicinity of sharp gradients. This is primarily of importance if the advected tracer quantity is coupled to physical or chemical processes. For instance spurious oscillations may develop in cloud water or water vapor, which have large spatial gradients in the vicinity of clouds, giving rise to cloud formation in unsaturated environments. Similarly, the effective radius of cloud droplets mainly depends on cloud liquid water and droplet number concentration, which is known to contain large spatial gradients. In Enviro-HIRLAM all cloud radiative properties are parameterized via the effective radius [243] and negative values would result in the model atmosphere behaving as an unphysical light source. For chemistry negative concentration values also poses a problem, consider the following photolysis reaction:

$$NO_2 + h\nu \rightarrow O(^3P) + NO$$
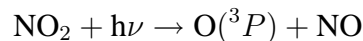
whereby NO_2 is converted to NO and triplet state Oxygen via interaction with sunlight. NO_2 and NO typically peaks over urban areas and posses sharp horizontal gradients in the urban-rural transition zone, during night. Assume that NO_2 constitutes a constant non-zero background, a condition that might occur during daytime when NO_2 concentration decreases. Let ψ_{NO_2} and ψ_{NO} represent the mass concentrations of NO_2 and NO and assume that NO_2 is converted to NO at a rate χ. Disregarding all other dynamical, physical and chemical processes the continuity equation for the two species in the x-direction becomes:

$$\frac{\partial \psi_{NO_2}}{\partial t} + u\frac{\partial \psi_{NO_2}}{\partial x} = -\chi\,\psi_{NO_2}\psi_{NO} \tag{4.2}$$

$$\frac{\partial \psi_{NO}}{\partial t} + u\frac{\partial \psi_{NO}}{\partial x} = \quad \chi\, \psi_{NO_2}\psi_{NO} \qquad\qquad (4.3)$$

Due to numerical dispersion effects when using the Eulerian core (Leapfrog in time and centered in space) oscillations (overshoots and undershoots) will develop in the transition zone giving rise to unphysical negative values of ψ_{NO}. If $\psi_{NO} < 0$ and $\psi_{NO_2} > 0$ in some point then the undershoot will be enhanced by equation (2.3) while increasing ψ_{NO_2}, eventually leading to destabilization of the numerical solution. Had there been no coupling between the two equations this error would likely have remained small. Hence, it is clear that the existence of negative concentration values is not acceptable for neither meteorological applications or air pollution applications. In the current version of HIRLAM the negative tracer values are removed by resetting the concentration to zero in these grid points.

The consequence of this is that mass conservation is lost (mass is gained). Mass conservation is generally accepted to be of importance in atmospheric chemistry where small changes in mass or mixing ratio may lead to large changes in the solutions of the generally highly non-linear chemical solvers. Considering the highly in-homogeneous distribution of sources and sinks for trace gases in the atmosphere, it must be anticipated that species with lifetimes longer than a few days may experience significant drift and distortions in their mass budget. The mass conservation properties of the semi-Lagrangian and Eulerian approaches in HIRLAM have previously been investigated. In a study using a predecessor version of Enviro-HIRLAM (denoted DMI-HIRLAM-TRACER) a simulation of a point source release of a passive tracer, showed that for both the Eulerian and semi-Lagrangian approaches the total tracer mass, increased by approximately 50 % over a 25 hour period after stop of emission and after 65 hours the total mass had increased by 80 % [37].

Mass conservation may be restored by using a mass-fixing algorithm. One algorithm that ensures positive definitness and mass conservation redistributes mass from grid points with positive values to grid points with negative values [187], however, this algorithm is not straight forward to apply in a limited area model. Advection across the lateral boundaries may contribute significantly to the mass budget which makes it difficult to apply the algorithm consistently. Many other mass-fixing algorithms have been developed [184, 17, 134], however, they have one deficiency in common, they only restore global mass conservation, i.e. the continuity equation is not necessarily fulfilled in each grid box.

Another way to proceed is to implement a new dynamical core which contains all the relevant properties, including local mass conservation, positive definitness, accuracy and computational efficiency. This work is currently being carried out at the University of Copenhagen, where the semi-Lagrangian dynamical core in Enviro-HIRLAM is being replaced by a modified version of the Cell Integrated semi-Lagrangian approach [160, 109, 40]. Meanwhile, based on experiences with DMI-HIRLAM-TRACER a separate scheme, developed by Bott [22, 23] is used for the advection of the tracers. The Bott scheme is an Eulerian advection scheme and the length of the time step is therefore limited by the CFL criterion. It is based on the upstream method, which is positive definit and numerical dispersion has been greatly reduced [15, 208]. The original Bott scheme is slightly unstable in deformational flow tests and had some phase speed and amplitude errors. These has been eliminated in the an updated version where the non-linear positive definite flux limitations are replaced by monotone flux limiters [24]. Similarly, errors connected with time-splitting for multi-dimensional applications where removed in [25]. Other updates of the Bott scheme exists [38, 45], but in the current version of Enviro-HIRLAM updates ensuring less phase speed error and improved stability in deformational flow, by [53] are used.

In this set-up the advantages of long time stepping in the dynamical core, which is very important for

operational applications of chemical weather models where chemical solvers usually are the bottleneck both in terms of cpu-time and memory usage , is retained while positive definitness and mass conservation is ensured by the Bott scheme. However, this set-up introduces the issue of inconsistency, which may lead to loss of mass conservation. This issue is discussed in the next section.

Different coupling strategies

Development of a chemical weather model consists of coupling an NWP model and a CTM. This can be achieved in various ways, which each have limitations [13]. There are two main types of coupling strategy, offline and online. Offline coupled models comprise a separate CTM forced by preprocessed meteorological data. This data may be generated on the basis of one to six hourly output from a mesoscale NWP model, output, at coarser time resolution, from a global general circulation model or measurement data. Online models comprise online access and online coupled models. In the online access framework the CTM and its meteorological driver are executed simultaneously and data is exchanged at every time step of the meteorological model using some interface. This is achieved either by using a coupler, such as the Ocean Atmosphere Sea Ice Soil (OASIS) coupler [228] or by keeping all exchange information in memory, thereby decreasing cpu-time considerably. In online coupled models the CTM is integrated into the meteorological driver resulting in a unified model, solving equation 4.1 along with the equations for the meteorological variables in one time step, with no need of the interface step.

Offline models are frequently used for air quality forecasting and are often convenient when considering various emission scenarios with fixed meteorology, such as in air quality impact assessments or when performing sensitivity analysis on dispersion models, assuming that feedbacks with meteorology do not play an important role.

However, during preprocessing the meteorological fields, such as the wind components, are interpolated to the CTM-grid and often the numerical schemes used in the CTM's are incompatible with the schemes in the meteorological driver, leading to loss of mass conservation or monotonicity irrespective of the properties of the intrinsic numerical advection scheme used to advect species in the CTM. This arises because the interpolated wind fields are not necessarily consistent with the surface pressure from the meteorological models and the interpolation process may cause extra convergence or divergence. The importance of dynamical consistency between the meteorological driver and the CTM has been highlighted by several authors [130, 31, 32]. Typical solutions for removal of the mass-wind inconsistency includes adjustment of the input wind field so that it matches the surface pressure of the meteorological driver by using a pressure fixer [183]. Letting $P_{s,ctm}$ represent the surface pressure consistent with the interpolated wind field and $P_{s,mod}$ represent the surface pressure consistent with the winds of the meteorological driver, then:

$$\frac{\partial P_{s,ctm}}{\partial t} = -\nabla \cdot C \qquad (4.4)$$

$$\frac{\partial P_{s,mod}}{\partial t} = -\nabla \cdot M \qquad (4.5)$$

where C and M are the vertically integrated mass fluxes consistent with the interpolated and non-interpolated wind fields respectively. The problem arises because $C \neq M$ leading to changes between $P_{s,ctm}$ and $P_{s,mod}$. When using a pressure fixer a correction, COR, is added to C such that:

$$\nabla \cdot (C + COR) = \nabla \cdot M$$

thereby insuring consistency. From the above condition an equation for COR may be derived:

$$\nabla \cdot COR = -\frac{\partial P_{s,mod}}{\partial t} - \nabla \cdot C$$

Hence, consistency may be fulfilled by solving the above equation and adding a correction to the mass fluxes. Several algorithms for solving the above equation have been developed [183, 196] and other fixes exists as well [32], however, for offline models output must always be preprocessed before it is used to drive the CTM's in order to ensure that the solutions do not blow up. Current short and medium range meteorological forecast models are well within the mesoscale. The Danish Meteorological Institute is currently switching to 0.025 degree resolution in the horizontal with 60 levels. For a CTM using the same or higher resolution than its meteorological driver, the time it takes to preprocess the input data may be problematic, especially in the future when the data amounts are expected to increase.

In an online model this problem is not encountered and the preprocessing step is avoided. When using an online model the intrinsic consistency is increased, but not guaranteed. Inconsistency may still be induced regardless of coupling strategy if the pressure based coordinate (e.g. hybrid or sigma levels) is changed inconsistently [106]. This may happen if an online model employs different numerical schemes for advection of air and tracer -mass. The following arguments uses Enviro-HIRLAM as a specific example, but they apply more generally. The hybrid coordinates (η) are fully specified from surface pressure (P_s) by:

$$P_{k+\frac{1}{2}} = A_{k+\frac{1}{2}}(\eta) + B_{k+\frac{1}{2}}(\eta)P_s(\lambda,\theta)$$

where P represents pressure and $k \in \{1,...,n+1\}$ where n is the number of model layers and k the layer index. Here k is counted from top to bottom, i.e. towards increasing pressure and the coefficients, A and B, are defined in appendix 11. The total tracer mass is given by:

$$M_{global}^t = \frac{1}{g}\sum_{i,j,k} A_{i,j} \Delta P_{i,j,k}^t \psi_{i,j,k}^t \tag{4.6}$$

where i and j are horizontal indices, t is a temporal index, A represents the grid cell area, ΔP is the pressure difference between full levels and g is the gravitational acceleration. Consider time-step t_0. Between time-step t_0 and t_1 the numerical advection scheme redistributes tracer mass leading to changes in surface pressure, $P_s^{t_1\prime}$ and since the vertical levels are specified solely by surface pressure, the pressure levels are modified as well. The problem arises because $P_s^{t_1\prime}$ is generally not identical to $P_s^{t_1}$, which is the surface pressure implied by the dynamical core of the model. Following 5.3 this inconsistency leads to variations in global mass. At $t_1\prime$ the tracer concentration is valid at the vertical grid implied by the advection scheme and must be re-associated with the model grid. This is typically done on an index to index basis. The numerical advection scheme employed for the tracers is therefore only intrinsically mass conserving in its own grid and some kind of remapping, replacing the index to index re-association, each time step is necessary. The problem is, however, that any remapping will lead to loss of information and generally degrade the global mass conservation implied by the tracer advection scheme [106]. The only way to guarantee consistency is to develop an online coupled model in which the numerical solution of the tracer advection equation is the same as the numerical solution of the continuity equation in the dynamical core of the model.

Offline models require time averaged output from their meteorological driver and this is typically available every one to six hours. In between updates the meteorological forcing fields are interpolated retrospectively in time, by some models, to achieve the necessary update frequency. Hence, the offline models rely on the assumption that disturbances with time scales less than the

coupling interval can be satisfactorily represented by interpolation. Mesoscale disturbances in the meteorological fields are known to affect pollutant concentration [3]. These short time scale (ranging from less than one hour to days) disturbances include frontal circulations, development of clouds and precipitation, orographically forced flows, urban circulations, sea breezes etc. Unresolved horizontal variability is typically accounted for by tuning horizontal diffusion coefficients, leading to large values in the range $10^3 - 10^5 \ \mathrm{m^2 s^{-1}}$ [50]. While interpolation and smoothing may be an appropriate representation of subgrid-scale turbulent eddies it is not the case when mesoscale disturbances are resolved by the meteorological model, since growth, decay and structural changes to the pollutant fields are not considered. Therefore, the assumption may not be valid if short time scale disturbances exist in the meteorological fields. Online models, on the other hand, do not require a cutoff in the variability of the input fields since the meteorological forcing is updated at each time step of the meteorological model and, hence, take full advantage of the variability of the meteorological fields (see figure 4.1). This issue is considered in more detail in chapter 4.
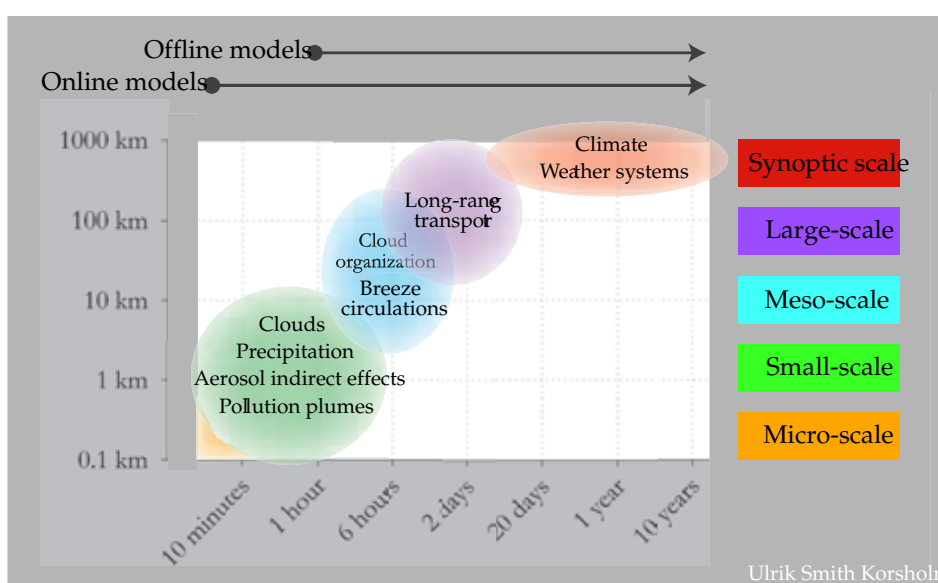
Figure 4.1: Characteristic temporal and spatial scales of processes of importance to the aerosol and trace gas distributions along with the ranges resolved by online and offline models. Note that an online access model may in principle resolve aerosol-meteorological feedbacks.

The issue raised above has special implications when considering pollutant-meteorology feedbacks. Since aerosols are of fundamental importance in cloud and precipitation development such feedbacks (including first indirect effect, second indirect effect, dispersion effect, semi indirect effect) are often mediated through clouds. The characteristic time scales of such effects are the same as that of the clouds, i.e. typically less than one hour (figure 4.1). Hence, online models with sufficient short time scales and sufficiently high horizontal resolution, are needed if feedbacks are to be simulated.

Issues when coupling simple and complex models

Development of an online coupled model involves the usage of 0-dimensional models (box models; here denoted simple models) to parameterize some physical or chemical processes, such as gas-phase chemistry, aerosol dynamics or deposition. As a first step the simple models should be thoroughly tested in a multitude of environments. Taking gas-phase chemistry as an example the simple model will be employed in regions with very sharp concentration gradients (rural to urban transition zone) and meteorological conditions span surface to top of the atmosphere conditions,

from $30°$ C to $-50°$ C. Often the 0-dimensional models have been employed in other studies and are therefore well tested at least near the surface, but neglect of the extreme environments may lead to problems in the form of crashes and difficulties in interpreting the results of the online coupled model, at a later point. The 0-dimensional model should also be evaluated against measurements or at least with respect to other similar models. There is no reason to believe that the coupled model will produce reasonable results if the simple model, on a stand alone basis, cannot.

The next step is to ensure consistency between the simple model and complex models. If processes are fully or partially accounted for in the complex model it will lead to erroneous results if they are also accounted for in the simple model. Although this point seems obvious, it is in fact often difficult to spot such errors. As an example consider the inclusion of ozone radiation absorption (a relevant feedback machanism) in Enviro-HIRLAM. Investigating the shortwave radiation parameterization reveals that it is developed by fitting measurement data and that the measurements include ozone absorption. Removal of this component of the radiation parameterization is not trivial, since this would require re-tuning of the radiation scheme. On the other hand the ozone measurements were based on natural background levels, so it may still be possible to include the effect of anthropogenic ozone, i.e. ozone originating from anthropogenic emissions of the generating species (NO_x, VOC, etc.). Another example considers cloud radiative properties. These are defined on the basis of the effective radius of the cloud droplets. The effective radius is strongly dependent on the droplet number concentration, which is fixed in the model. If the fixed value includes a contribution from anthropogenic sources any implementation of the first and second indirect effects would be inconsistent and extracting the natural part of the CCN contribution leading to droplet formation would require re-tuning of the entire model (the implementation of feedbacks is considered in chapter 3).

Another point which must be investigated is the applicability of the simple model as parameterization. Using aerosol number concentration as an example again it is well known that species concentrations may span many orders of magnitude, for example from 0 m^{-3} to 10^{11} m^{-3} in highly polluted urban regions (nucleation mode particles). If for example the tracer advection scheme of the online coupled model cannot handle such a large span in magnitude the model may crash or if cutoff's are applied a significant portion of the aerosol mass may be removed and mass conservation lost. Another applicability issue which should be addressed is the influence of the simple model on the parallelization of the online coupled model. If there are horizontal dependencies or statements that hinder parallelization the simple model may not be compatible with the parallelization strategy of the coupled model. Parallelization errors are very difficult to detect and may lead to everything from model crashes, unphysical results to subtle changes. The most effective way to investigate whether a parallelization error is present is to compare runs with one and more processors and do difference plots of relevant fields. When playing with the contour intervals parallelization errors turns up as distinct patterns reflecting the division of the grid in sub-domains.

As an example consider the implementation of the Bott advection scheme, which is employed in Enviro-HIRLAM (this will be discussed more fully in chapter 3). The initial coded version of the scheme was made by [54]. Therefore, it does not comply with the current Enviro-HIRLAM parallelization strategy, in fact, the calculation of the mass fluxes has strong horizontal dependencies since it assumes an internal four point halo around each sub-domain. Enviro-HIRLAM employs a hardcoded one point halo, and therefore, the advection scheme cannot be used straight away, without major code changes in either Enviro-HIRLAM or in the advection code. If this issue is ignored it will in fact be impossible to see any differences in the tracer concentration field, between simulations with one and eight processors with the naked eye (at least in the most common meteorological situations, within a few days forecast time). If, however, difference plots are drawn, the boundaries

of the eight sub-domains are clearly seen. As tracer mass is transported towards the sub-domain boundaries it is not allowed to fully be transported to the other sub-domains since the halo is to narrow and it piles up on the sub-domain boundaries. The consequences of this depends on the meteorological situation. If the wind is strong and the tracer impinges on the boundaries the concentration may rise to unrealistic values fast, however, if favoured by the wind, the accumulation may be slow and only give rise to subtle changes within the forecast and in this situation it may be very difficult to locate the problem. This discussion illustrates the importance of testing the code for parallelization errors in different meteorological conditions. The parallelization strategy and the implementation of the Bott scheme is discussed in detail in chapter 3.

Validity of the coupled model

The validity of the coupled model may be checked by comparing measurement data, typically generated during an observation campaign, with model predictions. The relevant concentration field is interpolated to the location of the measurements and temporal and spatial statistical quantities may be calculated to aid the comparison. By comparing to other such exercises it is possible to get an idea of the validity of the model, this procedure will be described more fully in chapter 4, but a few comments are appropriate here.

When a simple model has been implemented it is necessary to test the combined model, even though it is consistent, well tested and applicable. Assume that the simple model performed satisfactory on a stand-alone basis, then the results cannot be directly transferred to the coupled model because it includes much stronger mixing and generally smaller concentrations of the species. Subtle problems in the mathematical or numerical treatment of the sub-model or technical problems in programming may lead to errors. Such errors may be difficult to isolate and therefore it is important to test the model in as many different meteorological situations as possible. Here open source code models with a wide user community has a great advantage. When many different users employ the model the various errors are more likely to be identified quickly and the model may be tested more thoroughly. Therefore, the long term strategy for Enviro-HIRLAM involves collaboration with a wide variety of international institutes (see next section for a discussion of these issues), this also have the benefit of more model development.

The quality of the model should also be evaluated to test how reliable it is. If for instance the gas-phase chemistry scheme is not able to satisfactory simulate the sources and sinks of HNO_3 then this might generate a bias in the aerosol fields and thereby wrongly affect the interactions between aerosols and meteorology. The addition of a new simple model may not improve performance. Consider the situation where feedbacks between aerosols and clouds, are added consistently, in an online coupled model. Then, ideally, the simulation of clouds and precipitation should improve in the statistical verification because their description is more accurate. This is, however, not necessarily the case. Using Enviro-HIRLAM as an example, the meteorological part of the model is heavily tuned towards the weather in Scandinavia and the addition of a new simple model to account for the feedbacks requires retuning of the combined model system before any improvements can be expected. Considering the case where an existing online coupled model is being updated with a more complex chemistry scheme (including more reactions). The updated model will not necessarily lead to better statistical scores in the evaluation of, e.g. the NO_x concentration. In fact, the inclusion of a more complex description of the gas-phase chemistry is only a necessary condition for better statistical scores. If the new module has greater affinity towards errors in the input data then these errors may now be of much more importance and, hence, for a given set of input data the more simple scheme might provide better verification scores.

Strategy for Enviro-HIRLAM development

Since meteorological and air pollution models are now operating well within the mesoscale interactions between the two communities are feasible through the development of online coupled models. There are many areas of common interest where development could lead to synergy to the greater good of both communities. Examples of such areas include boundary layer structure (boundary layer height, mixing strength, etc.) which is of great importance when modeling the dispersion of air pollutants, but also for momentum and heat transport within the boundary layer and thereby for short-range numerical weather prediction (SRNWP). The same is true for convection parameterizations, prediction of precipitation and clouds or the usage of satellite derived land-use products. The greatest benefit, of such a coupling, for the SRNWP models may be through the development of more precise cloud and precipitation parameterizations (cloud-aerosol microphysics) and through feedbacks, while the air pollution community benefits from more precise dispersion and deposition of pollutants.

From the very beginning it has been an important part of the Enviro-HIRLAM strategy to utilize such synergy and bring the communities together. Enviro-HIRLAM is, however, a much larger project than this thesis alone. The idea is to develop a model which can be used in both operational and research mode for both air pollution and SRNWP purposes. This has the consequence that a wide variety of chemistry and aerosol schemes should be available for experimentation and some schemes should be economical enough (in relation to cpu-time and memory consumption) to be used for operational purposes. This thesis has focused on the operational applications by implementing and testing a chemical and aerosol scheme which has been designed especially for online coupled modeling. A range of other schemes (adapted from the WRF-CHEM model) are available for research purposes (such as RADM, RACM, CBIV, MADE) but have not yet been integrated in the code.

In addition to the advantages of online coupled modeling discussed earlier, it might be mentioned that it is advantageous to execute several operational models at the same time. For instance it is in the Enviro-HIRLAM long term strategy to use it for pollen forecasting, air pollution forecasting and weather prediction, in a nested set-up where it generates boundaries for the DMI 2.5 km resolution model. In this way fewer operational models and more people with hands on experience with the operational model and less cpu-usage is achieved, since we skip the post-processing steps for air pollution and pollen forecasting. Also on the longer term it is planned to investigate the usage of online coupled models for emergency preparedness.

The coding of Enviro-HIRLAM has been done to facilitate portability, by using the FORTRAN 90 memory allocation features (modularity). The general structure of the code follows HIRLAM as closely as possible to facilitate easy version updates and easy implementation of new features (chemical schemes etc.). In order to maximize development capabilities and testing of the model, the code is open to everyone who wish to contribute or use the model (non-HIRLAM members must sign a contract stating the rules of usage of the model). Seven different European groups are either working on, or will start working on, Enviro-HIRLAM. Another collaborator is the HIRLAM consortium. A HIRLAM chemistry branch will soon be opened (hosted by DMI) for easy downloading, code sharing, and version control. Enviro-HIRLAM will be used as a starting point for further developments and as more developers and users join in the model capabilities increase. Further discussion of the strategy and the relation to the HIRLAM consortium is discussed in [10].

From the above it is clear that Enviro-HIRLAM is an on-going project and this thesis contributes with an initial model version, testing and usage. The following plan for code development has been followed during this study:

- Updating, testing and evaluating tracer transport and dispersion

- Implementing and testing convection of tracers

- Implementing, testing and evaluating deposition of gases and particles

- Implementing, testing and evaluating gas-phase chemistry

- Implementing and testing wet aerosol model and thermodynamic equilibrium

- Implementing, testing and evaluating feedbacks through the first and second indirect effects

Summary and conclusions

Online coupled models are developed by coupling 0-dimensional chemistry, aerosol and deposition model components from a CTM. Any remaining part of the CTM disappears since the online coupled model applies the same numerical solution schemes and the same grid as the meteorological quantities. At each time step the model solves the coupled partial differential equations describing the evolution of both the meteorological and chemical fields.

The choice of chemical and aerosol solver must be carefully evaluated to match the usage of the model. In all cases the simple models must be consistent, applicable and well-tested and the validity of the coupled model must be evaluated in comparison with measurement data in an attempt to rule out technical or other errors. The main advantages of online models in comparison to offline models are that no spatial or temporal interpolation are necessary, since all processes are on the same grid, no temporal interpolation since the meteorological fields are available at each meteorological time-step, no artificial cut-off in meteorological variability, inconsistencies may be removed and feedbacks may be accounted for. The main disadvantage of online models is that they require quite large computer to run, because the computational requirements are concentrated in a short time interval. When using an offline model the computations are spread out over a longer time interval, i.e. it is more time consuming.

Model description

Parts of this chapter has been submitted as [121]

The first attempts at using HIRLAM as an air pollution model was made by [54]. She implemented a simplified sulfur chemistry scheme into HIRLAM, using the Bott advection scheme and the default vertical diffusion scheme. The Sulfur scheme followed [16] and considered three advected species: gaseous SO_2, particulate SO_4^{2-} and SO_4^{2-} dissolved in cloud water and kept all other species needed in the chemistry calculation (including O_3, HO^- and H_2O_2) constant at prescribed values. Dry deposition was included in a resistance approach based on look-up values of dry deposition velocity and wet deposition followed [16]. Comparison with measurements, in summer and winter cases, showed that the model overestimated SO_2, while particulate SO_4^{2-} was underestimated. Also SO_4^{2-} dissolved in cloud water showed poor agreement with observations and in general these issues were connected to the poor quality of the HIRLAM cloud cover and precipitation forecasts.

Further work was done by [37, 36] who considered the effect of using the Eulerian, semi-Lagrangian and Bott schemes for advection of a passive tracer in the operational HIRLAM version at DMI. Also the effect of vertical and horizontal diffusion were considered. He found that vertical diffusion is of great importance to the ability of the model to simulate passive tracer transport, while horizontal diffusion may be of importance at high resolution. Amongst the tested advection schemes the Bott scheme was preferred, due to its mass conservation properties and low computational cost when used in combination with the semi-Lagrangian scheme. The model development presented below is to be seen as a continuation of the work done by the above authors.

Processes of importance

Before model development may commence it is important to clearly define what the model should be used for and then investigate which physical, chemical and dynamical processes that are of importance to the problem and therefore should be included in the model. The focus of this work is aerosol-cloud interactions through the first and second indirect effects. The detailed implementation of these will be considered later in this chapter and here it will suffice to say that what is needed is a representation of the anthropogenic contribution to the cloud droplet number concentration. All dynamical and physical processes which are of importance to cloud life cycles, such as convection, entrainment/detrainment, vertical diffusion, advection and the flow on larger scales in general is represented in HIRLAM and will be described below.

The anthropogenic fraction of the cloud droplets may be calculated if the accumulation mode aerosols are well represented, since, aerosol in this mode have sizes relevant to droplet activation. Aerosols in the accumulation mode are either primarily emitted into the mode (examples include SO_4^{2-}, NO_3^-, NH_4^+, CO_3^{2-} and black carbon (BC) from industrial emissions and BC, SO_4^{2-}, Fe from fossil-fuel emissions) or are generated by growth of primary (examples include SO_4^{2-}, BC and Fe from fossil-fuel emissions) or secondary (including H_2SO_4 - H_2O nucleation) nucleation mode aerosols. Hence, in order to represent the accumulation mode aerosol the model must also account for the nucleation mode, whereas, the coarse mode, which is largely inactive with respect to clouds, may be neglected.

Nucleation and accumulation mode aerosols may grow by condensation of gaseous compounds, including water vapor, or by collision and coagulation. Coagulation is a volume preserving, growth and number reducing process (a new larger aerosol particle is generated on the expense of smaller particles). Using Smoluchowski's equation the effect of Brownian coagulation on the aerosol

number concentration may be expressed as:

$$\frac{\partial N(r_i)}{\partial t} = \frac{1}{2}\sum_{i \neq j} \beta_{i,j} N(r_i - r_j)N(r_j) - \sum_{0}^{\infty} \beta_{i,j} N(r_i)N(r_j)$$

where $N(r_i)$ is the number concentration of aerosols with radius r_i and β is the Brownian coagulation kernal:

$$\beta_{i,j} = 4\pi(r_i + r_j)(D_i + D_j) \tag{5.1}$$

with D_i and D_j the diffusion coefficients for small and large particles respectively. Using this kernel the time scale of coagulation may be approximated by division with the total volume $(4\pi(r_i + r_j)^3/3)$. Using $r_j = 0.1\ \mu m$ and $D_{0.1} = 6.75\ 10^{-10}\ m^2 s^{-1}$ and $D_1 = 2.77\ 10^{-11}\ m^2 s^{-1}$ [43], it is found that a $1\ \mu m$ particle is lost due to coagulation after approximately $0.5\ 10^{-3}$ seconds.

For condensational growth (for example water vapor condensing on a particle) the characteristic time scale may be approximated by using the radial diffusion equation:

$$\frac{\partial r}{\partial t} = \frac{D_v m_v N_v}{\rho_p r} \tag{5.2}$$

where D_v is the vapor diffusion coefficient, m_v is the mass of a vapor molecule and N_v is the number concentration of vapor molecules and ρ_p is the particle density. For H_2SO_4 with a vapor concentration of $10^7\ cm^{-3}$, $m_v = 98.08$ Da, $\rho = 0.5$ g cm^{-3} [43] and $D_v = 10^{-5}\ m^2 s^{-1}$ the growth rate of a 10 nm particle becomes approximately 12 nm hour^{-1} and for a $1\ \mu m$ particle it is approximately 0.1 nm hour^{-1}.

Particle ageing is the processes whereby an initially insoluble particles becomes more soluble through coagulation, condensation and chemical transformation of gaseous compounds on the particle surface. For the purpose of finding the characteristic time scale of condensation ageing the flux (F) of gas onto the particle surface may be described as: $F = D_v N_v/r$ For a 100 nm particle the time it takes to form a mono-layer of H_2SO_4 with 10^{19} molecules per cubic meter is approximately 3 hours, when $N_v = 10^7\ cm^{-3}$ and $D_v = 10^{-5} m^{-2} s^{-1}$.

The time-scales of nucleation in the boundary layer has been measured by several authors and amounts to $1 - 10^8\ cm^{-3} s^{-1}$ [124]. The characteristic time-scale of dissolution of a gas-phase species in an aqueous droplet has been evaluated in [153]. The process consists of diffusion to the particle and equilibration of the droplet into thermodynamic equilibrium. For accumulation mode the time-scale is typically hours, whereas for coarse mode particles the equilibrium is often not met (on the order of days). The time-scales have been summarized in table 5.1. The table shows that when using a short-range model, with forecast length of the order of days, neither of the processes can be neglected, at least not on the basis of time-scales alone, and must be accounted for in the model. However, in the current version of Enviro-HIRLAM insoluble material is not included in the aerosols and on that basis the effects of cloud ageing has been neglected.

The composition of atmospheric aerosols is dominated by Sulfate (SO_4^{2-}) and organic Carbon (C(org)) [205]. Over urban areas the average percentage distribution in tropospheric aerosol is approximately 30 % SO_4^{2-} and 30 % C(org), while the reminder mainly is composed of NH_4^+ and NO_3^-. Non-urban and remote areas contains more SO_4^{2-} than C(org), but in general there are large fluctuations in aerosol composition depending on region and type of pollution in this region. The influence of aerosol composition on cloud properties is not a settled issue. Observations and measurements are inherently difficult, but cloud resolving models may give some insigths into the importance of solubility. Organic compounds tend to act as surfactants lowering the surface tension

Table 5.1: Summary of time scales for various processes of relevance to aerosol-cloud interactions.

Mode	Process	Sec – Min – Hour – Day – Week
Nucleation[a]	Nucleation	———————
Nucleation	Condensation	—————————
Nucleation	Ageing	———————
Nucleation	Coagulation	—————————
Nucleation	Equilibration	———
Accumulation	Condensation	———————
Accumulation	Ageing	———————
Accumulation	Coagulation	———————
Accumulation	Equilibration	——————
Coarse	Condensation	———————
Coarse	Ageing	———————
Coarse	Coagulation	———————
Coarse	Equilibration	———————

[a]The dependence on aerosol size is covered by dividing the size ranges into three modes: nucleation mode (diameter of order 0.01 μm), accumulation mode (diameter of order 0.1 μm) and coarse mode (diameter of order 10 μm).

of individual droplets and thereby affecting further condensation. This, however, is believed to be a minor effect and in general the results of cloud resolving models show that up-draught velocity and CCN number concentration are more important in the sense that cloud and precipitation development is more sensitive to these parameters in cloud resolving models. For this reason the organic compound of the aerosols has been neglected and aerosols thus consist of $SO_2(aq)$, HSO_3^-, SO_3^{2-}, HSO_4^-, SO_4^{2-}, NH_4^+, $NH_3(aq)$, $HNO_3(aq)$, NO_3^- and H_2O.

Governing equations

From the above it is clear that the model must account for emission, advection, vertical diffusion, convection, gas-phase chemical transformations, aerosol thermodynamic equilibrium, aerosol nucleation, aerosol coagulation, gas and aerosol deposition and cloud and precipiation development, in addition to the larger scale dynamical and physical processes, in order to simulate and investigate the aerosol indirect feedbacks. The general equation describing these processes was given in equation 4.1. Including the advection term in $\mathcal{L}$ it may be expanded as follows:

$$\mathcal{L} = \mathcal{L}_{emis} + \mathcal{L}_{advn} + \mathcal{L}_{diff} + \mathcal{L}_{conv} + \mathcal{L}_{chem} + \mathcal{L}_{aero} + \mathcal{L}_{deps} + \mathcal{L}_{indt}$$

where $\mathcal{L}_{emis}$ describe primary emissions of gases and particles, $\mathcal{L}_{advn}$ describes advection, $\mathcal{L}_{diff}$ describes horizontal and vertical diffusion, $\mathcal{L}_{conv}$ described subgrid-scale convection of gases and particles, $\mathcal{L}_{chem}$ describes chemical transformations of gases, $\mathcal{L}_{aero}$ describes concentration changes due to the formation of secondary aerosol and transformations due to coagulation and condensation, $\mathcal{L}_{deps}$ describes dry and wet deposition of gases and particles and $\mathcal{L}_{indt}$ describes changes in gas and particle concentrations due to cloud aerosol interactions, i.e. feedbacks. The equation governing the development of the mass concentration of a given species may then be expressed as:

$$\frac{\partial \psi}{\partial t} = (\mathcal{L}_{emis} + \mathcal{L}_{advn} + \mathcal{L}_{diff} + \mathcal{L}_{conv} + \mathcal{L}_{chem} + \mathcal{L}_{aero} + \mathcal{L}_{deps} + \mathcal{L}_{indt})\psi \qquad (5.3)$$

Solution of the governing equations

As mentioned in chapter 2 equation 5.3 is generally nonlinear and can only be solved analytically in idealized situations. There are basically two approaches for its numerical solution, either a nonlinear equation solver (such as the SUNDIALS suite which include the GEAR and VODE solvers [29]) or operator splitting [150] must be used. Operator splitting has the advantage that separate numerical solution schemes may be applied to different dynamical, physical or chemical processes, i.e. a very precise, but computationally heavy, numerical solution scheme may not be appropriate if the given parameterization is very simplified. On the other hand it requires a new set of boundary conditions for each intermediate solution.

With operator splitting the contribution to ψ from individual processes is solved independently and then coupled together, hence, each process contributes part of the total change. These processes may correspond to the physical processes mentioned above as suggested by [?] or may be groupings of physical processes. Let $\Delta\psi = \psi(t + \Delta t) - \psi(t)$ be the total change in ψ due to all processes in time Δt. In the approach used here the effect of each process is applied in series (as opposed to in parallel, where each contribution is decoupled) and provisional values of ψ are generated and used as input for the next process; the procedure is as follows:

$$
\begin{aligned}
\psi^1(t + \Delta t) &= \mathcal{L}_{emis}(t)\psi(t) \\
\psi^2(t + \Delta t) &= \mathcal{L}_{advn}(t)\psi^1(t) \\
\psi^3(t + \Delta t) &= \mathcal{L}_{diff}(t)\psi^2(t) \\
&\vdots \\
\psi(t + \Delta t) &= \mathcal{L}_{indt}(t)\psi^7(t)
\end{aligned}
$$

where ψ^1 includes the effect of emissions, while ψ^2 includes the effect of emissions and advection, etc. The error induced due to operator splitting is of order Δt and should approach zero as $\Delta t \to 0$. The maximum value of Δt, however, cannot easily be determined and is process dependent. In general the procedure will converge if each of the numerical schemes applied for the provisional values are convergent. The order of the schemes are also of importance. Following [150] the advective part is solved using a symmetric permutation of the coordinate directions, i.e. solutions are first computed in the x, y and z directions and then in z, y and x, during the same time step. In the above notation $\mathcal{L}_{deps}$ only covers wet deposition, while dry deposition is not treated as a separate process in the operator splitting approach. Dry deposition is applied as lower boundary condition for the vertical diffusion, i.e. dry deposition and vertical diffusion are solved together. Similarly, gas-phase chemistry, aerosol-gas thermodynamic equilibrium, aerosol dynamics and nucleation are solved together. The HIRLAM model schemes are used to solve the individual processes, when possible, and therefore a brief overview of the HIRLAM model is given below. The reminder of this chapter describes the numerical solution procedures for each of the individual processes mentioned above.

The high resolution limited area model

In this chapter the solution methods employed in HIRLAM are outlined, for a full description the reader is referred to the HIRLAM documentation [226]. HIRLAM contains two main components, a dynamical module and a physical module, mainly describing transport and diabatic processes respectively. The dynamical cores are based on the primitive equations and were described in chapter 2, while the physical module includes parameterizations of processes such as radiation, vertical diffusion, convection and condensation and land-use properties. Tendencies from the physical module are computed separately and added to the primitive equations as source/sink terms.

The model is hydrostatic and the prognostic variables comprise the velocity components, temperature, specific humidity, cloud water, turbulent kinetic energy (TKE) and surface pressure. With the addition of chemistry and aerosols in Enviro-HIRLAM the number of prognostic variables increases by the number of chemical and aerosol species.

In both the Eulerian and semi-Lagrangian dynamical cores, semi-implicit adjustment treats gravity waves and allows for long time-steps, however, the dynamical equations are transformed to Helmholtz type equations:

$$f - H\nabla^2 f = g$$

which must be solved on each time step; the general expressions for f, H and g may be found in [226]. The solution of the Helmholtz equation proceeds by decoupling in the vertical and subsequent solution of a set of independent two-dimensional equations. These are found by using Fourier-Sine-transforms in the west-east direction and applying Gaussian elimination in the south-north direction, followed by an inverse Fourier sine transform in the west-east direction. The total solution is found by vertical coupling of the two-dimensional equations. To maintain stability for large time steps the fields are diffused in the horizontal using a fourth order explicit or a sixth order implicit scheme. The sixth order equation for a field f is defined as:

$$\frac{\partial f}{\partial t} = K\left(\frac{\partial^6 f}{\partial x^6} + \frac{\partial^6 f}{\partial y^6}\right)$$

The simplified implicit diffusion equation only considers sixth order terms in longitude and latitude and is solved using a two-step implicit time splitting scheme. Since fields at time level $n + 1/2$ are potential sources of instability, the non-linear fields are further filtered by:

$$
\begin{aligned}
f^{n+1/2} &= \frac{1}{2}(3f^n - f_f^{n-1}) \\
f_f^n &= f^n + \epsilon(f^{n+1} - 2f^n + f_f^{n-1})
\end{aligned}
$$

where $\epsilon = 0.1$ is the default value.

All meteorological fields are arranged on a rotated latitude-longitude Arakawa-C grid with wind components and geopotential defined on grid-cell intersections and temperature, specific humidity, cloud water and surface pressure are carried in the grid-cell center. In Enviro-HIRLAM the tracer mass concentration is also carried at cell mid-points and thereby they represent the grid-volume averaged mass concentrations. Meteorological fields are calculated by the dynamical and physical cores and is used for driving chemical and aerosol processes, which may feed back onto the meteorological fields through cloud processes. In the vertical a hybrid between terrain following σ-coordinates and pressure coordinates is used. The hybrid vertical coordinate (η) is defined in terms of pressure (p): $p_{k+1/2} = A_{k+1/2}(\eta) + B_{k+1/2}(\eta)p_S(\lambda, \theta)$ where k is a level index and A and B are fixed constants (see appendix 1). As A approaches zero η approaches σ-coordinates and as B approaches zero η approaches pressure coordinates. For the vertical discretization wind, temperature, specific humidity (and tracer mass concentration in Enviro-HIRLAM) are defined on full levels, while pressure, geopotential and vertical velocity are defined on half levels. The Eulerian core uses a three time level leapfrog scheme for iterating forward in time, while the semi-Lagrangian core uses a two time level semi-implicit scheme.

At the lateral boundaries the fields are relaxed towards externally imposed fields, in a pre-specified boundary zone, in order to prevent sharp gradients across the boundaries (shock effects). The external fields are either output from a global model or output from a limited area model running on

a larger domain. Over-specification of the fields on the lateral boundaries may be a source of error through the development of slow Rossby waves or fast gravity waves propagating from the boundaries into the domain. The slow waves may be avoided by situating the boundary zone sufficiently far away from the region of interest and the fast waves are removed by having a damping zone adjacent to the boundary zone. Initial and boundary conditions for the trace gases and aerosols are discussed later in this chapter.

At analysis time the state of the atmosphere is initialized by digital filtering [139]. If the initial mass and wind fields are not sufficiently consistent spurious high-frequency oscillations (gravity-inertia waves with unrealistically large amplitudes) may develop in the meteorological fields. The digital filter is applied to time series of input fields by first switching off all irreversible physics and running the model backwards in time, while accumulating the filtered field. Then a forward integration is performed until the analysis time is reached. As the model runs back and forth the initial fields are filtered and the final initial state contains only damped high-frequency noise, decreasing the meteorological spin-up time (spin-up when chemistry is included is discussed later in this chapter).

Emission mechanisms

Emissions are currently handled as Eulerian point sources located within the lowest model layer, extending approximately 32 meters above the surface. It is necessary to assume that the emitted species is well mixed within the grid box containing the emission point. Given the emission rate, emission time interval and the location of the emission point, the grid box volume may be calculated to give the emitted mass concentration ($Q_{i,j,k}$) per time interval in grid-point (i, j, k), where the indices represent longitudinal, latitudinal and vertical directions respectively. The modification of $\psi_{i,j,k}$ then follows the Leapfrog scheme:

$$\psi_{i,j,k}^{t+1} = \psi_{i,j,k}^{t-1} + 2\Delta t Q_{i,j,k}$$

The grid point closest to emission point is assumed to contain the emission grid box. The volume of this, and therefore the emitted concentration, is dependent on the current resolution of the model. Hence, the higher the resolution the higher the emitted concentration. This influence of the resolution on the species concentration is mainly visible close to the source (neighboring grid boxes) and disappears as the concentration field spreads. The emission rate, location and temporal development of the emission may be prescribed directly in the code for point source releases. For areal sources, which are treated as a sequence of point sources, this information may be supplied by emission files generated from emission inventories. A corresponding emission pre-processor has been developed in order to generate the necessary emission files. The pre-processor reads the GEMS-TNO [231] inventory (figure 5.1), unpacks the temporal variations of the species, implements splitting of the volatile organic compounds, handles unit conversions and prepare the data on the model grid, accounting for grid rotations. The inventory is in $0.125° \times 0.0265°$ (longitude $\times$ latitude) resolution and provides full geographical coverage for Europe, from Ireland to Kazakstan and contains 2003 emissions. It includes acidifying pollutants (SO_2, NO_X, NH_3, CO, Non methane VOCs (NMVOC), CH_4 and particulate matter (PM)) and is divided into 10 SNAP (Selected Nomenclature for sources of Air Pollution) codes (table 5.2).

NO_X values are partitioned as 90% NO and 10% NO_2. The VOC split follows [220], while the lumping mechanism used for the NWP-Chem gas-phase chemistry scheme, which is currently the default scheme in Enviro-HIRLAM, follows the procedure used in RACM (the Regional Acid Deposition Model [212]). Temporal development of the selected SNAP codes may be either monthly, weekly, daily or hourly. The procedure for translating monthly emissions into hourly emissions is accomplished by using the default temporal allocation profiles. These profiles assign

Figure 5.1: Example of the NO_x ($NO_2 + NO$) component of the GEMS-TNO inventory (tonnes/year); ship tracks are not included in this plot.

Table 5.2: SNAP codes available in the GEMS-TNO emission inventory.

SNAP code	Description
1	Energy transformation
2	Small combustion plants
3	Industrial combustion
4	Industrial processes
5	Fossile fuel production
6	Solvent and product use
7	Road transport
8	Non-road transport and mobile machinery
9	Waste disposal
10	Agriculture

portions of the total monthly emissions to each day of the month and then assign portions of the daily emissions to each hour of the day. The temporally resolved emission data, containing contributions from some or all of the SNAP codes, is then reassigned to the model grid (gridded). The griding procedure proceeds by interpolating between the inventory and model grid, taking the appropriate area corrections into account in order to conserve species mass. The procedure may be written as: $Q_{grid} = \beta Q_{inventory}$ where Q is the emission rate and β is the area correction factor defined as the ratio of corresponding grid-cell areas in the Enviro-HIRLAM and inventory grid, assuming that the emission per grid-cell area is the same in the two grids. Output is written to an external emission file which is read once at the beginning of the Enviro-HIRLAM forecast. All emission information is kept in memory, so that the mass concentration fields may be updated at a time interval corresponding to the selected temporal resolution of the emission data.

Advection

The advective part of the continuity equation (equation 5.3) for chemical species is given as:

$$\mathcal{L}_{advn}\psi = -\nabla \cdot (\psi\vec{v})$$

stating that the mass concentration of the species can only change in regions of flux convergence or divergence. Here it has been assumed that the type, density, shape etc. of the species are not of importance when considering advection. Hence, the problem of advecting the species is well understood and well described mathematically. There is, however, a problem since the above equation is non-linear and cannot be solved analytically, except in very idealized situations, where the wind components are not allowed to evolve freely [242]. The native semi-Lagrangian and Eulerian advection schemes may be used to advect the species. However, mass conservation of chemical species is expected to be of great importance to chemistry and therefore these schemes are not sufficient, when developing an online coupled model [37]. In order to improve mass conservation the Bott advection scheme is used for chemical species and aerosols, while the semi-Lagrangian scheme is used for meteorological quantities, thereby, facilitating fast simulation times. This inconsistency does not seem to cause loss of mass conservation on the short time-scales considered here [36]. However, it is planned that the model will be used for longer term simulations, ranging from a month to a year, and in this situation the solution strategy should be reconsidered. Currently, at the University of Copenhagen, a new scheme for solving the continuity equation, which is locally mass conserving, is being implemented in Enviro-HIRLAM, thereby removing the inconsistency. Full consistency is only achieved if the algorithms of the underlying dynamical core are fully consistent with the solution of the continuity equation for each species. The new scheme consists of a simple and cost effective method to ensure local (inherent) mass conservation in traditional semi-implicit (SI), semi-Lagrangian (SL) models and an efficient locally mass conserving spatial filter. The locally mass conserving SL method (LMCSL) is relatively simple to construct from existing SL schemes [109, 128]. The LMCSL based dynamical core in Enviro-HIRLAM has come quite far and the model seems to be able to run stably with realistic results. The main obstacle in the implementation has been the inclusion of Lagrangian vertical coordinate. The increase in numerical cost of the new scheme relative to traditional SI-SL schemes is expected to be small, particularly, when there are several passive tracers.

The SL implementation in HIRLAM is coupled with a two time-level SI time stepping routine. The air parcels are tracked backwards at each time-step along the trajectories from the forecasted arrival points to the departure points. Once the departure point is located the concentration value is found by interpolation from the previous time-level. Considering the Lagrangian form of the continuity equation the new concentration, at time level n+1 is then given as:

$$\psi^{n+1} = \psi_\star^n + \Delta t\{\psi\nabla \cdot \vec{v}_\star\}^{n+\frac{1}{2}}$$

where $\star$ denotes the departure point and Δt is the dynamical time-step. A more detailed description of the SL-SI implementation in HIRLAM is given in [148].

The Bott advection scheme is an Eulerian flux based scheme inspired by the upstream method, thereby retaining positive definiteness, conservatism and reducing numerical diffusion. In order to illustrate the implementation of the Bott advection scheme, assume that advection is the only process of importance:

$$\frac{\partial\psi}{\partial t} = \mathcal{L}_{advn}\psi \tag{5.4}$$

Using the upstream method one may discretize equation 5.4:

$$\psi_{i,j,k}^{n+1} = \psi_{i,j,k}^n - \frac{\Delta t}{\Delta x}(F_{i+1/2}^n - F_{i-1/2}^n) - \frac{\Delta t}{\Delta y}(F_{j+1/2}^n - F_{j-1/2}^n) - \frac{\Delta t}{\Delta z}(F_{k+1/2}^n - F_{k-1/2}^n)$$

where (i, j, k) are the longitudinal, latitudinal and vertical indices and $F_i^n = (\psi u)_i$ is the species mass flux in the longitudinal direction at the center of the grid cells at time n. In Bott's scheme the fluxes are defined as:

$$F_{i+1/2} = \frac{1}{\Delta t} \int_{x_{i+1/2}-u\Delta t}^{x_{i+1/2}} \psi_i \mathrm{d}x$$

where the fluxes are defined identically in the other coordinate directions. hence, $F_{i+1/2}$ is the mass flux through the right hand boundary of the grid-cell in time Δt and a corresponding expression for $F_{i-1/2}$ may be found by substituting i with $i-1$. The distribution of ψ_i inside the grid-cell is found by fitting area preserving polynomials of order q. The area under the polynomial in grid-cell i should equal $\psi_i \Delta x$ for mass to be conserved:

$$\psi_i \Delta x = \int_{x_{1-1/2}}^{x_{1+1/2}} \sum_{p=0}^{p=q} a_{i,p} \left(\frac{x - x_i}{\Delta x} \right)^p \mathrm{d}x$$

where the coefficients $a_{i,p}$ are functions of ψ and may be found by interpolation from the neighbouring points. Currently, the scheme is implemented with fourth order polynomials in the horizontal directions and second order polynomials in the vertical (coefficients up to fourth order are given in [22]. The positive definiteness of the scheme is ensured by requiring that the total flux out of a grid cell is positive and less than the available mass in the cell. On the lateral boundaries the advected chemical and aerosol fields are relaxed towards background values, as for the meteorological fields. The scheme has been extended to three dimensions by using a splitting procedure, in which the one-dimensional solution scheme is applied alternately in each direction [150]. In order to assure that the CFL criterion is fulfilled in each direction at each time step the scheme is typically called three times inside a dynamical time step (at a horizontal resolution of 15 km).

Turbulent mixing

Vertical mixing of aerosols and chemical species is parameterized using the native dry TKE-1 scheme by [48] (denoted the CBR-scheme), the same scheme which is used for all other vertically mixed quantities. The scheme was originally developed for the Meso-NH model, for both large eddy and mesoscale simulations, but has been adapted to HIRLAM [226]. The vertical turbulent fluxes of ψ (F_ψ) are defined as:

$$F_\psi = -K_\psi \frac{\partial \psi}{\partial z}$$

where K_ψ is the turbulent diffusion coefficient. The basic idea when using a TKE scheme is to close the turbulence calculation by approximating any unknown term in dimensionally correct and physically consistent model variables. In the CBR scheme the diffusion coefficient is chosen proportional to a velocity and a length scale which represents the largest transporting eddies. The velocity scale (v_{turb}) is given as: $v_{turb} = \sqrt{E}$ where E represents the TKE. TKE is a prognostic variable and is computed from the full TKE equation:

$$\frac{\partial E}{\partial t} = -\overline{u\prime w\prime}\frac{\partial u}{\partial z} - \overline{v\prime w\prime}\frac{\partial v}{\partial z} + \frac{g}{\theta_v}\overline{w\prime\theta_v\prime} - \frac{\partial}{\partial z}(\overline{w\prime E} + \overline{w\prime p\prime/\rho}) - \epsilon$$

where primes denote the turbulent part of the fields (differences from average values) and averages are denoted by an overbar, g is the gravitational acceleration, θ_v is the virtual potential temperature and ρ is the density of air. On the right hand side the first two terms represents shear production of turbulence, the third term represents buoyancy production and consumption, the fourth term represents transport by turbulence and pressure forces and ϵ is the dissipation term, representing the energy cascade from the largest to the smallest scales. The model solves this equation for E, with

appropriate boundary conditions, at each time-step. The length scale formulation is the main difference between the original and the HIRLAM versions of the CBR-scheme. The characteristic turbulent length scale represents the largest turbulent eddies feeding the energy cascade. Since, the resolution is not sufficient to resolve the turbulent eddies the length scale must be parameterized. The formulation used in HIRLAM is based on a combination of length scales for stable and unstable conditions. Consider an air parcel moving upwards due to turbulence, i.e. in unstable conditions. Let l_{up} denote the maximum and l_{dwn} the minimum vertical displacements of the air parcel. In HIRLAM these are parameterized as functions of stability F.

$$
\begin{aligned}
l_{up} &= \int_{z_{bottom}}^{z} F(N_b^2) \mathrm{d}z\prime \\
l_{dwn} &= \int_{z}^{z_{top}} F(N_b^2) \mathrm{d}z\prime
\end{aligned}
$$

where N_b^2 is the Brunt-Väisala frequency and z_{top} and z_{bottom} are the upper and lower boundary of the mixing domain. For unstable conditions: $F(N^2) = \alpha_n - \alpha_r \alpha_d \arctan(\alpha_d N^2)$ where α_n, α_r, α_d are tuning constants ensuring reasonable behaveiour of the scheme in the near neutral and convective limits. The total length scale in unstable conditions (l_{int}) is given as: $l_{int}^{-1} = l_{dwn}^{-1} + l_{int}^{-1}$. In the stable case the length scale (l_s) is given as: $l_s = c_{m,h}\sqrt{E}/N$ where the constant $c_{m,h}$ may differ for heat and momentum transport, $c_h = 0.2$ and $c_m = 0.8$. The total length scale formulation is then given as: $l_{m,h}^{-1} = (\max(l_{int}, l_{min}))^{-1} + l_s^{-1}$ where l_{min} has been introduced to ensure a contineous transition between the stable and unstable regimes, it is defined as: $l_{min}^{-1} = l_{limit}^{-1} + (c_n \kappa z)^{-1}$ where κ is the ratio of the gas constant and specific heat for dry air and $c_n = 3.3^{-1/2}$.

Stability parameters and eddy diffusivities are explicitly calculated while the solution of the diffusion equation is done implicitly. Aerosols and chemical species are implemented as moisture and cloud water, using the length scale formulation for heat. As lower boundary condition, the dry deposition flux towards the surface, is used thereby simulating the removal of aerosols and gas species due to dry deposition.

Convection

The vertical velocity as diagnosed in HIRLAM represents the resolved dynamical velocity, however, at certain points convection may produce very large vertical velocities (up to 30 or 40 m/s) at sub-grid scales. As gases heat they become buoyant and start to rise. Similarly, particles caught in such updraughts may be lifted out of the boundary layer and into the free atmosphere. Convection plays an important role in moving aerosols into cloud environments and therefore convection of particles is of importance in the study of cloud/aerosol feedbacks and must be included in the model.

Convection of chemical species and aerosols follows the approach for moisture in the Soft TRAnsition COndensation (STRACO) scheme, except evaporation and condensation of water vapor from aerosols is not accounted for, i.e. they are passively convected. Here the features relevant to the species and aerosols are described, for a detailed description of the STRACO scheme see [226].

Convection and associated condensation and evaporation is dependent on both resolved and sub-grid scale vertical motion. Hence, the computations of convective processes is also dependent on the formulation of model dynamics and vertical diffusion. The vertical diffusion accounts for small scale vertical transport through the boundary layer, while the convective parameterization described vertical transport up to the depth of the troposphere.

The STRACO scheme relies on moisture budget closure, i.e. it is assumed that convective activity proceeds only if there is moisture convergence. In the current development version of STRACO, this

constraint is being relaxed and convection in strongly unstable situations without moisture convergence is allowed. Convection may be triggered from any level in the model using trigger perturbations for temperature (T) and specific humidity (q):

$$\Delta T = \frac{1}{a_1 + a_2\sqrt{\frac{D_T}{\Delta X}}}$$

$$\Delta q = \frac{1}{a_3 q_k \sqrt{\frac{\Delta X}{D_T}}}$$

where $a_1 = 0.6 \text{ K}^{-1}$, $a_2 = 0.5 \text{ K}^{-1}$, $a_3 = 0.02 \text{ K}^{-1}$ and $D_T = 10^4$ m. When triggered the scheme proceeds by determination of the vertical extent of the convective cell by adiabatic cloud parcel lifting. It is assumed that the parcel remains saturated, at the saturation specific humidity, at the corresponding temperature which evolves during the lifting process and due to lateral entrainment until the buoyancy becomes negative. The vertical redistribution of the vertically integrated concentration then proceeds according to the lateral entrainment. The change in aerosol or chemical species mass concentration inside the convective cell is calculated according to the convective equation:

$$\frac{\partial \psi}{\partial t} = \left(\frac{\partial \psi}{\partial t}\right)_{dyn} + \left(\frac{\partial \psi}{\partial t}\right)_{turb} + \hat{Q}_\psi \frac{F_\psi}{\hat{F}_\psi} + S_\psi$$

where $(\partial \psi / \partial t)_{dyn}$ and $(\partial \psi / \partial t)_{turb}$ are the provisional values of the changes due to dynamics and vertical diffusion, $\hat{Q}_\psi$ is the total concentration source vertically averaged over the convective cell, S_ψ represents entrainment through the cloud top, while F_ψ is the redistribution function, describing the vertical variation of convective concentration supply, accounting for lateral entrainment: $F_\psi = \psi_c - \psi_e$, where ψ_c is the concentration inside the convective entity and ψ_e is the corresponding stable environment value at the same level. $\hat{F}_\psi$ is the vertically averaged distribution function.

Clouds and indirect effects

The STRACO convection scheme describes the redistribution of temperature, specific humidity, cloud condensate and chemical and aerosol species inside the convective entity, however, it also accounts for the sub-grid scale distribution of humidity. In both the unstable (convective) and stable (stratiform) cases the humidity varies according to a probability distribution function (PDF). For some cloud condensate the cloud cover is defined as the saturated fraction of the grid box and is, therefore, defined in terms of the PDF. In the convective case a rectangular asymmetric PDF is employed resulting in the following expression for the cloud cover:

$$f = \frac{1}{1 + \sqrt{\frac{q_s - \overline{q}}{\overline{q}_c}}} \qquad \text{if} \quad q_s \geq \overline{q}_{tot}$$

$$f = \frac{1}{2} + \frac{\overline{q}_{tot} - q_s}{2 A_c \overline{q}_{tot}} \qquad \text{if} \quad \overline{q}_{tot}(1 - A_c) \leq q_s \quad \text{and} \quad q_s < \overline{q}_{tot}$$

$$f = 1 \qquad \text{if} \quad q_s < \overline{q}_{tot}$$

where A_c is a dimensionless parameter defining the width of the PDF, q_s is the saturation specific humidity, where saturation is calculated with respect to the temperature inside the convective entity, $\overline{q}$ is the grid-cell mean specific humidity, $\overline{q}_c$ is the grid-cell mean specific humidity inside the convective entity and $\overline{q}_{tot}$ is the grid-cell mean total humidity, i.e. $q_{tot} = q + q_c$. For a stratiform cloud cover a symmetric rectangular PDF is used resulting in the following expression for the cloud cover:

$$f = \frac{1 + A_{st} - q_s/\overline{q}_{tot}}{2 A_{st}}$$

where saturation is calculated with respect to the grid-cell averaged temperature and A_{st} is the amplitude of the PDF. For values below zero or above one f is reset to zero or one respectively. For the calculation of formation and fall-out of precipitation a description of cloud micro-physics is needed, this is also provided by the STRACO scheme. The description of cloud microphysics in the STRACO scheme is based on the Sundqvist parameterization [216, 217, 218]. STRACO has been extended to include the effects of cloud drop number concentration and characteristic droplet radius r, by combining the autoconversion term for cloud water from [188] with the existing formulation in the STRACO scheme [198]. In STRACO precipitation release is written $G_p = \Phi q_c (1 - \exp(-X^2))$ where $X = \hat{q}_c / \mu$ and $\hat{q}_c = q_c / f$ is the in-cloud specific cloud condensate. The Φ term is defined as: $\Phi = \Phi_1 \Phi_2 \Phi_3 \Phi_4$ where Φ_2 describes the effect of collision/coalescense and the Bergeron-Findeisen mechanism, Φ_3 expresses a temperature dependency at cold temperatures, Φ_4 is height dependent and describes an enhanced sedimentation of cloud droplets from fog (clouds at very low levels) and Φ_1 is the autoconversion term which is now defined as:

$$\Phi_1 = C_{l,out} \hat{q}_c \frac{\rho_a}{\rho_w} \left(\hat{q}_c \frac{\rho_a}{\rho_w} N \right)^{\frac{1}{3}} H(r - r_0)$$

Here ρ_a represents air density, H is the Heavy-side step function, $C_{l,aut}$ is a constant [188], r_{eff} is the cloud droplet effective radius (ratio of total droplet volume to total droplet surface area and r_0 is a constant threshold drop radius (currently fixed at $5~\mu$m following [188]). For water clouds r_{eff} follows [144]:

$$r_{eff} = [(3\rho_a q_c)/(4\pi N \rho_w)]^{1/3} \qquad (5.5)$$

Rasch and Kristjansson refer to a need of reducing the term Φ_1 by an order of magnitude to obtain a sufficiently damped autoconversion when precipitation release is not well developed. Here the Sundqvist term (X) as given above has been introduced in order to achieve the same effect in a more physically based way. The effect of the X term is to make precipitation release less efficient at small amounts of in cloud condensate. The parameter is affected by the denominator μ which implies increasing X with increasing precipitation release entering the grid-box from above and depends on the temperature. N represents the cloud droplet number concentration, which, assuming a natural background CCN concentration, is fixed at 10^8 m^{-3} over marine regions and $4 \cdot 10^8$ m^{-3} over continental areas. Herein lies a possibility to parameterize the second indirect effect. By perturbing the natural background value of N with an anthropogenic component, precipitation release would be delayed and cloud lifetime and cloud cover would be affected (the second indirect effect is discussed in detail in chapter 5). Hence, $N = N_{back} + N_{anthr}$ where N_{back} depends only on surface type and represents the natural background and N_{anthr}, represents the anthropogenic component, and is calculated using input from the aerosol module and a parameterization directly connecting sulfate aerosol number concentration (N_{aero}) and cloud droplet number concentration (N_{anth}) [26]:

$$\begin{aligned} N_{anth} &= N_{aero}^{0.48} 10^{8.06} \qquad \text{over continental areas} \\ N_{anth} &= N_{aero}^{0.26} 10^{2.24} \qquad \text{over marine areas} \end{aligned}$$

Since the use of the Rasch-Kristjanson autoconversion formula in STRACO has not been properly verified it is necessary to compare the accumulated precipitation of a simulation with the new formula with an identical simulation using the standard STRACO scheme. If the accumulated precipitation does not differ significantly between the two simulations it is likely that the new formula performs reasonably well at least in the simulated case. Figure 5.2 displays an example of a comparison between the new and old formulation for the simulations presented in chapter 5. A similar approach is followed in order to parameterize the first indirect effect. Cloud radiative properties are parameterized on basis of the cloud droplet effective radius. The parameterization is
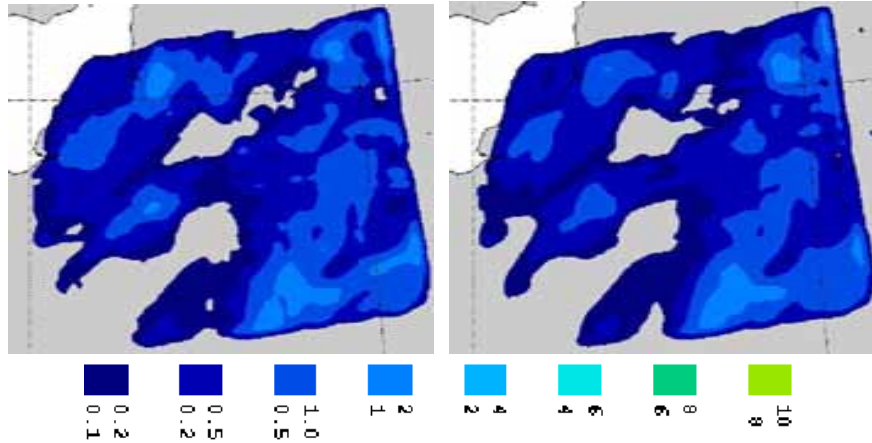
Figure 5.2: Accumulated precipitation (mm) over 24 hours (30 June 2005 at 00 UTC to 1 July 2005 00 UTC) from simulations using the new (left) and old (right) STRACO autoconversion formulations. The horizontal resolution is $0.05° \times 0.05°$. The case is described in more detail in chapter 5.

based on a five band radiative transfer model [200] and for clouds the shortwave absorptivity ($\hat{A}$) and transmissivity ($\hat{T}$) are:

$$\hat{A} = b_{10}(b_{11} + \cos(\theta))\log(1 + b_{12}\hat{M}) \tag{5.6}$$

$$\hat{T} = \frac{\hat{T}_1}{\hat{T}_1 + \hat{M}} \tag{5.7}$$

where $\hat{T}_1 = b_{13}(b_{14} + \cos(\theta))$ and θ is the solar zenith angle and $\hat{M}$ is a modified cloud condensate content. At a given level it is defined as:

$$\hat{M} = f_{max}^{-1} \int_{z}^{z_{top}} q_c(z\prime)f(z\prime)\mathrm{d}z\prime$$

where z_{top} is the top model level and f_{max} is the maximum cloud cover in the column. The parameters b_{10} and b_{13} depends on the effective cloud droplet radius, which is defined in equation 5.5 for water clouds and in [169] for ice clouds. For the shortwave they are defined as:

$$b_{10} = b_{10a}r_{eff} + b_{10b}$$
$$b_{13} = b_{13a}r_{eff} + b_{13b}$$

where b_{10a}, b_{10b}, b_{13a} and b_{13b} are constants. The values of all the b-parameters in equations 5.6 and 5.7 can be found in appendix 2. Hence, the same approach as for the second indirect effect may be followed and the natural background cloud droplet number concentration may be perturbed by the anthropogenic fraction, while keeping q_c unchanged. This will lead to a decrease in the cloud droplet effective radius and a corresponding decrease in $\hat{A}$ and $\hat{T}$ and an increase in the reflected fraction of the incoming shortwave radiation, i.e. a whitening of the cloud [243].

Deposition mechanisms

Dry deposition refers to the processes by which gases and aerosols are removed from the atmosphere, in the absence of precipitation, at the atmosphere - surface interfaces (such as canopy, leafs, trees, water surfaces, grass surfaces etc.). Wet deposition refers to the processes by which gases and aerosols are removed from the atmosphere due to precipitation release. Below-cloud scavenging is the process whereby ambient gases and aerosols receding below cloud base are

removed by rain or snow fall while in-cloud scavenging is the processes by which gases and aerosols receding inside the cloudy environments are removed. Both dry and wet deposition is known to be of importance when modeling the distribution of aerosol and chemical species and therefore their effects must be accounted for in the model.

Dry deposition

There are two aspects which must be considered when modeling dry deposition; the transport of the aerosols or gases from the atmosphere to the reacting surface and the interaction with the surface. The small scale transport from the near surface environment to the surface can conceptually be viewed as occurring in two steps. During step one the particles are transported from the atmosphere across the surface layer and into the laminar sub-layer[1]. The governing processes are vertical mixing and gravitational settling. Step two accounts for transport across the laminar sub-layer onto the surface. Brownian diffusion and gravitational settling are governing processes but also phoretic effects, impaction and interception are relevant in this region. Once at the surface species specific interactions may take place. The dry deposition velocity is defined as:
$v_d^i(x, y, t) = -F_i(x, y, t)/\psi_i(x, y, z = z_r, t)$ where F_i is the flux of species i from the atmosphere to the surface (downward flux is defined to be negative) at position x, y with $z = z_r$ a reference height, taken to be the lowest full model level and t a time variable. Defined in this manner parameterizations of v_d^i will yield the requested flux. Following [236] v_d^i is parameterized using an an electrical analog; the resistance approach. The dry deposition velocity may then be written as $v_d^i = 1/r_{total}^i$ where r_{total}^i is the total resistance of species i to dry deposition. This parameterization is convenient because the total resistance may be split into component resistances, representing different parts of the atmosphere, which are coupled in series. By coupling the resistances in parallel, mass transport can occur through parallel paths, such as through plant stomata and leaf surfaces.

The dry deposition flux to the surface provides the lower boundary condition for the vertical diffusion of gases and aerosol number and mass concentration (zero'th and third moment of the size distribution). Deposition is done in each aerosol size mode separately (see aerosol section below) using the deposition velocity for the mass concentration as described below and using the geometric mean radius of each aerosol mode as the aerosol size. Considering the fluxes of aerosols through each of the layers one may derive an expression for r_{total}, where i is now omitted, since, aerosol species are only distinguished by their size, it follows:

$$v_d = \frac{1}{r_{total}} = (r_a + r_b + r_a r_b v_g)^{-1} + v_g$$

Hence, the deposition velocity of the aerosols may be viewed as the reciprocal of three resistances in series and one in parallel. In this expression r_a is termed the aerodynamic resistance describing the turbulent transfer of particles to the laminar sub-layer, r_b is the resistance to Brownian diffusion across the laminar sub-layer, $r_a r_b v_g$ is an artifact of the equation manipulation and v_g is the gravitational settling velocity.

Gravitational settling, v_g, is calculated according to the size of the aerosols using Stoke's law in the laminar regime or an iterative procedure in the intermediate or turbulent regime [162]. The Cunningham correction factor accounts for non-continuum effects, while parameterizations of r_a and r_b follows [236, 248] and is generally dependent on atmospheric stability, land-use, friction velocity, wind speed, kinematic viscosity and Brownian diffusivity. For gas-phase species $v_g = 0$ and the term $r_a r_b v_g$ is replaced by r_s which describes the surface resistance due to direct

---

[1]here the laminar sub-layer describes the lowest part of the surface layer, starting a few centimeters above the surface, where molecular transport dominates turbulent fluxes

species-surface interaction, this term is zero for aerosols since they are assumed to stick to the ground once impacted. Resuspension of aerosols could be implemented by adjusting this parameter, but this has not been included in the present version of the model. The resistance should represent the major serial and parallel deposition pathways. Over land these include the stomata and mesophylic pathways into active plants (r_{plant}), the canopy pathway (r_{canopy}) and the pathway directly into the ground (r_{ground}), therefore:

$$r_s = \frac{1}{r_{plant} + r_{canopy} + r_{ground}}$$

The resistance of deposition in plants is considered to consist of two parallel pathways, represented by the stomatal and mesophylic resistances (r_{st} and r_m respectively), so that $r_{plant} = 1/(r_{st} + r_m)$. The canopy resistance is splitted into the upper canopy (r_{uc}) and the lower canopy which includes two parallel paths, the resistance to buoyant convection (r_{dc}) and the resistance to uptake in leaves, twigs and other exposed surfaces (r_{cl}). For the canopy $r_{canopy} = 1/r_{up} + 1/(r_{dc} + r_{cl})$ is used. The ground resistance comprises two parallel paths, a transfer resistance due to processes which is only dependent on canopy height (r_{ac}) and a resistance against uptake in soil, leaf litter, etc. on the ground (r_{gs}). The ground resistance may then be written $r_{ground} = 1/(r_{ac} + r_{gs})$. Following [236] these resistances are typically dependent on season and land-use and in Enviro-HIRLAM they are adjusted for solar insolation and surface wetness. Following [204] the surface resistance over water is given as:

$$r_s = \frac{1}{3.9 \times 10^{-5} H T_s u^*}$$

where T_s is the surface temperature, H is the effective Henry's law constant and u^* is the friction velocity.

Wet deposition

Wet deposition processes are parameterized via the scavenging coefficient $\Lambda^i(x, y, z, t)$:

$$\frac{\partial \psi_i}{\partial t} = -\Lambda^i \psi_i$$

and is carried out for gases and in each aerosol mode separately, using corresponding species dependent scavenging coefficients. Dissolution of gases in aqueous aerosols, involves the iteration of a thermodynamic equilibrium between gases and aerosol water as is described in the aerosol section below. In-cloud and below-cloud scavenging of aerosols by rain is dependent on the aerosol radius and rain rate and follows the extensions in [9]:

$$\Lambda = \alpha_0 q^{0.79}, \qquad\qquad\qquad\qquad\qquad r \leq 1.4 \ \mu m$$
$$\Lambda = (\beta_0 + \beta_1 r + \beta_2 r^2 + \beta_3 r^3)(\alpha_1 q + \alpha_2 q^2), \ \ 1.4 \ \mu m \ < \ r \ < \ 10 \ \mu m$$
$$\Lambda = \alpha_1 q + \alpha_2 q^2, \qquad\qquad\qquad\qquad\qquad r \geq 10 \ \mu m$$

Here $\alpha_0 = 8.4 \ 10^{-5}$, $\alpha_1 = 2.7 \ 10^{-4}$, $\alpha_2 = -3.618 \ 10^{-6}$, $\beta_0 = -0.1483$, $\beta_1 = 0.3220133$, $\beta_2 = -3.0062 \ 10 - 2$, $\beta_3 = 9.34458 \ 10^{-4}$. Rain-out of aerosols in the stratiform case may be simulated as above for $1.4 \ \mu m \ < \ r \ < \ 10 \ \mu m$ and in the convective case $\Lambda = \alpha_3 q^{0.79}$, with $\alpha_3 = 3.36 \ 10^{-4}$. Snow scavenging below cloud base and scavenging between cloud top and cloud base follows [145] $\Lambda = \alpha q^\beta$, with $\alpha = 3.36 \ 10^{-4}$ and $\beta = 0.79$ in the convective case and $\alpha = 8.0 \ 10^{-5}$ and $\beta = 0.305$ in the stratiform case.

For gases there are two main mechanisms regarding the scavenging of ambient gases; they may be removed by uptake in falling precipitation (both in-cloud and below-cloud) and they may be removed by dissolution in cloud water which is sub-subsequently scavenged by precipitation (in-cloud). The parameterization of Λ for these processes follows [205]. Assuming that the ambient gases are ideal and that a steady-state equilibrium exists between the gaseous and aqueous phases in cloudy grid-boxes, the fraction of dissolved gas is given by: $\psi_i^{aq}/\psi_i^{gas} = H_i$, where H_i is the Henry's law constant adjusted for temperature, ψ_i^{aq} the aqueous phase concentration (dissolved in cloud water) and ψ_i^{gas} the remaining gaseous concentration. The temperature dependence of the Henry's law constant may be expressed as: $H_i = k_i RT \exp[A(1/T_0 - 1/T)]$ where k_i (M/atm) is the Henry's law constant for species i, T (K) is temperature, $T_0 = 298K$, R is the ideal gas constant and A (K) is the temperature dependency factor.

Considering the scavenging of gases by rain, the residence time of a rain drop in a given gird-box is to short to establish an equilibrium between the ambient gases and the rain water, therefore, the transfer of gas into the rain water must be calculated explicitly. The rate of transfer of a gas to a drop of water is given as $W = K_c(H_i \psi_i^{gas} - \psi_i^{aq})$, where K_c the mass transfer coefficient [?]SP), is defined as:

$$K_c = \frac{D_g}{d_d}\left[2 + 0.6\left(\frac{v_d D_d}{\nu}\right)^{1/2}\left(\frac{\nu}{D_g}\right)^{1/3}\right]$$

where D_g and ν are the gas and air molecular diffusivity, v_d is the drop fall speed and d_d is the drop diameter. The drop diameter and fall speed may be related to rain rate $q(x, y, z)$ (mm/hr) via $d_d = 9 \cdot 10^{-4} q^{0.21}$ and $v_d = 3100 \ d_d$ [203, 205]. The tendency of ψ_i^{aq} may be represented by the mass balance:

$$\frac{1}{6}\pi d_d^3 \frac{d\psi_i^{aq}}{dt} = \pi d_d^2 W$$

Assuming that the ambient gas concentration, pH and rain drop size are constant throughout a model layer of height Δz (m) and that $\psi_i^{aq,0}$ is the aqueous concentration at the top of the layer, the mass m_i^{aq} scavenged by a drop falling through the layer becomes:

$$m_i^{aq} = \frac{1}{6}\pi d_d^3 (H_i \psi_i^{gas} - \psi_i^{aq,0})\left[1 - \exp\left(\frac{6K_c \Delta z}{d_d v_d H_i}\right)\right]$$

after integration over z. The rain drop number concentration, $N_d \ [m^{-3}]$ may be parameterized in terms of precipitation rate:

$$N_d = \frac{2.8 \cdot 10^{-7} q}{\pi d_d^3 v_d/6}$$

Multiplying m_i^{aq} by N_d and dividing by the ambient gas concentration ψ_i and the time it takes for the drops to fall through Δz yields the scavenging rate of in-cloud ambient gases due to uptake in falling

rain: following [205] the scavenging coefficient for in-cloud scavenging of ambient gases becomes:

$$\Lambda_i^{g,in}(x,y,z) = \frac{2.8 \cdot 10^{-7} q}{\psi_i \Delta z}(H_i \psi_i^{gas} - \psi_i^{aq,0})\left[1 - \exp\left(\frac{6K_c \Delta z}{d_d v_d H_i}\right)\right]$$

where Δz is the layer thickness, $\psi_i^{aq,0}$ is the aqueous concentration at the top of the model layer under consideration, d_d is the rain drop diameter and v_d is the fall speed. The drop diameter and fall speed are related to q using the parameterization by [203]. Similarly, the scavenging rate due to uptake of ambient gases in rain below cloud base becomes:

$$\Lambda_i^{g,below}(x,y,z) = \frac{2.8 \cdot 10^{-7} q}{\psi_i \Delta z}(H_i \psi_i - \psi_i^{aq,0})\left[1 - \exp\left(\frac{6K_c \Delta z}{d_d v_d H_i}\right)\right]$$

so that all the ambient gas is affected by the falling rain.

The fraction of the gases dissolved in cloud water may be scavenged by collection of cloud droplets by falling rain drops. A falling rain drop sweeps a volume $V = (d_d + d_c)^2 v_d \pi/4$ where d_c is the cloud droplet diameter. Assuming $d_d >> d_c$ the number of droplets inside V may be found as $d_d^2 v_d N_d \pi/4$ and assuming a collection efficiency $E = 0.9$ [205] and multiplying by the aqueous to ambient concentration ratio, the scavenging coefficient becomes:

$$\Lambda_i^{l,in} = 4.2 \cdot 10^{-7}\frac{Eq\psi_i^{aq}L_c}{\psi_i \rho_w d_d}$$

where L_c is the cloud water content and ρ_w is the water density. The total in-cloud scavenging of ambient gases then becomes $\Lambda_i^{in,tot} = \Lambda_i^{g,in} + \Lambda_i^{l,in}$

Chemical mechanisms

The NPW-Chem mechanism was developed at DMI for usage in online coupled models, where the number of species may be a limiting factor due to memory and cpu-time consumption. Hence, the philosophy has been to develop a scheme that describes the basic chemistry of volatile organic compounds (VOCs) photo-oxidation, nitrogen oxides, ozone and sulfur while using as few species as possible. These reactions have been chosen because of their importance in aerosol formation and as air pollutants. The organic chemistry has been significantly reduced, compared to other schemes such as RACM [213] or SAPRC-07 [34], and VOC emissions are described by only HCHO and a lumped variable HC representing all remaining organics.

The quasi steady state approximation (QSSA) is used for solving the chemical equations [86]. Consider the equation describing the evolution of the concentration field, ψ_i, of some species i:

$$\frac{d\psi_i}{dt} = P_i(t) - L_i(t)\psi_i \tag{5.8}$$

where P and L are the production and loss terms and all variables depend on their spatial indices (not shown in the equation). Assuming that each equation in 5.8 are independent and following it is found that for $\Delta t L > 10$, i.e. the lifetime of the species is smaller than the time step, the steady state solution ($d\psi_i/dt = 0$) may be used. In this case:

$$\psi_i(t+1) = P_i(t)/L_i(t) \tag{5.9}$$

Using a first order forward Euler algorithm, the solution to equation 5.8 becomes:

$$\psi_i(t + \Delta t) = \psi_i(t) + \Delta t(P_i - L_i\psi_i(t)) \tag{5.10}$$

Table 5.3: Gas-phase chemical reactions in NWP-Chem.

Reaction type	Reaction
Photolysis	
1	$NO_2 + hv \rightarrow O(^3P) + NO$
2	$O_3 + hv \rightarrow O(^1D) + O_2$
3	$HCHO + hv \rightarrow 2\,HO_2 + CO$
4	$HCHO + hv \rightarrow H_2 + CO$
Inorganic	
5	$O(^3P) + O_2 \rightarrow O_3$
6	$O(^1D) + N_2 \rightarrow O(^3P) + N_2$
	$O(^1D) + O_2 \rightarrow O(^3P) + O_2$
7	$O(^1D) + H_2O \rightarrow HO + HO$
8	$HO_2 + NO \rightarrow NO_2 + HO$
9	$O_3 + NO \rightarrow NO_2 + O_2$
10	$CO + HO \rightarrow HO_2 + CO_2$
11	$HO + NO_2 \rightarrow HNO_3$
12	$HO_2 + HO_2 \rightarrow H_2O_2 + O_2$
13	$HO_2 + HO_2 + H_2O \rightarrow H_2O_2 + H_2O + O_2$
Organic	
14	$HC + HO \rightarrow RO_2 + H_2O$
15	$RO_2 + NO \rightarrow HCHO + HO_2 + NO_2$
16	$HCHO + HO \rightarrow HO_2 + CO + H_2O$
17	$RO_2 + HO_2 \rightarrow ROOH + O_2$
18	$RO_2 + RO_2 \rightarrow prod$
Sulfur	
19	$HO + SO_2 \rightarrow H_2SO_4 + HO_2$

This algorithm is stable for $\Delta t L_i < 0.01$. For $0.01 < \Delta t L_i < 10$ is is assumed that P_i and L_i are constant over the time step equation 5.8 reduces to a first order ordinary differential equation with constant coefficients which may be solved analytically:

$$\psi_i(t + \Delta t) = P_i/L_i + (\psi_i(t) - P_i(t)/L_i(t))\exp(-L_i(t)\Delta t) \qquad (5.11)$$

In order to increase accuracy for species in instantaneous equilibrium with other species (such as HO and HO_2) five iterations are performed in each time step. The concentration of the radicals HO, $O(^1D)$ and $O(^3P)$ is always low and they are assumed to be in steady state and equation 5.9 is used. The chemical mass imbalance is reduced to avoid time steps which are too small, by introducing the following lumpings [86, 78]: $[O_3NO]=[O_3]-[NO]$, where the square brackets indicate a concentration and $[NO_x] = [NO] + [NO_2]$. The lumping species are solved for using equation 5.10 and 5.11. The concentration of O_3, NO and NO_2 are then estimated as follows. [NO] is found using equation 5.11 and if $[O_3] > [NO]$ it is found that $[O_3](t + \Delta t) = [O_3NO](t + \Delta t) + [NO](t + \Delta t)$. For $[O_3] < [NO]$, $[O_3]$ is calculated according to equation 5.11 and NO follows from $[NO](t + \Delta t)$ $= [O_3](t + \Delta t) - [O_3NO](t + \Delta t)$. The NO_2 concentration is calculated according to: $[NO_2](t + \Delta t)=[NO_x](t + \Delta t)-[NO](t + \Delta t)$.

Aerosol dynamics

The default aerosol module in Enviro-HIRLAM has been taken from the CAC (Cloud-Aerosol-Chemistry)-model [77], used for operational ozone forecasting at DMI. It is based on the modal description of the particle distributions as developed by (Whitby and McMurry, 1998). The aerosols are divided into three size modes, the nuclei mode (i) consisting of aerosols generated by nucleation (typical diameter 0.01 μm), the accumulation mode (j) consisting of aged aerosol and cloud condensation nuclei (typical diameter 0.1 μm), and the mechanically generated coarse mode (c) (typical diameter 10μ m). The definition of the k'th moment, M_k, of the distribution is:

$$M_k = \int d^k n(\ln d) d(\ln d)$$

where n is the aerosol size distribution and d is the aerosol diameter. Following [238] it is assumed that the size distribution in each mode is log-normal:

$$n(\ln d) = \frac{N}{\sqrt{2\pi}\ln\sigma_g}\exp\left[-\frac{1}{2}\left(\frac{\ln\frac{d}{d_g}}{\ln\sigma_g}\right)^2\right]$$

where N is the number concentration, d_g is the geometric mean diameter and σ_g is the geometric mean standard deviation for the modes. This assumption closes the equations and the k'th moment of each mode may be written:

$$M_k = Nd_g^k\exp\left(\frac{k^2}{2}\ln^2\sigma_g\right)$$

M_0 represents the total number concentration in a given mode, M_2 is proportional to the total aerosol surface area and M_3 is proportional to the total aerosol volume and therefore to the total aerosol mass concentration. Assuming that σ_g is constant in time, prediction of two moments, M_0 and M_3, allows the number and mass concentration as well as geometric mean diameter to be diagnosed. Hence, in this model formulation it is sufficient to advect the M_0 and M_3 modes. The model may now be formulated in terms of the effect of the aerosol dynamical processes on the moments of the size distribution. For accumulation mode the rate of change for the k'th moment becomes:

$$\frac{\partial M_{kj}}{\partial t} = G_{kj} - C_{kjj} + C_{kij} + E_{kj}$$

where G_{kj} is the condensation growth term, C_{kjj} represents the moment loss due to intra-mode coagulation, C_{kij} is the gain in moment due to inter-mode coagulation and E_{kj} represents primarily emitted accumulation mode aerosols. A similar equation governs the rate of change of the k'th moment in nuclei mode:

$$\frac{\partial M_{ki}}{\partial t} = \dot{M}_{ki} + G_{ki} - C_{kii} - C_{kij} + E_{ki}$$

where $\dot{M}_{ki}$ is the production rate of the k'th moment due to nucleation. For the coarse mode it si found:

$$\frac{\partial M_{kc}}{\partial t} = E_{kc}$$

Under the assumption of log-normal size distributions analytical expressions may be found for the terms on the right hand side of the above equations and we can solve for the evolution of the number concentration and mass concentration for each mode. Advection, convection, diffusion and deposition of these modes proceeds as explained in the previous sections.

Emissions of sulfate aerosols are estimated from the GEMS-TNO inventory from PM2.5 and PM10; as an example table 5.4 shows the relative distribution of sulfate in PM10 and PM2.5. The

Table 5.4: Example of composition of particulate matter.

SNAP code	PM10 Sulfate percentage[a]	PM2.5 Sulfate percentage
1	10	15
2	2	2
3	7	10
4	2	3
5	0	0
6	0	0
7	1	1
8	2	3
9	0	0
10	0	0

[a]Mass percentage of sulfate in PM10 and PM2.5 aerosols for each SNAP code; see table 5.2 for an explanation of the SNAP codes.

contribution to the zero'th ($k = 0$) and third ($k = 3$) mode then follows from:

$$E_{3n} = \frac{6}{\pi} \frac{E_n}{\rho_n}$$

$$E_0 = \frac{\sum_n E_{3n}}{d_g^3 \exp(\frac{-9}{2}\ln^2 \sigma_g)}$$

where E_n denotes the emission rate of aerosol species n.

Homogeneous nucleation follows [123] and both nucleation and accumulation mode aerosols may grow by condensation thereby affecting mass concentration. A general expression for G_{kj} is given as:

$$G_{kj} = \nabla \cdot \int_0^\infty d^k \nabla n_j(d) dd$$

For H_2SO_4-H_2O aerosols the water mole fraction (χ), in a given mode, follows [239]:

$$\chi_j = \frac{\chi_{par}}{1 + d_{par}/d_{g,j}}$$

where d_{par} represents a critical diameter at which the Kelvin effect becomes substantial and χ_{par} is a limiting value for large particles. The two parameters are found by fitting to experimental values and depends on relative humidity (see [239] for values).

Coagulation of aerosol particles is also accounted for and is expected to be particularly important for low humidity and low geometric mean diameter. Following [238] the inter and intra-mode coagulation terms for accumulation mode may be expressed as:

$$
\begin{aligned}
C_{kij} &= \int_0^\infty \int_0^\infty (d_1^3 + d_2^3)^{\frac{k}{3}} \beta(d_1, d_2) n_i(d_1) n_j(d_2) dd_1 dd_2 \\
&\quad - \int_0^\infty \int_0^\infty d_2^k \beta(d_1, d_2) n_i(d_1) n_j(d_2) dd_1 dd_2 \\
C_{kjj} &= \frac{1}{2} \int_0^\infty \int_0^\infty (d_1^3 + d_2^3)^{\frac{k}{3}} \beta(d_1, d_2) n_j(d_1) n_j(d_2) dd_1 dd_2 \\
&\quad - \int_0^\infty \int_0^\infty d_1^k \beta(d_1, d_2) n_j(d_1) n_j(d_2) dd_1 dd_2
\end{aligned}
$$

where β is the Brownian coagulator kernel (equation 5.1). Using the log-normal size distribution, as defined above, the integrals reduce to:

$$
\begin{aligned}
C_{kij} &= N_i N_j F_{kij} \\
C_{kjj} &= N_j^2 F_{kjj}
\end{aligned}
$$

where F_{kij} and F_{kjj} depends only on d_g and σ_g for the accumulation mode. The equation describing the time evolution of N_j may then be written:

$$
\frac{\partial N_j}{\partial t} = E_0 - N_j^2 F_{0jj} \tag{5.12}
$$

where E_0 refers to the emission into accumulation mode. The solution to this logistics type equation for $E_0 \neq 0$ is:

$$
N_j(t) = \frac{\alpha(1 - \gamma \exp(2\alpha t))}{F_{0jj}(1 + \gamma \exp(2\alpha t))}
$$

where $\alpha = \sqrt{F_{0jj} E_0}$ and $\gamma = (\alpha - F_{0jj} N_j(t_0))/(\alpha + F_{0jj} N_j(t_0))$. For $E_0 = 0$ the solution reduces to:

$$
N_j(t) = \frac{N_j(t_0)}{1 + F_{0jj} N_j(t_0) t}
$$

Similar equations may be derived for the nuclei mode, where an additional production term must be included in the tendency equation for N_i in order to account for nucleation and a loss term must be added due to inter-mode coagulation:

$$
\frac{\partial N_i}{\partial t} = E_0' - N_i^2 F_{0ii} - N_j N_i F_{0ij}
$$

where E_0' represents primary and secondary production of nucleation mode particles. Since, the derivation of the solution in nucleation mode is almost identical, the formulation is not described here. Note that a production term due to inter-mode coagulation is not accounted for in equation 5.12, due to the general assumption that the coagulation of a small and a large particle leads to loss of a small particle, but not to a gain of a large particle, i.e. the large particle already existed. There is, however, a transfer of mass from nuclei to accumulation mode and the tendency equation for the mass concentration (ϕ) in nucleation and accumulation mode becomes:

$$
\begin{aligned}
\frac{\partial \phi_i}{\partial t} &= P_i - L\phi_i \\
\frac{\partial \phi_j}{\partial t} &= P_j + L\phi
\end{aligned}
$$

where P_i is a production term due to emission, nucleation and condensation, P_j is a production term accounting for emission and condensation and $L = N_i N_j F_{3ij}/M_{3i}$ describes the transfer of mass due to inter-mode coagulation. Holding the coefficients constant for a time step and using an Eulerian forward step the solution becomes:

$$
\phi(t) = \frac{P}{L} + \left(\phi(t_0) - \frac{P}{L}\right) \exp(-Lt)
$$

Table 5.5: Gas-aerosol equilibrium reactions included in Enviro-HIRLAM.

Number	Reaction
1	$SO_2(g) \rightleftharpoons SO_2(aq)$
2	$SO_2(aq) + H_2O(aq) \rightleftharpoons HSO_3^- + H^+$
3	$HSO_3^- \rightleftharpoons SO_3^{2-} + H^+$
4	$H_2SO_4(aq) \rightleftharpoons HSO_4^- + H^+$
5	$HSO_4^- \rightleftharpoons SO_4^{2-} + H^+$
6	$NH_3(g) \rightleftharpoons NH_3(aq)$
7	$NH_3(aq) + H_2O(aq) \rightleftharpoons NH_4^+ + HO^-$
8	$HNO_3(g) \rightleftharpoons HNO_3(aq)$
9	$HNO_3(aq) \rightleftharpoons NO_3^- + H^+$
10	$NH_4NO_3(s) \rightleftharpoons NH_4^+ + NO_3^-$
11	$(NH4)_2SO_4(s) \rightleftharpoons 2\,NH_4^+ + SO_4^{2-}$

Aerosol thermodynamic equilibrium

Many gas-phase species are water soluble and sulphate and ammonia together with water take part in binary/ternary nucleation. In order to consider these processes a simplified liquid-phase equilibrium mechanism, with the most basic equilibria, is included in NWP-Chem. At present this equilibrium module is solved using the analytical equilibrium iteration (AEI) method [98]. The reactions are summarized in table 5.5 (equilibria containing anthropogenic organic compounds is planned to be included in the furture).

The thermodynamic equilibrium between gases and aerosols must be solved iteratively and poses a potential problem for online models, since the convergence cannot always be guaranteed within a reasonable amount of time. The AEI method is designed to eliminate iterations of the individual equilibria (table 5.5), but not among all the reactions. The solutions found by this scheme are identical, to within several decimal places, to those found by methods where all iterations are accounted for, such as the mass flux iteration method [98], however, the AEI method is significantly faster. To illustrate the solution method consider a reaction of the form: $D(gas) \rightleftharpoons A(aq)$ and let ψ_D and ψ_A denote the concentrations (mol cm$_{air}^{-3}$) in the gas and liquid phase respectively. Assuming equilibrium an equilibrium constant K_r may be defined as:

$$\frac{\psi_A}{\psi_D} = \frac{\psi_{A,0} + \Delta X_{fin}}{\psi_{D,0} - \Delta X_{fin}} = K_r$$

where the subscript 0 indicates initial values and K_r is in mol mol^{-1}, i.e. a fraction of compound D is moved to the liquid phase. Solving this equation one finds: $\Delta x_{fin} = (C_{D,0}K_r - C_{A,0})/(1 + K_r)$ which is then substituted into the above equation to obtain the converged solution. For this type of reaction the K_r is defined as: $K_r = m_A c_w M_w RT/p_D$ where c_w and M_w are the aerosol liquid water content and molecular weight of water respectively, R is the gas constant, T is temperature, p_D is the vapor pressure of compound D and m_A is the molality of compound A. For a series of reactions ΔX_{fin} is found for the first reaction and used as input for the next etc. at the end the convergence criteria, that the percentwise change in species concentration is less than 0.001% is checked, if it is not fulfilled the iteration procedure is carried out again.

Initial and boundary values

Initial and boundary conditions for the meteorological fields have already been described, this chapter contains a description of the initial and boundary values for chemical and aerosol fields. Since detailed information about the vertical profiles of all the chemical species are not readily available, Enviro-HIRLAM uses idealized climatological profiles for initialization if measurement data is not available. Following the procedure in WRF-CHEM the initial profiles for NO_x and HNO_3 is taken from the NALROM chemistry model [172], for clean northern hemisphere mid-latitude conditions, while the profiles for O_3 and SO_2 are measurement based, taken from the New England Air Quality Experiment [117] (figure 5.3). For the rest of the species climatological values along with a latitudinal, land-use and temporally dependent formulation from [78]. Aerosol number and mass concentration in nuclei and accumulation mode is taken from the climatological values in [205]. Following [97] the number and mass concentrations in each mode decays exponentially upwards so that a 20'th of the surface value is reached around 850 hPa.
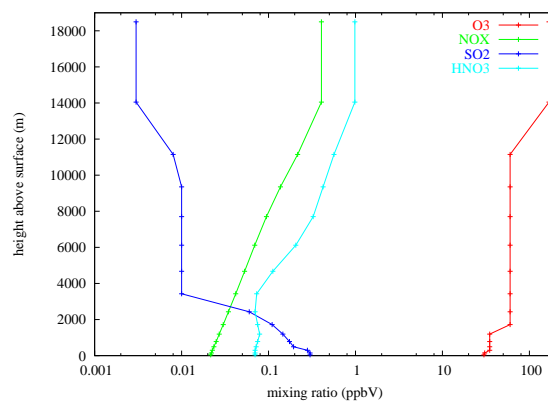

Figure 5.3: Initial vertical profiles for NO_x, HNO_3, SO_2 and O_3, from the NALROM chemistry model and the New england Air Quality Experiment, currently used in ENviro-HIRLAM.

In the simulations presented in this thesis inflow across the lateral boundaries was neglected, however, in a routine production environment the inflow would be generated by an outer nesting and treated as the meteorological fields during the boundary preprocessing. In the boundary zone the fields are relaxed towards the imposed field. In the absence of an imposed field they are relaxed towards a clean background as specified by the initial conditions. The surface boundary conditions are specified in the vertical diffusion routine and depends on the dry deposition flux of a given species as well as the emission strength of that species:

$$\left(v_d\psi - k_\psi \frac{\partial \psi}{\partial t} \right)_{z=klev} = E$$

where E is the emission rate of the species and $klev$ represents the lowest model layer. In the top of the atmosphere, which is at approximately 10 hPa the boundary condition becomes reflecting:

$$k_\psi \left(\frac{\partial \psi}{\partial t} \right)_{z=1} = 0$$

where $z = 1$ represents the upper most full model level. This condition is not believed to be of relevance, since the troposphere is far removed from this boundary.

Spin-up

Spin-up refers to the time it takes before the meteorological or chemical fields become independent of the initial conditions. It is basically the time it takes for a signal on the boundary to traverse the

domain. Hence, the spin-up time may be estimated as: $\Delta x/u_{max}$, where u_{max} is a measure of the maximum wind speed in the x-direction, but the use of dampers and filters on the initial fields may shorten this period. The effect of the initial conditions in the total solution for, e.g. the concentration of a chemical species, decays exponentially in time [205], however, the decay constant (rate of decay) may vary substantially between different types of chemistry schemes. After the spin-up period the concentration values are mainly dependent on emissions, boundary conditions, transport and chemical transformations. The spin-up may, also be estimated from plots of the temporal development of a given field in various points, since the tendency in such a plot should be zero as an equilibrium is reached. Considering the spin-up of meteorological fields in a limited area model, the absolute value of the three-hourly domain averaged surface pressure tendency (NN):

$$ NN = \frac{1}{N_{max}} \sum_{n=1}^{N_{max}} \left| \frac{\partial p_s}{\partial t} \right| $$

where N_{max} is the total number of grid-points in the domain, is a basic measure of the high frequency noise, i.e. surface fields are not expected to vary at high frequency, in a simulation. For a well balanced field NN should be approximately 1 hPa/3h; figure 5.4 displays an example of a simulation, presented in chapter 5 (the reference simulation, denoted REF), that does not employ digital filtering initialization. In this case digital filtering could shorten the spin-up time substantially, a feature which is important when executing the short-range model in operational cycles. Since the digital filter is computationally heavy, i.e. takes up a substantial part of the total forecast time at any forecast length, and since chemical spin-up is longer, it has been switched off.
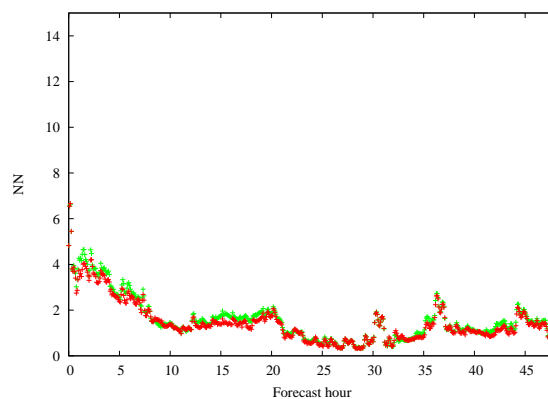

Figure 5.4: Domain averaged absolute change in surface pressure over three hours (NN) (hPa/3h) versus forecast hour for the reference run (green) and an identical run except it includes the first and second indirect effects. These results are discussed in chapter 5.

For meteorological fields the spin-up time is mainly established by transport processes in the atmosphere. When including chemistry in an online model these processes will also affect the spin-up time of the chemical and aerosol species, however, the reaction times are also of importance in reaching equilibrium between the chemical species. Therefore, the spin-up time of the combined system will depend on the reactions included in the chemical solver, i.e. slow reaction rates produces longer spin-up times than fast reactions. If the initial chemical state of the atmosphere is far from equilibrium, e.g. if all gas-phase species are initialized to zero (and emissions are included), the spin-up time may be several days and hence, much longer than for the pure meteorological fields. The thermodynamic equilibrium between aerosols and gases is essentially an iterative one and therefore the spin-up time may also be affected by the choice of convergence criteria in this solver. For online coupled models where chemical, aerosol and meteorological fields must reach a balanced state also through feedbacks the spin-up time may be even longer. In my experience with

Enviro-HIRLAM it is always found that the chemical spin-up is the limiting factor, because it is quite difficult to find a balanced initial state of the chemical species, i.e. there is a lack of measurements. As an example figure 5.5 displays the temporal development of NO_2 and O_3 on a station located close to a forest $(49, 54$ N, $4, 38$ S) where NO_2 emissions are small, for the simulations presented in chapter 5. The spin-up of ozone takes longer than NO_2, since, it is not an emitted species and depends on the equilibrium between many species. The spin-up time on the small domain (500 km $\times$ 400 km in $0.05°$ horizontal resolution) surrounding Paris is approximately 24 hours. Within this time the meteorological fields have easily reached a steady state and the chemical solver is therefore the bottleneck, regarding spin-up time. Figure 5.4 also shows that including the first and second indirect effects in the model does not lead to increased spin-up, i.e. does not introduce more noise in the model and the balance between the chemical fields is the bottleneck.
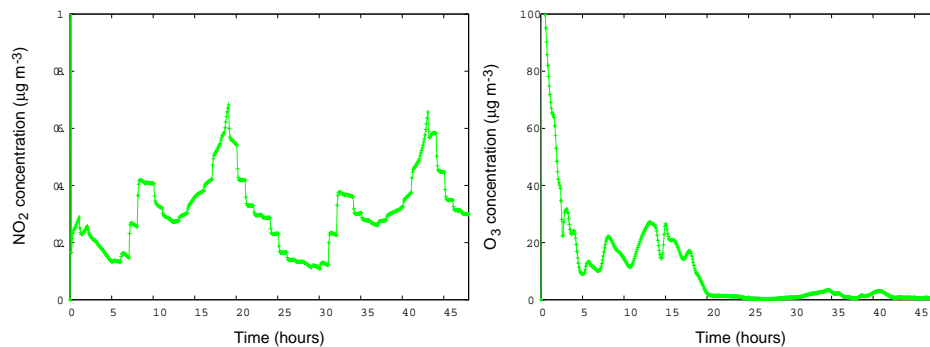

Figure 5.5: NO_2 (left) and O_3 (right) concentration (μg m^{-3}) versus forecast hour, starting 29 June 2005 at 00 UTC, on a station which experience only weak NO_2 emissions.

The choice of spin-up period should be based on the temporal development of species, in particular ozone at various stations in different environments (urban, forest, etc.) and should be repeated for each new simulation set-up.

Optimization

Enviro-HIRLAM is currently being executed on the NEC SX-6 supercomputer at DMI and the timings reported in this chapter refers to this computer. DMI has, however, acquired a new supercomputer, the CRAY-XT5, which has a different architecture, in the sense that it is not composed of vector processors, but of quadro-core scalar processors. Optimization for the XT5 has not yet commenced and will therefore not be described here. There are two main issues with regards to optimization for the NEC SX-6; the vectorization and parallelization of the code. HIRLAM was originally designed with one-dimensional long loops, facilitating good vector performance, however, parallelization required some restructering of the code structure. This issue is of minor importance now, due to the complexity of the SX6 FORTRAN compilers which very effectively optimize the code for vector processing.

The new code added in Enviro-HIRLAM has been made to complement the HIRLAM parallelization strategy and therefore a short account of this will be given here. The strategy is based on the single program multiple data programming paradigm, so that each processor performs all computations for only one subdomain. A two-dimensional latitude-longitude domain decomposition is used with subdomains consisting of contiguous vertical columns, extending from the surface to the top of the atmosphere. The NEC SX-6 architecture consists of eight nodes with eight vector processors on each node, hence, the system is distributed between the nodes and shared within the nodes. Therefore, inter-process communication is based on the message passing interface (MPI). MPI is implemented by using the General Communication package to assure portability. Inter-process communication is

not of importance in the physics part of the code, since there are no horizontal dependencies, however, it is of great importance in the dynamics. For explicit dynamics a halo size of one point is sufficient and the solution of the Helmholtz equation follows the outline given in the beginning of this chapter. The trajectory calculation in the semi-Lagrangian core requires a larger halo, dependent on the current wind speed, grid spacing and time step. It is currently fixed at five points. Fourth order horizontal diffusion is splitted into two second order operations each requiring a halo of one point.

At DMI an attempt has previously been made to use OpenMP within nodes and MPI between nodes for parallelization. The results, however, showed that the pure MPI strategy was more promising and therefore no OpenMP parallelization has been considered in Enviro-HIRLAM, an issue that might be re-addressed with the XT5. One advantage of using 0-dimensional models as parameterizations, such as with the NWP-Chem scheme in Enviro-HIRLAM, is that there are no horizontal dependencies and therefore the new parameterization fits easily into the HIRLAM parallelization strategy. The same may be said about the aerosol and deposition parameterizations, which have been made to fit the strategy, but not about the implementation of the Bott advection scheme. The version currently used in Enviro-HIRLAM is old and contains strong horizontal dependencies and therefore I implemented a quick-fix which solves the problem temporarily until the new dynamical core (LMCSL) is ready for implementation. The quick fix basically gathers all necessary fields on the master processor, executes advection and scatter the updated fields again. This solution hinders scalability and generally the model cannot take full account of the increased number of processors.

The implementations in Enviro-HIRLAM should also support other optimizations made for HIRLAM, in order to optimize performance. One example is the HIRLAM Grib file Server (HGS) which is a system which ensures asynchronious output. All input and output is kept in memory so that the model is free to proceed with model computations while output/input is being written/read to/from disk. Usually two processors are allocated to this task and it saves about 17% in total run time, i.e. it is important that Enviro-HIRLAM supports this feature.

Chemistry accounts for the largest bottleneck in run time and it is therefore of outmost importance to minimize the number of reactions and thereby the number of species, included in the scheme. NWP-Chem has been developed to optimize performance, with respect to run time and memory consumption, and employ as few species as possible. It is therefore especially suited for online modeling.

Summary and conclusions

Enviro-HIRLAM has been developed by consistently implementing descriptions of the following processes in HIRLAM: emissions, advection, turbulent mixing, horizontal diffusion, subgrid scale convective processes, gas-phase chemistry, aerosol-gas thermodynamic equilibrium, aerosol dynamics, dry and wet deposition of gases and aerosols and the first and second indirect effects. These processes has been chosen because of their importance in aerosol-cloud interactions, thereby, aiding in the fulfillment of the overall goal of this work. A schematic of the system is displayed in figure 5.6 and a partial call tree is displayed in appendix 3.
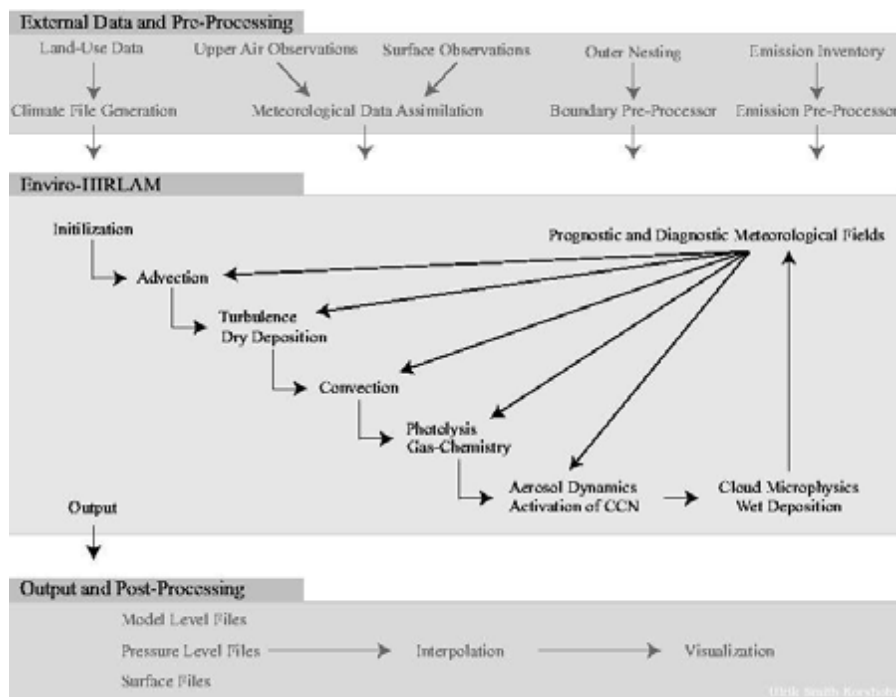
Figure 5.6: Overview of the Enviro-HIRLAM modeling system. Input and output is indicated and the inter-connection between the processes most important for chemistry, aerosols and indirect effects are displayed.

Testing the model

As described in chapter 2 it is of importance to test the reliability of the model components which have been implemented in order to identify errors in the implementation. The ability of the model to transport a passive tracer was tested by simulating the release made during the first European Tracer Experiment (ETEX-1), the ability of the model to deposit airborn material was tested by simulating the accidental release during the Chernobyl accident and the ability of the model to forecast concentrations of trace-gases was tested by simulating a typical pollution load episode. An additional test compared the effect of using an online model as compared to an offline model.

Statistical methodology

In order to calculate the level of agreement between modeled and observed concentration values it is necessary to apply appropriate statistics to the measured (M) and predicted (P) fields. The following statistical measures were computed: mean value, variance, normalized mean square error (NMSE), bias, fractional bias, correlation, figure of merit in time (FMT), fractional standard deviation, temporally integrated values and factor of exceedence (FOEX). In the following the main statistical measures, which follow [158] will be described in more detail. Some are temporal measures, i.e. the location is fixed and the temporal development of the measured and predicted fields are compared, while others are to be used for a global analysis, i.e. including all stations at all times.

The measurement data was filtered before use. Background values were subtracted so that only the pure tracer concentration was used. Measurements of zero concentration (concentrations below the background level) were included in time series to the extent that they lay between two non-zero measurements or within two before or two after a non-zero measurement. Hereby, spurious correlations between predicted and measured zero-values far away from the plume track were reduced.

Variance

The variance describes the degree to which a distribution spread out and is defined as:

$$\sigma_p = \frac{1}{N} \sum_i (P_i - \overline{P})^2$$

where N denotes the number of (P_i, M_i) pairs, i is a temporal index and $\overline{P}$ represents the average:

$$\overline{P} = \frac{1}{N} \sum_i P_i$$

The standard deviation is defined as the positive square root of the variance and a relative measure of the variance is given by the fractional standard deviation:

$$\text{FSTANDEV} = 2 \frac{\sigma_p^2 - \sigma_m^2}{\sigma_p^2 + \sigma_m^2}$$

If the variance of the measurements is well described by the predictions, FSTANDEV will be close to zero.

Normalized mean square error

The NMSE is a measure of the overall deviations between predicted and measured values and is calculated as a sum of absolute deviations:

$$\text{NMSE} = \frac{1}{N} \sum_i \frac{(\text{P}_i - \text{M}_i)^2}{\overline{\text{PM}}}$$

Bias

The bias is defined as the average difference between the (P_i, M_i) pairs and is a measure of the level of the general under-prediction or over-prediction by the model as compared to the observations:

$$BIAS = \frac{1}{N} \sum_i (\text{P}_i - \text{M}_i)$$

A corresponding relative value of the bias is given by the fractional bias:

$$\text{FBIAS} = 2\frac{\overline{P} - \overline{M}}{\overline{P} + \overline{M}}$$

If FBIAS is close to zero the model has only little bias.

Correlation

The linear correlation coefficient (R) is defined by:

$$R = \frac{\sum_i (\text{M}_i - \overline{\text{M}})(\text{P}_i - \overline{\text{P}})}{\sqrt{\sum_i (\text{M}_i - \overline{\text{M}})^2} \sqrt{\sum_i (\text{P}_i - \overline{\text{P}})^2}}$$

and if its calculation is based on log-transformed values it is given as:

$$R = \frac{\sum_i (\ln \text{M}_i - \overline{\ln \text{M}})(\ln \text{P}_i - \overline{\ln \text{P}})}{\sqrt{\sum_i (\ln \text{M}_i - \overline{\ln \text{M}})^2} \sqrt{\sum_i (\ln \text{P}_i - \overline{\ln \text{P}})^2}}$$

A value of 1 indicates complete positive correlation, i.e. all (P_i, M_i) pairs lies on a straight line with with slope 1 in a scatter diagram, a value of -1 indicates complete negative correlation while a value of 0 indicates no correlation. R is calculated on the basis of the logarithm of the concentration values due to the large range of the data values [158].

Integrated concentration

The integrated concentration, I, (also denoted dosage) is defined by:

$$\text{I(x)} = \sum_{j=1}^{N} \text{M}(\text{x}, \text{t}_j)(\text{t}_j - \text{t}_{j-1})$$

where x is a fixed location and t_j is a temporal index.

Figure of merit in time

For a fixed location, x, the FMT evaluates the overlapping concentration histogram normalized by the time series of the maximum concentration:

$$\text{FMT(x)} = 100\frac{\sum_j \min(\text{M}(\text{x,t}_j), \text{P}(\text{x,t}_j))}{\sum_j \max(\text{M}(\text{x,t}_j), \text{P}(\text{x,t}_j))}$$

If the FMT value is 100% then there is total overlap between the measurements and predictions and if FMT is 0% there is no overlap.

Figure of exceedence

The FOEX is defined by:

$$\text{FOEX} = 100\frac{\text{N}(\text{P}_i > \text{M}_i)}{\text{N} - 0.5}$$

where $\text{N}(\text{P}_i > \text{M}_i)$ is the number of points above the $45°$ line in a global scatter diagram. Hence, FOEX ranges from -50 to $+50$ and exposes the bias of the predictions. The FA2 and FA5 are connected to the FOEX and represent the percentage of predictions found within a factor of two and five above or below the measurements respectively.

Transport and dispersion

Parts of this chapter has been published as [120, 119].

Methodology

In order to test the ability of the model to transport and disperse an inert tracer gas, the ETEX-1 release of Perfluoro-Methyl-Cyclo-Hexane was simulated and output concentrations were compared to measurements taken during the ETEX-1 campaign. The release was carried out from a site in northern France (Brittany, $2.01°$ W and $48.06°$ N) eight meters above ground at a constant average rate of $7.95 \, \mathrm{g\,s^{-1}}$ during meteorological conditions producing only little dispersion, i.e. the plume did not break up due to dispersional effects [80]. It commenced on 23 October 1994 at 16:00 UTC and lasted 11 hours and 50 minutes. Measurement stations in northern and central Europe were employed in deriving the horizontal and temporal development of the plume (figure 6.1). During real-time and retrospective analysis (Atmospheric Transport Model Evaluation Study II (ATMES-II)) offline long range dispersion models were evaluated against the measurements [71, 158]. In order to facilitate comparison with the results of ATMES-II the statistical methodology applied in here corresponds to that used during the ETEX-1 model evaluation studies.
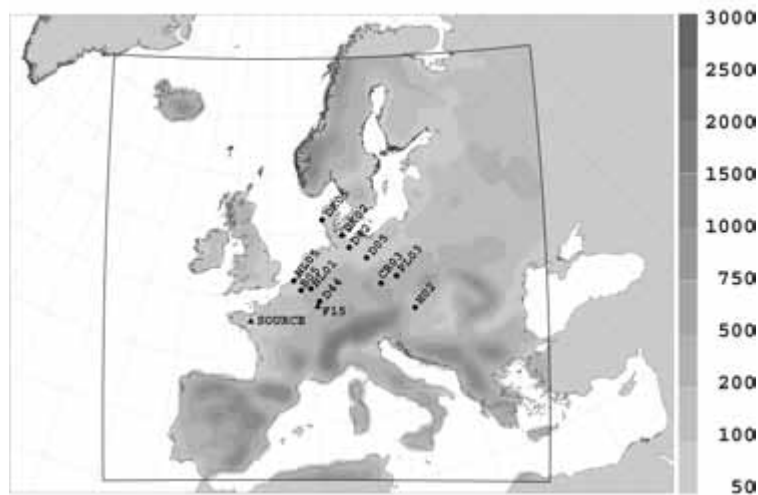

Figure 6.1: Area covered in simulations, displayed as surface geopotential height (meters). Positions of measurement stations (identified by the ETEX naming convention) referred to in the text along with the source point for the ETEX-1 release is also indicated.

Model set-up

All chemical, aerosol and deposition options were switched off, so that only emission, advection and vertical diffusion was active (horizontal diffusion was neglected). Point source emissions with a prescribed release rate was used. The nearest grid-point to the release site was ascribed the emissions, which was converted to mass concentration by division by the grid cell volume. The horizontal resolution was $0.40° \times 0.40°$ while there were 40 unequally spaced levels in the vertical, with the top level at 10 hPa. The model grid was rotated so that the north pole was located at $(0.0°E, 25.0° \, \mathrm{S})$ with a domain covering most of Europe (figure 6.1). Analysis and six-hourly boundaries were supplied by the European Center for Medium Range Weather Forecasts and digital filtering was used to initialize the model which used a time step of 10 minutes. The Analysis time was 23 October 1994 at 12:00 UTC, four hours before the start of the release, and the model was integrated out to 80 hours.
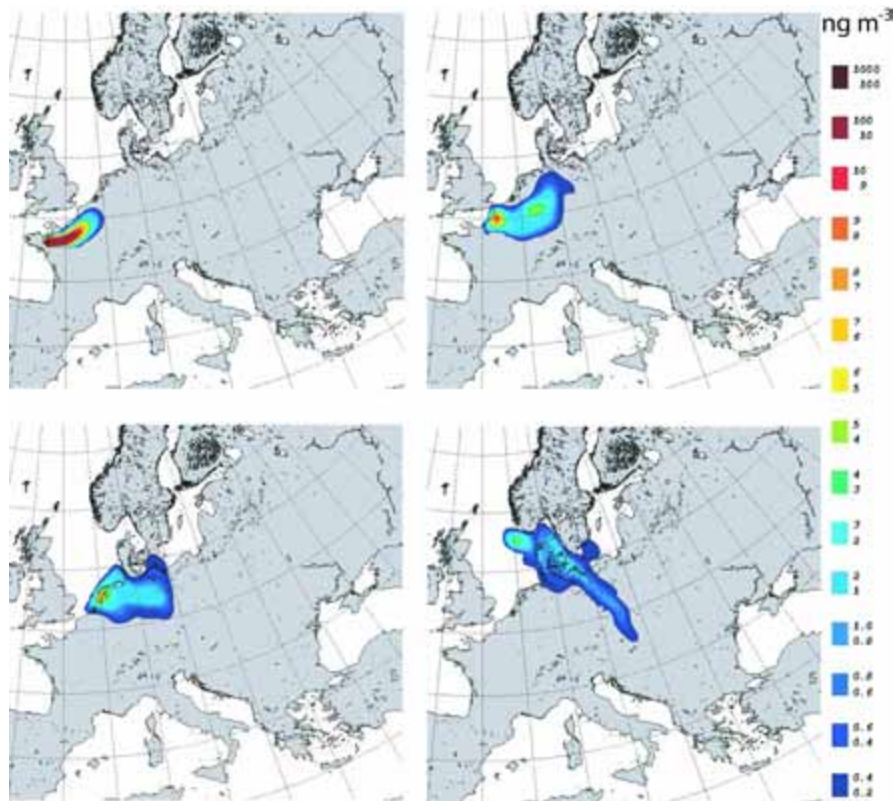
Figure 6.2: Tracer concentration (ng m^{-3}) at 12, 24, 36 and 48 hours after release (upper left to lower right) for the simulation of ETEX-1.

Results and discussion

The synoptic situation in the days following the ETEX-1 release has previously been described in detail [80, 71, 161] and represents a typical meteorological situation. On 24 October there is an unstable flow over the release area, and the presence of a deep low pressure system north of Scotland maintains south-westerly winds. On 25 October the wind speed decrease further due to the northerly movement of the low. Showers prevail over Holland due to the presence of a cold front. On 26 October the low is still present and winds change towards west-south-west while showers are still prevailing over the advection area. Correspondingly, the model plume was initially advected by the south-westerly flow, mainly influenced by synoptic-scale forcings, in a north-easterly direction. The spatial structure of the model plume resembled the observations (as compared to [158]) (figure 6.2) and the plume retained its continuity throughout the forecast period. After 36 hours the model plume had attained a U-shaped deformation receding over northern Germany. An identical deformation also exists in ETEX-1 simulations by other models and although less distinct, a similar structure is present in the observations [158]. The model, thus, over-predicted the development of the deformation, which extended further to the north. In line with the measurements the model plume was stretched and its axis tilted, so it was oriented in a north-west to south-east direction, after 48 hours. The peak concentration, however, was located too far to the north. After 60 hours the largest concentration values were still found in the North Sea, a feature which is also present in the observations.

The global statistics contain information from all stations at all times and thus represents a more general approach to the quality of the model. Table **??** displays the results of the global analysis. There are 20.8% of the predictions within a factor of two and 36.5% within a factor of five from the measurements. The low FOEX value indicates that predictions are nearly equally distributed around the measurements, which is also confirmed by the scatter diagram (figure 6.3). The bias and
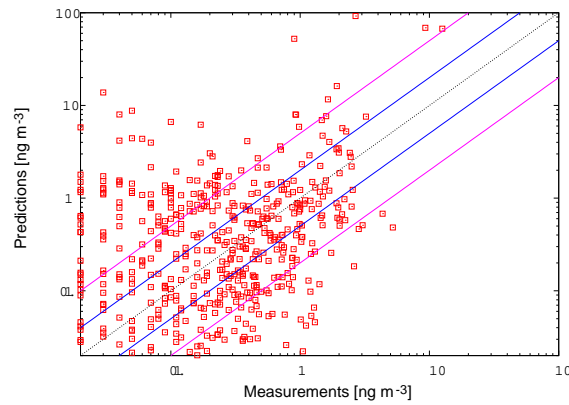
Figure 6.3: Global scatter diagram, along with factor of two (FA2) and factor of five (FA5) lines in blue and red respectively. The number of points is 1243 and FA2 $= 20.84\%$, FA5 $= 36.52\%$ and FOEX $= -0.93$

Table 6.1: Model ranking procedure used during the ETEX-1 real time long range dispersion model evaluation.

Statistic	1[a]	2	3	4
Normalized mean square error	x<15.0	15.0<x<25.0	25.0<x<50.0	x>50.0
Bias (ng m^{-3})	x<0.3	0.3<x<0.5	0.5<x<1.0	x>1.0
Correlation	x>0.5	0.4<x<0.5	0.3<x<0.4	x<0.3

[a]1 is the best ranking and 4 as the worst. x denotes the statistical measure in consideration.

fractional bias suggests that the model has a tendency to overpredict the concentrations. The correlation indicates a rather good correlation between measurements and predictions. The large NMSE suggests that the predictions have large spread around the measurements, which is also confirmed by the value of the fractional standard deviation. From inspection of the statistics at each individual station it is clear that the large value of NMSE results from overpredictions at stations close to the source. In an attempt to investigate the agreement to include zero values if there is a non-zero neighbour or a non-zero next to neighbour was investigated by including only zero values if there was a non-zero neighbour. In this case the NMSE decreases to 90 while the bias and correlation does not change appreciably, underlining the importance of comparing models based on the same statistical methodology and assumptions. The global statistical measures compare well with the models participating in the ATMES-II exercise [158]. During the ETEX-1 real time long range dispersion model evaluation [71] the models were ranked according to their global statistical measures for NMSE, bias and correlation. The criteria for the ranking is shown in table **??**. Using this ranking the NMSE is placed in ranking group 4, while the bias is in group 2 and the correlation is in group 1. In order to facilitate comparison with the ATMES-II model evaluation [158], 11 measurement stations (B05, CR03, D05, D42, D44, DK02, DK05, H02, NL01, NL05, PL03), representing short-range and long range transport, were selected for the temporal analysis (figure **??**). The predicted and measured temporal development of the tracer concentration is displayed in figure 6.4, while the corresponding statistical measures are shown in table 6.3 and 6.4.

The performance at stations in the second arc is in general better than at stations in the first arc. This is especially seen in the integrated concentration and variance fields (figure 6.5). The largest bias is found at stations B05 and NL05, while the largest NMSE is found at station NL05 and the lowest FMT at station B05. Similarly, the largest difference between mean measured and predicted values is
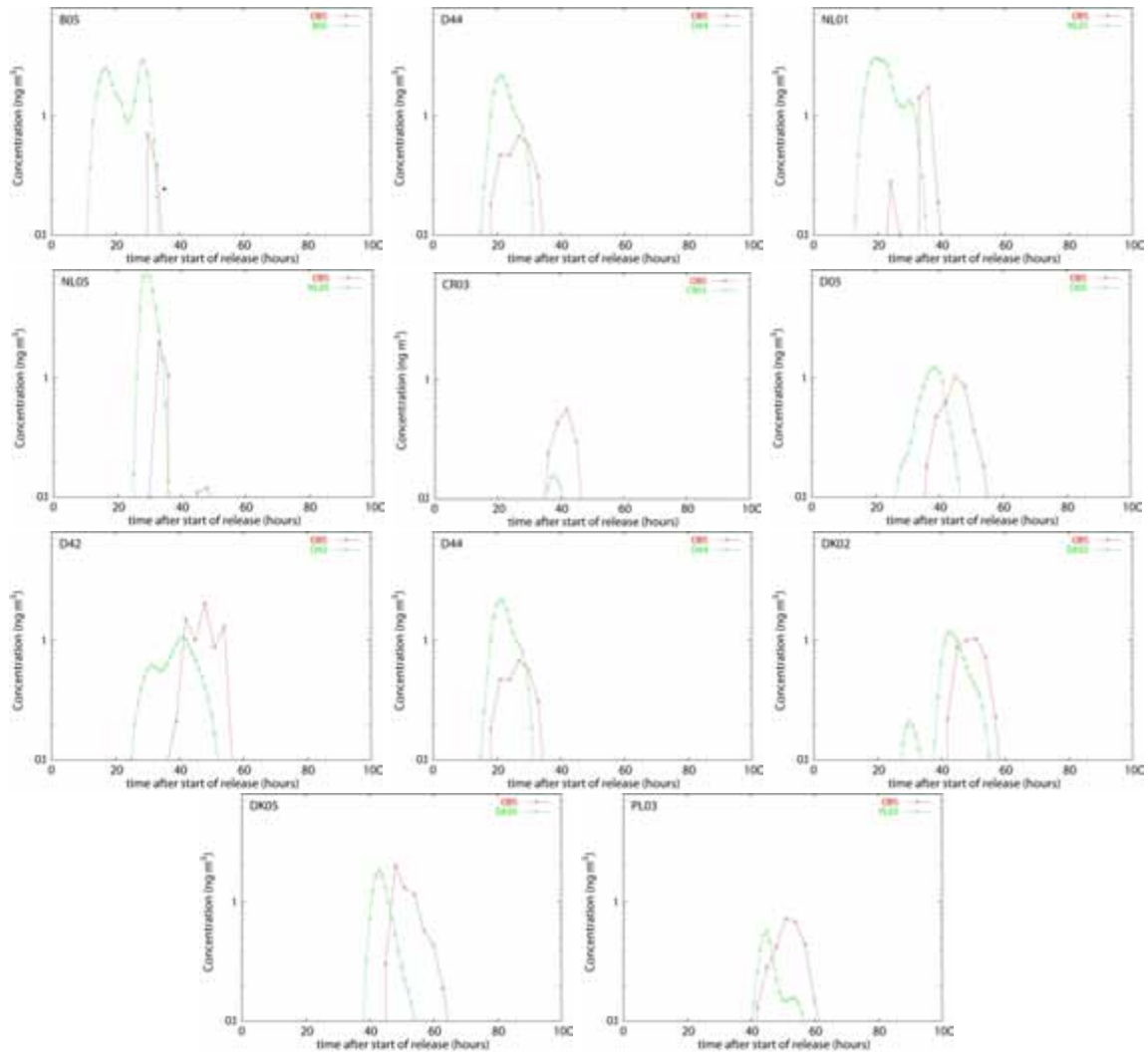
Figure 6.4: Temporal development of the tracer cloud as it passes measurement stations in the first and second arch, from upper left to lower right the stations are B05, D44, NL01, NL05, CR03, D05, D42, D44, DK02, DK05, PL03. Red lines are observations, while green lines are predictions.

Table 6.2: Global statistical measures taken over all ETEX-1 measurement stations at all times. Number of points: 1243.

Statistic	Predicted	Measured
Mean (ng m^{-3})	0.26	0.23
Variance (ng^2 m^{-6})	17.83	0.41
Fractional standard deviation	1.91	–
Normalized mean square error	104.59	–
Bias (ng m^{-3})	0.39	–
Fractional bias	0.92	–
Correlation	0.57	–
FA2 (%)	20.84	–
FA5 (%)	36.52	–
FOEX (%)	−0.93	–

found at stations B05 and NL05, 0.76 ng m^{-3} and 0.56 ng m^{-3} respectively. The worst correlation is found at station NL01. These features correspond very well to the findings during ATMES-II. The Eulerian treatment of point sources, whereby the emission rate is divided by the grid cell volume, may lead to unrealistic values close to the source. Stations such as B05, NL01 and NL05 are located in the margin of the tracer cloud and experience only weak concentrations. In such regions the tracer cloud is more sensitive to small errors in the meteorological fields or mesoscale influences which may not be well represented by the model. This result is consistent with the result that the large global NMSE is caused by overprediction at stations close to the source. Amongst the stations with the worst correlation DK05, which is located in the second arc, is found. In this case the degraded correlation is caused by a temporal shift, of a few hours, in the plume. Double peak structures in the observed temporal evolution (figure 6.4), which is indicative of mesoscale influences during the transport, was seen at several stations. Unresolved mesoscale activity may also lead to a degradation of the statistics. This issue is discussed more fully in chapter 4.5. The mean bias in the first and second arc is 0.59 ng m^{-3} and -0.07 ng m^{-3} respectively, suggesting that the model has a tendency to overestimate the concentration close to the source, while there is a slight underestimation far from the source. In connection with this it is worth noticing that the meteorological measurements themselves also contain errors and one may question whether the density of the network close to the source is representative, i.e. idealy the density of the measurement stations should increase as the source point is approached from the direction of the plume.
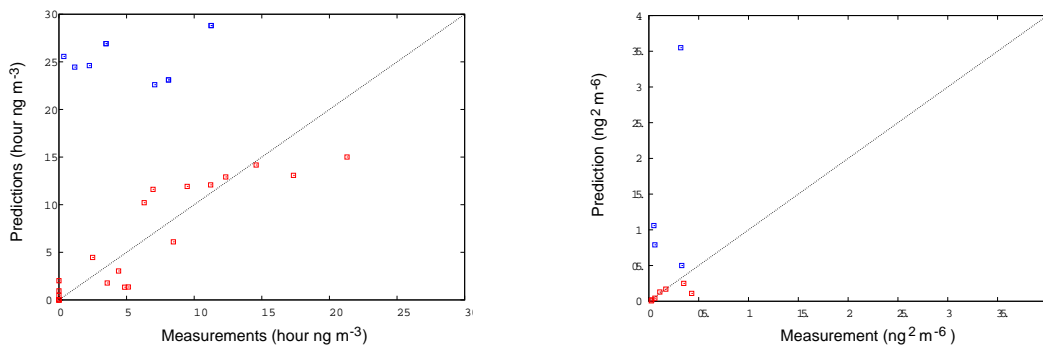
Figure 6.5: Left: scatter plot of integrated concentration, for the 11 selected stations. There are points at 30, 48 and 60 hours after start of release. Right: scatter plot of variance, for the 11 selected stations. In both plots blue points represent stations in the first arch, while red points represent stations in the second arch.

During the ETEX-1 real time long range dispersion model evaluation the models were also ranked in the temporal analysis. Indices were defined according to NMSE, bias, R, FMT and cumulated concentration. Out of the 11 selected stations the number of sites with NMSE less than 10, bias between -0.14 and 0.30, R greater than 0.70, FMT greater than 20% and cumulated concentration differences less than a factor of 2.5 after 48 hours were counted. With 9, 6, 3, 6 and 6 sites in each category respectively and using the indeces defined in [71] the total score becomes 24, which is amongst the five best performing models in the ETEX-1 real time long range dispersion model evaluation.

Conclusions

Away from the source point the model performs satisfactory, both with respect to correlation, bias, NMSE and variance, and in comparison to the models which were evaluated during the ETEX-1 real

Table 6.3: Temporal statistical measures at stations in the first arc.

Statistic[a]	B05	D44	NL01	NL05
Observed mean (ng m^{-3})	0.12	0.25	0.31	0.27
Predicted mean (ng^2 m^{-6})	0.88	0.70	0.80	0.15
Observed I (48 h) (ng h m^{-3})	3.48	8.10	11.25	10.20
Predicted I (48 h) (ng h m^{-3})	24.60	23.12	28.81	36.02
NMSE	12.94	4.54	4.47	14.88
BIAS (ng m^{-3})	0.77	0.96	0.49	0.65
R	0.80	0.64	-0.05	0.29
FMT (%)	12.90	32.05	16.00	19.07

[a]included obs. for B05: 10, D44: 11, NL01: 12, NL05: 13

Table 6.4: Temporal statistical measures at stations in the second arc.

Statistic[a]	CR03	D05	D42	DK02	DK05	H02	PL03
Observed mean (ng m^{-3})	0.12	0.29	0.48	0.34	0.41	0.12	0.22
Predicted mean (ng^2 m^{-6})	0.03	0.31	0.33	0.33	0.29	0.09	0.15
Observed I (48 h) (ng h m^{-3})	4.86	9.48	14.58	6.30	6.96	3.57	2.49
Predicted I (ng h m^{-3})	1.35	11.92	14.17	10.21	11.62	1.78	4.47
NMSE	7.96	2.00	2.25	0.94	4.77	1.06	1.96
BIAS (ng m^{-3})	-0.08	0.02	-0.15	-0.01	-0.11	-0.02	-0.06
R	0.92	0.29	0.46	0.68	0.08	0.86	0.43
FMT (%)	26.06	29.60	32.70	51.38	15.43	49.25	38.42

[a]Included obs. for CR03: 16, D05: 13, D42: 15, DK02: 12, DK05: 15, H02: 14, PL03: 14

time long range dispersion model evaluation and ATMES-II Enviro-HIRLAM performs well. Close to the source point there is a tendency to overprediction of the tracer concentration, resulting in a large global NMSE.

Testing deposition

Parts of this chapter has been published as [119].
The Chernobyl accident occurred on 25 April 1986 at 21:23 UTC at the Chernobyl nuclear power plant in Ukraine ($51°17'$ N, $30°15'$ E). Two explosions and subsequent fires emitted large amounts of radioactive material into the atmosphere in the form of gases and fuel core fragments containing radioactive isotopes, including We, I, Ba, Mo, Ru, Sr, Cs. Due to its long half-life (30 years) and the large amount emitted, Cesium has the strongest long term radiological influence. The purpose of this experiment is to evaluate the ability of the model to simulate the deposition of Cesium 137 (Cs^{137}) .

Methodology

The main difference between these simulations and the one presented for ETEX-1 is that here an accident is modeled and therefore the source term is very uncertain. Measurements of total accumulated deposition were extracted from the Radioactivity Environmental Monitoring database

(REMdb) at the Joint Research Centre, Ispra, Italy (http://rem.jrc.ec.europa.eu/37.html). The comparison date was chosen to be 1 May 1986 at 12:00 UTC, since at this time the greatest number of measurements were available. Statistical measures were calculated following the recommendations of the Atmospheric Transport Model Evaluation Study (ATMES) final report [118]. Correlation was calculated using log-transformed deposition fields, with a cut-off at 0.001 Bq m^{-2}. Since only few daily measurements were available and due to the accumulated nature of the deposition field only global statistics were considered.

Model set-up

The total amount and corresponding temporal development of the Cs^{137} emission has been estimated [51, 49, 175] but is still associated with at least 50 % uncertainty. The current simulation considered the transport, dispersion and deposition of Cs^{137} and employs vertically stratified point sources in order to simulate the explosions and following fires. The size distribution of particles containing Cs^{137} is not known and here only mono-disperse particles are considered with a radius of 0.5 μm and a density of 1.88 g cm^{-3}. The horizontal resolution was $0.45° \times 0.45°$ and the area covered a region which includes northern Africa, the arctic regions, northern America, Europe and a large part of northern Russia (figure 6.6). The start time was at 25 April 1986 at 18 UTC and the model was integrated two days ahead and then reinitialized and restarted until 7 May at 18 UTC. Surface analysis and 3DVAR upper air analysis was used as initial conditions for the meteorology at the beginning of each cycle and six hourly boundaries were post-processed from the ECMWF (European Center for Medium Range Weather Forecasting) model IFS (Integrated Forecast System).
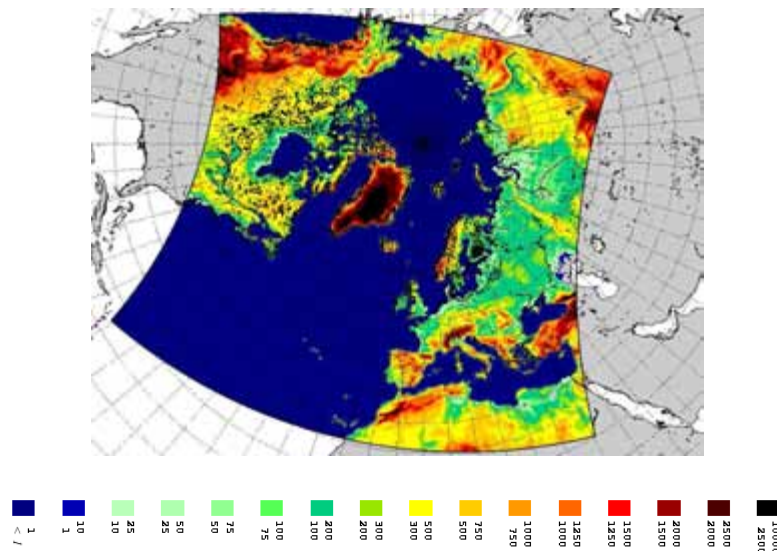
Figure 6.6: Model area used for the simulation of the Chernobyl accidental release, displayed as surface geopotential heights (meters).

Results and discussion

Figure 6.7A and 6.7B displays the dry and wet deposited Cs^{137} fields and figure 6.8 shows the total measured deposited Cs^{137}. Considering the large uncertainty of the emission data, the uncertainty in the measurements, the mono-disperse nature of the simulation and the coarse horizontal resolution, the model reproduce (spatially) most features of the deposition field satisfactory. This includes the peaks close to the accident site, in southern Finland, Suisse, Austria and Italia. The band of increased activity extending from Southern Finland across Sweden and Norway is not well captured and is known to be caused by wet deposition. In the model the precipitation falls in a band further south causing the shift in the wet deposition pattern.

Figure 6.7: Accumulated dry (left column) and wet (right column) deposited Cs^{137} in kBq m^{-2} on 12 UTC 1 May 1986. A and B are predictions using $0.45°$ resolution and C and D are predictions using $0.15°$ resolution.
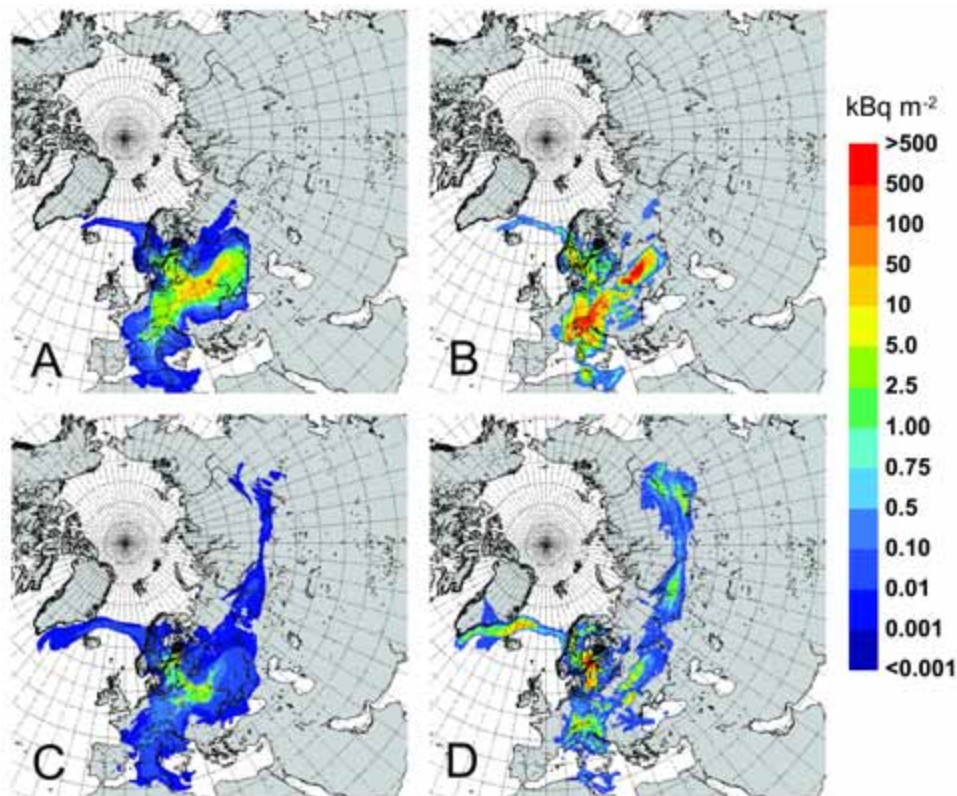
Table 6.5 displays the statistical scores and figure 6.9 shows the global scatter diagram. There are 24.05% of the predictions within a factor of two and 55.06% within a factor of five above or below the measurements. The large bias and fractional bias suggests that the model has a strong tendency to overestimate, this is also confirmed by the scatter diagram and the large FOEX value. This may, in part, be due to the misplacement of the band of wet deposition across Sweden and Norway, but also biases in the source term and errors in the estimated release height may contribute. Due to the uncertainty in the emission estimates, some of the bias may be removed by correcting the source term, however, this has not been done.

Comparing to the models which participated in ATMES the correlation and NMSE are amongst the best performing models while the bias is amongst the worst performing models. In the ETEX-1 simulation it was found that the model has a tendency to overestimate close to the source. From figure 6.7 it is found that this may also explain some of the bias.

Another reason for the large global bias could be due to insufficient horizontal resolution. The simulations were repeated in $0.15°$ resolution, keeping everything else as described above. The cumulated deposition fields are displayed in figure 6.7(C and D). The band of wet deposited Cesium across Sweden and Norway is not better resolved in higher resolution. The model rain out in the Bay of Finland, instead of in Sweden, generating a large peak of deposited Cesium. Although the concentration in the emission grid box generally increase, with increasing resolution, the dry deposition field generally decreases over much of the domain. This is confirmed by the statistical scores (table 6.5) which all improve, except for the correlation. As resolution increased so did the vertical mixing and more mass was transported into the jet stream residing at about 600 hPa. The stream transported Cesium towards the east with a speed of approximately 30 m/s, leading to a band of increased dry and wet deposition in northern Russia. The increased mass at higher levels caused
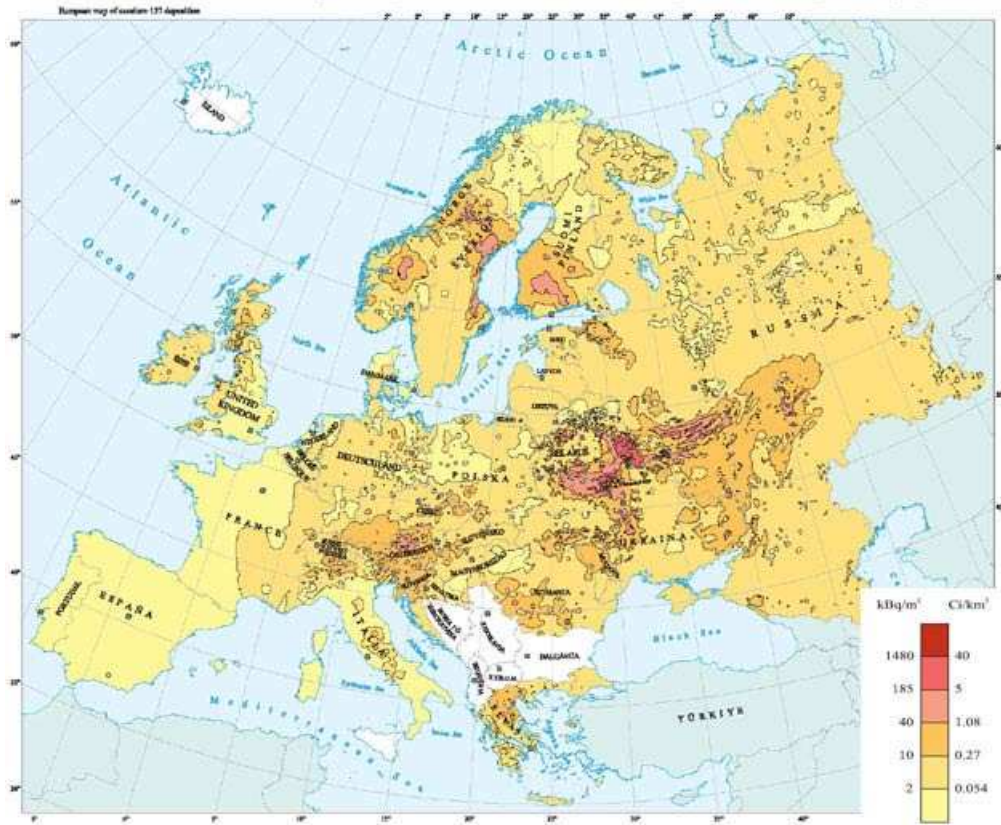
Figure 6.8: Measured accumulated Cs^{137} deposition in kBq m^{-2} [49].
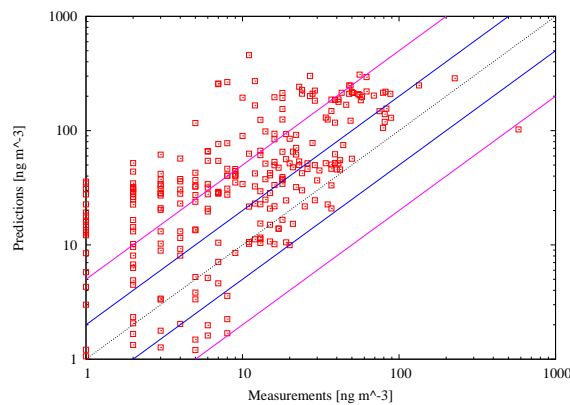
Figure 6.9: Global scatter diagram for total cumulated Cs^{137} deposition on 1 May 1986. Number of points is 316, FA2 = 24.05%, FA5 = 55.06% and FOEX = 22.47%.

the surface concentration to decrease and wet deposition near the east coast of Greenland to increase. Hence, the bias improved from increasing the resolution, however, it is seen that the correlation decrease due to overestimation of the total deposited field. In $0.45°$ resolution the numerical diffusion from the advection scheme is sufficient to balance the real physical horizontal diffusion. This may, however, not be the case at $0.15°$ resolution, where it is likely that 'extra' diffusion is needed, since more variability is explicitly resolved. In the simulations presented here the horizontal diffusion of the tracer field was switched off, because the fourth order scheme described in chapter 3 is not mass conserving. Including horizontal diffusion in the $0.15°$ simulations would likely decrease the concentration at all levels and thereby the deposited fields, leading to an increase in correlation. It is therefore necessary that a mass conservative horizontal diffusion scheme is implemented for

Table 6.5: Global statistical measures for the Chernobyl simulations.

Global statistic	0.45°	0.15°
Number of points	316	326
NMSE	6.34	0.83
BIAS ($kBqm^{-2}$)	38.77	2.17
FBIAS	1.04	0.70
R[a]	0.59	0.38
FMT (%)	26.29	45.11
FA2 (%)	24.05	45.10
FA5 (%)	55.06	78.83
FOEX (%)	22.47	39.57

[a]Lower cut-off for log transformation is 0.001

future use of the model.

Conclusion

The model has a large positive bias, but considering the large uncertainty in the emission strength, release height and the simplicity of the simulation the model performs well. This was also confirmed when comparing to the models evaluated during the ATMES exercise, where the model was among the best with respect to NMSE and correlation. The BIAS may be partly explained by overestimation of the concentration close to the source, due to the basic treatment of point sources, and partly by insufficient horizontal resolution. A mass conservative horizontal diffusion scheme should be implemented and tested in the future, for use in high resolution simulations.

Gas-phase chemistry

NWP-Chem is a new gas-phase chemistry scheme designed for operational usage in online coupled models. In this chapter an evaluation of the Enviro-HIRLAM chemistry for a single meteorological case is considered. It is not possible to give any general conclusions regarding the quality of the predictions by the model when using NWP-Chem on this basis, however, the chosen case corresponds to the case considered in chapter 5.3 and is therefore of importance to this study. Zero-dimensional tests of the scheme have previously been performed at DMI [79]. The scheme has been shown to compare well with the more detailed RACM scheme for the species of importance in aerosol formation and gas-aerosol equilibration. In appendix 4 some of these results have been reproduced for completeness.

Three-dimensional testing

Enviro-HIRLAM was executed with full gas-phase chemistry, aerosol dynamics and gas-aerosol equilibration on a domain surrounding Paris (figure 6.10). The model was initialized at 00 UTC 29 June 2005 and integrated for 48 hours until 00 UTC 01 July 2005 and the first 24 hours were disregarded as spin-up. The horizontal resolution was $0.05° \times 0.05°$ and 40 levels was used in the vertical with the lowest level about 30 meters above the surface and the top level around 10 hPa. Inflow of chemical species across the boundaries was neglected since the wind at higher levels was

weak and westerly, i.e. there were only low anthropogenic emissions from the north-western part of France and the northern atlantic region. The meteorological boundaries and initial conditions were interpolated from the DMI-HIRLAM-S05 model used for operational weather forecasting at DMI. All other aspects of the simulation and model set-up were as described in chapter 3.

Figure 6.10: Model area displayed as surface geopotential height (meters). The black names refer to stations employed in the NO_2 comparison and the location of Paris is shown with a red dot.

Measurements of NO_2 was taken from the European air quality database (AIRBASE) [1] and was used to compare predicted and measured concentration values. The model area contained 248 measurement stations sufficiently removed from the domain boundary zone. Recasting these onto a 50×50 km grid and retaining only one to three stations within each grid cell, to achieve an even coverage in the modeling domain, results in 64 evenly distributed stations. Urban stations were disregarded, due to the tendency for overestimation near the source points. Data at some stations was not available and in the 27 stations, each containing hourly NO_2 concentration measurements, representing the modeling domain (figure 6.10) were retained.
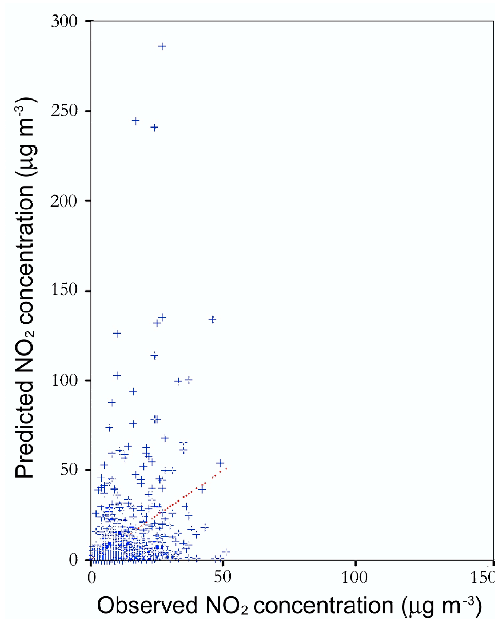

Figure 6.11: Global scatter plot of NO_2 concentration ($\mu g\ m^{-3}$). Global BIAS $= 0.34\ \mu g\ m^{-3}$, FBIAS $= 0.02$, NMSE $= 1.12$, R $= 0.38$, number of points: 648.

Results

The general performance of the model is summarized in figure 6.11. The global bias, fractional bias and NMSE compares well with other models (e.g. [66]), however, they cover a large range of values. There are a few very large predictions (compared to the measurements) occurring primarily at stations which are close to and downwind of the Paris metropolitan area, such as station FR1396A. At such stations the concentration is influenced by the general overestimation of the concentration close to the source point (see chapter 4.2 and 4.3). Disregarding these stations the bulk of the points in figure 6.11 are located below the $45°$-line suggesting a general underestimation at stations away from the source. The global bias is generally negative during day and positive during night -time and varies between -20 and $10 \ \mu g \ m^{-3}$. Figure 6.12 displays the temporal development of the NO_2 concentration at various stations along with the average over all stations. At station FR1252 (figure 6.12F) the prediction greatly underestimates the amplitude of the diurnal cycle, while at station FR1233 (figure 6.12E) the amplitude is overestimated. At these stations the predictions are consistent with errors in the modeled cloud cover. Underprediction of the cloud fraction leads to enhancement of the photochemically driven part of the diurnal cycle, while overprediction leads to excessive damping of the diurnal cycle. On the other stations (figure 6.12A-D) the amplitude and temporal and phase is well predicted. On average the diurnal cycle is well represented. The largest deviation from measurements occur during night, where the model overestimates the concentration with up to $10 \ \mu g \ m^{-3}$. During day there is a general underestimation of approximately $5 \ \mu g \ m^{-3}$. It is also worth noting that the measurement data contains some representivity errors. There are interference from other NO_x species during the measurements which may lead to deviations between modeled and measured values. The importance of such errors in this case study are not known.
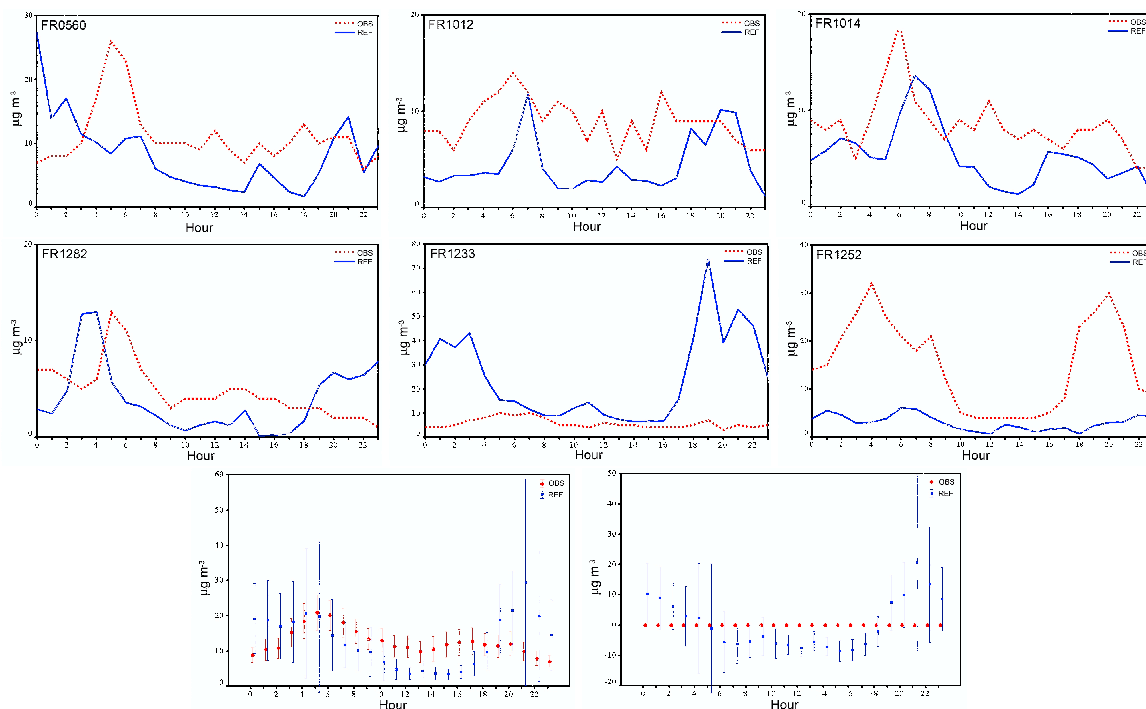
Figure 6.12: Predicted and measured temporal development of NO_2 concentration at representative stations (A-F) (see figure 6.10 for station locations), along with station averaged temporal development and station averaged deviations from observations (G-H).

Conclusion

The NWP-Chem scheme for gas-phase chemistry performs well, compared to other more elaborate schemes, in one-dimensional simulations. They covered a range of meteorological conditions in both the boundary layer and in the free troposphere. Considering a single meteorological case the full three-dimensional model was shown to compare well with measurements of NO_2 away from the major source area. Some overpredictions during night and underpredictions during daytime, in the range 5 - 10 μg m^{-3}, are found. Other aspects of this case are considered in chapter 5.3, where also the models ability to predict aerosol mass concentration is considered.

Differences between offline and online models

This chapter has been published as [120].

Abstract

Traditionally, transport and dispersion models are offline coupled to meteorological drivers, receiving preprocessed output at regular coupling intervals. However, today meteorological models have reached urban and cloud resolving scales and online models integrating meteorological and dispersion models have been developed. In this study the online coupled model, Enviro-HIRLAM, which can also run in offline mode, was used to compare online and offline representations of mesoscale disturbances. The online model was evaluated using data from the first European Tracer Experiment (ETEX-1) and produced satisfactory results. Mesoscale influences during the simulation pertube the plume during long-range transport, leading to a double peak structure at a specific measurement station. The mesoscale influence was investigated by varying the off-line coupling interval which was shown to be important in constraining the influence of mesoscale disturbances on plume structure in coarse resolution.

Introduction

Modeling studies of urban air-quality and the dispersion of air pollution has traditionally been carried out using offline[1] models. Such models are often convenient when considering various emission scenarios with fixed meteorology, such as in air-quality impact asse sments or when performing sensitivity analysis on dispersion models. They require time-averaged output from meteorological m odels to force transport and dispersion of pollutants. Such output is typically available every one, three or six hours (her e denoted the coupling interval) and in between updates the meteorological fields are interpolated retrospectively in time. Hence, offline models rely on the fundamental assumption that the variability present in the meteorological driver which is produced by disturbances with time scales shorter than the coupling interval can be satisfactorily reproduced during interpo lation.

In the planetary boundary layer short-term variability in the pollutant concentration field is generated by meso-sca le disturbances in the mean flow [3]. Generation mechanisms include atmospheric instability (e.g. conditional in stability [92, 233]), surface inhomogeneities and bifurcations in the wind field. Specific exampl es include flow over and around orographical features [176, 114], the effect of mega-cities on plume transpor t and meteorology, urban circulations (Piringer and Joffre, 2005), urban breeze circulations [168, 146], changes in wind structure due to enhanced roughness over urban agglomerations [241], interactions between urban and sea bree zes [131], building effects inside the urban canopy [195], lake effects [177], sea breezes, fr ontal circulations and associated rapid changes in wind direction [80], development of clouds and precipitation and up- and down-draughts in connection with single and multi-cell storms. The horizontal scale of such disturbances range f rom a few kilometers to several hundred kilometers while the time scale range from less than one hour to days.

Pollutant concentration fields are known to contain large temporal and mesoscale variability [178, 3]. The presence of such disturbances may significantly alter plume spread and structure and therefore the detailed po llution patterns [64]. Hence, uncertainties in plume development may be induced if the coupling interval does not r esolve the developments in mesoscale disturbances. Unresolved horizontal vaiability is typically accounted for by tuning ho rizontal diffusion coefficients, leading to large values in the range $10^3 - 10^5$ m^{2}s^{-1} [**?**]. While smoothing may be an

---

[1]The use of the term offline in this context has been ambiguous. A formal defi nition may be given as: separ ate chemical transport models forced by output from meteorological models, analyzed or forecasted meteorological data from a rchives or data sets, preprocessed meteorological data, measurements or output from diagnostic models.

appropriate representation of subgrid-scale turbulent eddies it is not the case when meso- scale disturbances are resolved by the meteorological model, since growth, decay and structural changes to the plume are not considered.

Consequently, the basic assumption may not be fulfilled if the meteorological fields contain mesoscale fluctuations not explicitly resolved by the coupling interval. This is particularily relevant for high resolution wind fields in which most of the variability stems from explicitly resolved eddies. This has recently been demonstrated in a study which showed that offline models are susceptible to large errors when variability in the vertical wind field is large. During a particular frontal passage the coupling interval of an offline model had to be as low as 10 minutes to capture 85% of the variability in the vertical velocity [75]. Hence, the basic assumption may be more appropriate for applications which do not require spatially detailed pollution fields.

The importance of the coupling interval has previously been highlighted [28, 149, 157, 81, 179]. In most of these studies the coupling interval was changed from 12 to 6 hours, demonstrating the importance of resolving the diurnal cycle, especially in relation to vertical mixing in the boundary layer. Mesoscale eddies, superposed on the diurnal cycle, have also been shown to affect plume structure both at its initial stage and during long range transport [161, 219].

Due to the great advances in computer power within recent decades meteorological models have reached high spatial resolution, resolving urban features, (horizontal grid spacings typically between 3 and 15 km) and it has become feasible to develop meteorological models which include transport and dispersion of particles and gases at each advection time step [75, 95]. In this context it is reasonable to question whether offline models are sufficient in applications where detailed (high spatial and temporal resolution) pollution levels are required (such as the spread of air pollution in complex terrain or urban exposure modeling). The purpose of this study is to demonstrate that even at coarse resolution (approximately 40 km grid-spacing) errors may be induced in offline models if the coupling interval does not resolve the evolution of horizontal mesoscale eddies. Section 2 contains a description of the methodology, while model description, results and conclusions are found in sections 3, 4 and 5, respectively.

Methodology

In the first European Tracer Experiment (ETEX-1) a controlled release of an inert tracer gas, along with measurements of its air concentrations at 168 stations, were conducted [165]. The release was carried out from a site in northern France (Brittany, $2.01\,^\circ$ W and $48.06\,^\circ$ N) eight meters above ground at a constant average rate of $7.95\,\mathrm{g\,s^{-1}}$ during meteorological conditions producing only little dispersion, i.e. the plume did not break up due to dispersional effects [80]. It commenced on 23 October 1994 at 16:00 UTC and lasted 11 hours and 50 minutes. Measurement stations in northern and central Europe were employed in deriving the horizontal and temporal development of the plume. During real-time and retrospective analysis offline long range dispersion models were evaluated against the measurements [71, 158].

Employing a recently developed online[2] coupled environment model Enviro-HIRLAM (High Resolution Limited Area Model) which has the ability to run in offline mode, the ETEX-1 measurements were used in a case-study and the effects of mesoscale disturbances on transport and dispersion were considered. Using a 10 minute coupling interval (which is also the length of the meteorological time step), corresponding to an online access run the model was evaluated against the ETEX-1 measurements.

In order to simulate the extreme case, where mesoscale disturbances are not resolved by the coupling

---

[2]The use of the term online in this context has been ambiguous. A formal definition may be given as: chemical transport models in which the meteorological forcing fields are available at each time step of the meteorological driver (on-line access models) and online integrated models which includes feedbacks between pollutants and meteorology (online coupled models.)

interval, variability was restricted by keeping the meteorological input, used for advection, constant between updates. Full variability was retained in the vertical so that only the effect of advection was considered. In five simulations the coupling interval was progressively increased (without changing the time step) attaining the values 30, 60, 120, 240 and 360 minutes (offline simulations). The concentration fields at two measurement stations, F15 ($49.05°$ N, $6.08°$ E) and DK02 ($54.50°$ N, $10.58°$ E), located at different distances from the release site (corresponding to short and long range transport) were analyzed allowing for an evaluation of the importance of the length of the coupling interval at those sites.

Model description

Enviro-HIRLAM is an online coupled meteorological, chemical transport and dispersion model developed at the Danish Meteorological Institute (DMI). At its core lies the High Resolution Limited Area Model (HIRLAM) version 6.3.7 which is employed for limited-area short-range operational weather forecasting at DMI [37]. For a detailed description of the features in HIRLAM the reader is referred to the HIRLAM reference guide [226]. In this study the transport and dispersion of a passive tracer was simulated using a one-way coupling from meteorology, i.e. there were no feedbacks and the model was run as an online access and offline model.

Point sources are parameterized by assuming that the tracer distribution is uniform within the grid box containing the release site. The emission is ascribed the grid point closest to the release site in the lowest model layer, corresponding to a height of approximately 30 meters above the surface. In a well-mixed boundary layer this height is not believed to affect the results away from the emission grid box.

The model contains several choices for advection, but in order to achieve sufficient tracer mass conservation and at the same time maintain large time steps in the meteorological model, advection was treated differently for meteorological quantities and for the tracer. The Bott scheme [22, 23] was employed for the tracer while a Semi-Lagrangian scheme was employed for meteorological fields. The mass conservation properties of the Bott scheme, during these meteorological conditions, have been tested [37] and found appropriate, hence, the inconsistency thus introduced is not believed to be of importance during this case study.

In the present study horizontal diffusion was switched off hence, the numerical diffusion arising from the Bott scheme was the only representation of subgrid-scale horizontal eddies [36]. In the vertical a modified version of the Cuxart, Bougeault, Redelsperger (CBR)-scheme developed for HIRLAM is employed [48]. It is based on turbulent kinetic energy, which is a prognostic variable in the model, and a stability dependent length scale formulation [226].

The model is hydrostatic and horizontal discretization is done on an Arakawa C grid, while in the vertical a hybrid between terrain-following Sigma and pressure coordinates is employed [226]. In the present set-up the model covered most of Europe (figure 6.1) with a horizontal resolution of $0.40°$ (92×86 points) on a rotated latitude-longitude grid, with 40 levels in the vertical, where 30 of these are inside the troposphere and the top level is at 10 hPa.

Analysis and six-hourly boundaries were supplied by the European Center for Medium Range Weather Forecasts and digital filtering was used to initialize the model which used a time step of 10 minutes. The Analysis time was 23 October 1994 at 12:00 UTC, four hours before the start of emission, and the model was run out to 80 hours.

Results and discussion

The current version of Enviro-HIRLAM has not previously been evaluated against the ETEX-1 measurements. To facilitate comparisons with models evaluated during the ATMES II (Atmospheric Transport Model Evaluation Study) model inter-comparison an identical statistical methodology was

employed [158]. Background Perfluoro-Methyl-Cyclo-Hexane values were subtracted so that only the pure tracer concentration was used. Measurements of zero concentration (concentrations below the background level) were included in time series to the extent that they lay between two non-zero measurements or within two before or two after a non-zero measurement. Hereby, spurious correlations between predicted and measured zero-values far away from the plume track were reduced.

The synoptic situation in the days following the ETEX-1 release has previously been described in detail [80, 71, 161] and represents a typical meteorological situation without frontal circulations. Correspondingly, the model plume was initially advected by a westerly flow, mainly influenced by synoptic-scale forcings, in a north-easterly direction. The spatial structure of the model plume resembled the observations (figure 6.2, [158]) and the plume retained its continuity throughout the forecast period. The plume is most sensitive to mesoscale perturbations during its initial development. Even though the bulk of the plume remained continuous the marginal structure may be affected by such disturbances and cause large errors in verification scores at specific stations. After 36 hours the model plume had attained a U-shaped deformation receding over northern Germany. An identical deformation also exists in ETEX-1 simulations by other models [158] and although less distinct, a similar structure is present in the observations [158]. The model, thus, over-predicted the development of the deformation, which extended further to the north.

In line with the measurements the model plume was stretched and its axis tilted, so it was oriented in a north-west to south-east direction, after 48 hours. The peak concentration, however, was located too far to the north. After 60 hours the largest concentration values were still found in the North Sea, a feature which is also present in the observations.

Following the methodology of ATMES II the time development of the model plume was evaluated at 11 selected stations [158]. These were chosen to constitute two arcs at different distances from the release site. The first arc (measurement stations: NL05, B05, NL01, D44) follows the eastern border of Belgium (figure 6.1). The arrival time at these stations ranged from 15 to 18 hours. The second arc (measurement stations: DK05, DK02, D42, D05, PL03, CR03, H02) extended from Denmark in the north to Hungary in the south, and the arrival times at these stations ranged from 30 to 39 hours. For the statistical analysis the following parameters were computed: linear Pearsson correlation (R), normalized mean square error (NMSE), bias and figure of merit in time (FMT). The FMT is computed as the ratio of the area of common ground and the area under the envelope of the measured (M) and predicted (P) time series at a specific location (x), a general expression may be given as: $\text{FMT} = 100 \times \sum_i min(\text{M}(x, t_i), \text{P}(x, t_i)) / \sum_i max(\text{M}(x, t_i), \text{P}(x, t_i))$ where t_i represents measurement times and $i \in \{1, ..., N\}$ where N is the number of measurements. The average R, NMSE, bias and FMT (table 6.3 and 6.4) at the stations were 0.49, 4.25, $0.18 \, \text{ng} \, \text{m}^{-3}$ and 29.35% respectively. These values are all acceptable when compared to the model scores during ATMES II (here the statistical results are grouped and a global correlation above 0.5, a global bias less than 0.3 $\text{ng} \, \text{m}^{-3}$ and a global NMSE below 15 are considered the best) [158]. All the scores were degraded by the values at the stations in the first arc, suggesting worse performance close to the release site than further away from it, which was generally also found during ATMES II.

Numerical noise due to the Eulerian treatment of point sources, in which emissions are resolution dependent, are only believed to be of importance within a few gridlengths of the release site and cannot explain the degraded performance close to the release site. One possible explanation is the influence of mesoscale disturbances during the initial development of the plume, which are not resolved by the model. The existence of a short wavelength disturbance (≈ 300 km) in the surface pressure field, during the release, has been reported [161]. If such a disturbance is not well represented its influence could lead to degraded statistical performance at stations close to the release site.

The global statistical scores provide a more comprehensive picture of the ability of the model to

simulate the tracer plume because it contains information from all the measurement stations at all times (table 6.3 and 6.4). Over- and under-predictions were equally distributed, but the large positive bias (relative to the mean value) suggests that the over-predictions generally are larger in magnitude than the under-predictions. The large value of the NMSE suggests that there is a large spread around the measurements, and the correlation coeficient indicates a good global correlation between predictions and measurements. The large value of the NMSE could be caused by temporal or spatial shifts of the predicted relative to the measured fields. The low value of the FMT indicates the existence of a temporal phase error.

In order to consider the influence of mesoscale eddies in more detail the temporal development at two stations, one near the first arc (F15) and another in the second arc (DK02), was considered. At station F15 the measurements were dominated by a single peak which was captured well by the simulation (figure 6.13; run with a 10 minute coupling interval). The result was not sensitive to variations in the coupling interval of up to six hours. This suggests that the peak is generated by transport of the bulk of the plume over the site without any influence from short time scale disturbances (less than six hours), i.e. the wind did not vary rapidly. At station DK02 the plume had traversed a region in which mesoscale disturbances are known to influence the dispersion [219]. The predicted development of the concentration field had a phase error of a few hours on the arrival of the plume but was otherwise in good agreement with the observations (figure 6.13). A false (not in observations) peak preceding the plume existed and is indicative of mesoscale influences during model plume development. Notice that the first peak does not contribute to the statistical scores because the observations are zero. As the coupling interval was increased, the main (second) peak remained unaffected while the amplitude of the first peak gradually increased. This suggests that the existence of the first (false) peak is related to short time-scale disturbances in the forecasted meteorological fields, while the second peak is generated by transport of the bulk of the plume. Mesoscale eddies are superposed on the mean flow generating cyclonic and anti-cyclonic perturbations in the plume. The eddies are visible as peaks in plots of relative vorticity (figure 6.14; the perturbations influencing the model plume structure are marked with arrows). The eddies filled the boundary layer between the surface and at least 800 hPa. The two eddies persisted at least 15 hours, had maxima of $+/- 6\,\mathrm{s}^{-1}$ respectively at the surface and tilted towards the NE with height. After 24 hours (from start of release) the model plume maximum had split into two separate parts. The head received cyclonic rotational momentum from a mesoscale disturbance and reached DK02 after 26 hours giving rise to the first peak. As the latter part of the cloud progressed it received anti-cyclonic momentum and after 36 hours the plume has attained the U-shaped deformation which was advected towards DK02. The rotational time scale of the eddies was not large enough (compared to the advective time scale of the plume) to cause a full revolution in the plume.

As the coupling interval was increased changes in the magnitude of the eddies were not resolved, and the U-shape extended further northwards leading to increased peak values in the concentration field at DK02 (figure 6.15). Increased temporal resolution constrained the evolution of the mesoscale disturbances, leading to better correspondence with measurements. Hence, even at coarse resolution it may be necessary to decrease the coupling interval in order to achieve correspondence with measurements at specific stations.

During this case-study I considered the sensitivity of horizontal dispersion. However, previous studies have shown that very short coupling intervals are necessary to constrain vertical mixing processes [75, 5]. In general, the appropriate length of the coupling interval will depend on the application and the mesoscale activity. From the current experiments it is not possible to give general recommendations along these lines, however, a coupling interval of three hours is not sufficient to constrain the development of the mesoscale disturbances. In high resolution (below 5 km) applications, most of the horizontal and vertical variability comes from explicitly resolved features. In order to achieve correspondence between the spatial and temporal scales and in order to
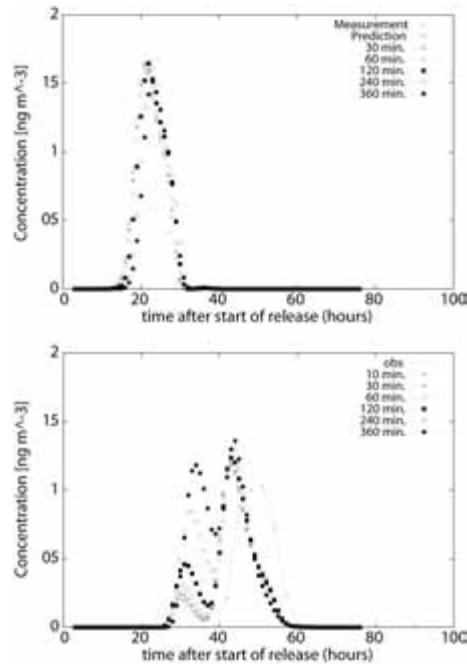
Figure 6.13: Top plot: Measured and simulated concentration (ng m^{-3}) as a function of time (hours) at ETEX-1 station F15 for coupling intervals: 30, 60, 120, 249 and 360 minutes. Bottom plot: Measured and simulated concentration (ng m^{-3}) as a function of time (hours) at ETEX-1 station DK02 for coupling intervals: 30, 60, 120, 249 and 360 minutes.
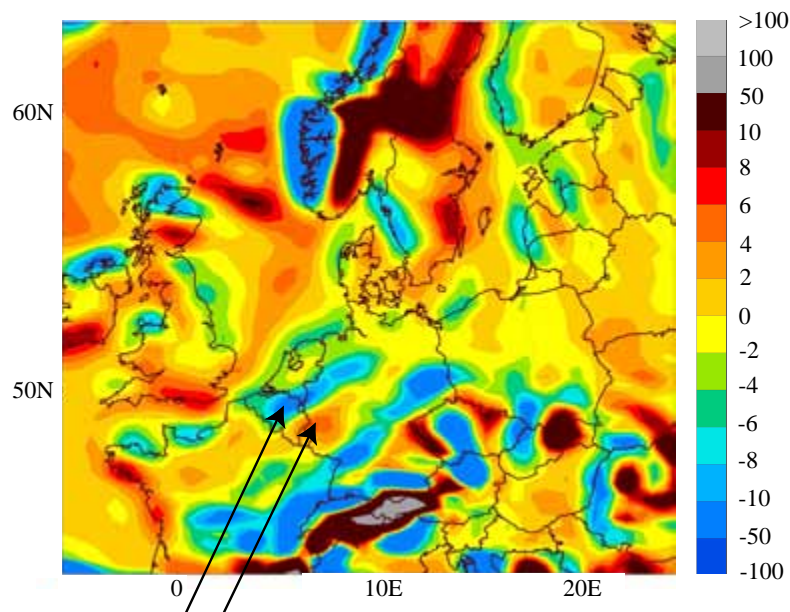
Figure 6.14: Relative vorticity (s^{-1}) at the lowest model level at 12 hours after start of release, from the online access simulation.

resolve the effects of mesoscale disturbances, it is necessary to use coupling intervals which are likely to be lower than one hour.

Conclusion

Enviro-HIRLAM performed satisfactorily when compared to the measurements made during ETEX-1. For stations close to the release site the model performed worse than for stations further
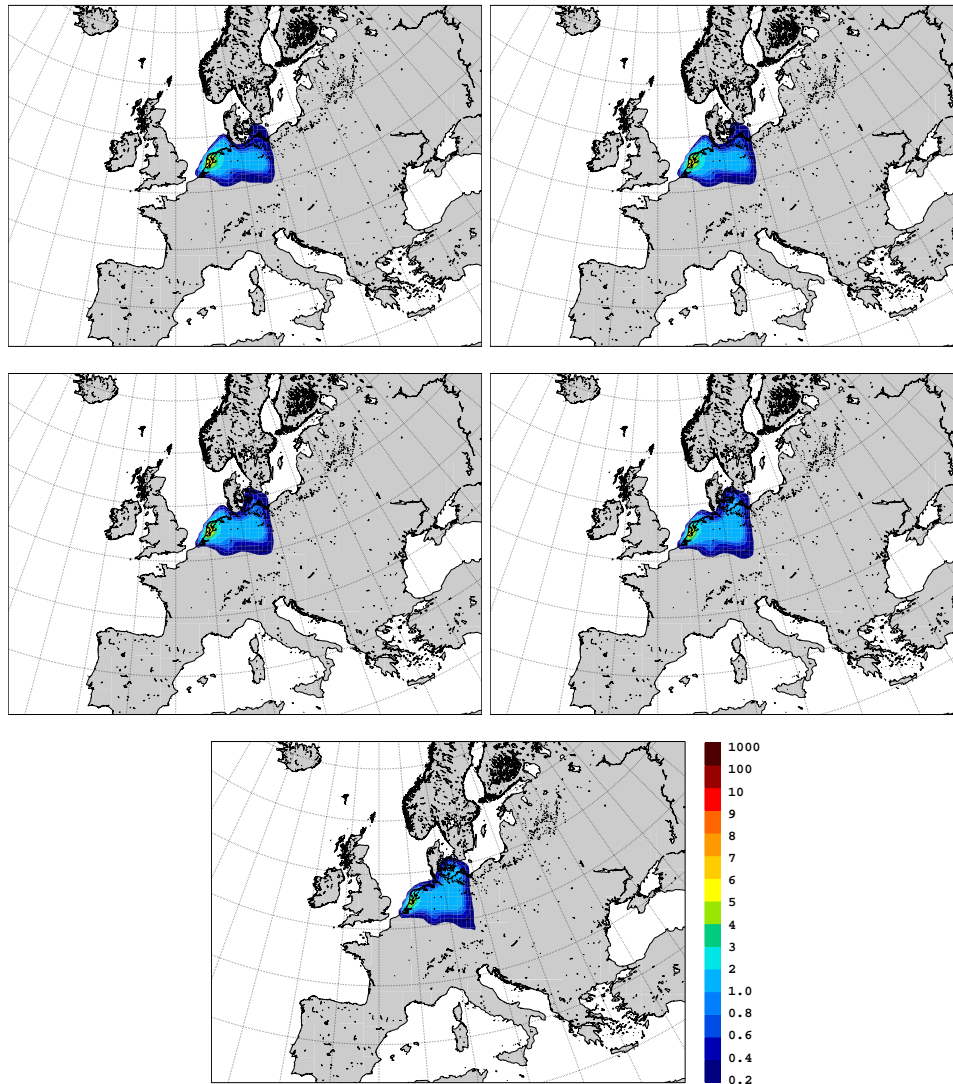
Figure 6.15: Surface concentration (ng m^{-3}) at 36 hours after start of release for coupling intervals: 30, 60, 120, 240, 360 minutes (left to right).

away, and an investigation into the large value of the global NMSE will be made in the future. The concentration field measured at station F15 was not influenced by mesoscale disturbances. At station DK02 mesoscale disturbances modified the plume structure (as found for other models as well), resulting in a double peak structure, which did not exist in the observations. The influence of the eddies was over-predicted as compared to the measurements which showed a similar structure further to the south. The over-prediction was due to insufficient temporal resolution, and as the coupling interval became shorter, the amplitude of the spurious peak decreased.
Mesoscale eddies may exert important influences on plume (urban or other) structure during long-range transport, and if the variability of a mesoscale disturbance is not resolved the coupling interval is an important factor in controlling the influence of the eddies on the plume. Hence, a coupling interval which is too large compared to the characteristic time-scales of the mesoscale eddies in a given meteorological situation, may result in large errors at specific stations, even at coarse resolution. Due to their short characteristic time scales mesoscale eddies are best represented in online access or online coupled models, where they are explicitly resolved.

Table 6.6: Different measures of computational performance for two simulations with and without chemistry and aerosols.

All processors	Without chemistry	With chemistry	Ratio[a]
Lon $\times$ Lat	730×682	90×74	–
Number of advected species	1	24	–
Number of procs.	6	8	–
Forecast length (h)	70	48	–
Real time (s)	62466	16866	39.25
Cpu-time (s)	374063	134298	52.19
Memory consumption (GB)	28.67	7.38	37.42
Vector optimization ratio ($\%$)	89	87	–
Average vector length	230	84	–

[a]A ratio larger than one indicates an increase when including chemistry. The ratio's are based on normalized values. Note that the values shown here were obtained on a non-dedicated system and therefore are associated with some uncertainty.

Computational performance

The computational performance is of great importance with respect to operationalization of the model, but not of particular importance when used in research mode, as in this project. Therefore, there has not been any efforts in trying to optimize the model, except for what has been described in chapter 3.

Table 6.6 compares two simulations, one including chemistry and aerosols and one without. The cpu-time is evenly distributed among the processors, indicating an even work load between the processors. In order to compare the output it is assumed that the scalability is good up to eight proessors and the simulation without chemistry is scaled to account for forecast length, number of processors and number of grid-points (Lon $\times$ Lat). The resultant ratios between real-time, cpu-time and memory comsumption are displayed in table 6.6. The large increase in real time (also denoted wall clock time), cpu-time (based on clock cycles) and memory consumption underlines the importance of generating effecient chemistry schemes for online models, using as few species as possible. The vector optimization ratio, which expresses the fraction of the code which has been vectorized, is quite low and does not change much when chemistry is added, i.e. the ability of the compiler (the NEC sxf90) to vectorize the coded is not affected by the inclusion of chemistry. However, the values in both cases are too low and should be closer to 98% for good optimization, this expresses a general problem with the HIRLAM optimization, rather than a problem with the chemistry code. The vector length, however, is severely reduced. On the SX6 architecture this value should be as close to 250 as possible and 87 is a very low value. Hence, the chemistry code should be optimized if the model is to executed operationally on a vector machine.

Summary and conclusions

Several simulations were carried out in order to investigate the models ability to transport, disperse, deposit and chemically transform species. Passive transport and dispersion was tested against measurements made during ETEX-1. The simulation showed that the model performed satisfactory but has a tendency to overpredict concentration values near point sources, which may in part be related to the use of resolution dependent Eulerian point sources. Another factor that might degrade performance is the presence of unresolved (spatially and temporally) mesoscale disturbances in the

meteorological fields. Several stations show double peak structures in the temporal development of the tracer concentration and the case study presented here indicates that if such disturbances are not resolved they may affect the statistical performance at stations located in the outer regions of the plume where concentration is low. Hence, part of the bias and NMSE may be explained by insufficient spatial and temporal resolution.

This issue, however, is of a more general nature. The temporal variability resolved by offline models is controlled by the coupling interval and in practice it may be necessary with coupling intervals below one hour in order to resolve the effect of mesoscale eddies on plume development. Hence, if detailed tracer concentrations are required, online access or online coupled models might be advantageous. It should be noted that during ATMES-II model ranking procedure they did not find any relationship between the level of sophistication of the models (or between Eulerian and Lagrangian models) and their ranking. However, the models employed all had rather poor resolution and therefore improvements are not necessarily expected.

The simulation of the Chernobyl accident showed that the model had a large positive bias, which is also connected to the issues mentioned above. However, considering the uncertainties in source strength, release height, that the particles were mono-disperse and the coarse horizontal resolution the model performs well.

One-dimensional testing of the gas-phase chemistry scheme showed that it performs well in comparison to more elaborate schemes. In a three-dimensional case study, including only a single case, it was shown that the model predicts NO_2 concentration satisfactory away from the source areas.

In all tests the model performs well in comparison with other models and the general conclusion is that the model performs satisfactory, however, keeping in mind the tendency to overpredict concentrations near point sources. There are two ways to prevent such overpredictions in the future and thereby make the model more precise close to the source regions. By implementing an emission model which assumes a distribution of the species inside the emission grid box, some of the problem may be solved. Currently, the source point is located in the lowest model layerwhich is located approximately 30 meters above the surface. Vertical redistributions of certain SNAP codes would also releave some of the problem. For example NO_x's are emitted both from traffic and from industrial stacks, hence, some of the mass corresponding to the stack emissions should be redistributed to higher levels. Preliminary testing of the computational performance of the model, showed that including chemistry and aerosols in Enviro-HIRLAM increases runtime by a factor of 40, however, there is room for strong optimization since the vector length decreases dramatically when chemistry and aerosols are included. These issues should be resolved before any operational testing commence.

Integrated modeling of aerosol indirect effects

It is well known that aerosol and trace gas distributions vary with very short time scales due to the influence of spatial and temporal variability in meteorological, chemical and emission fields. Chemical weather considers the aerosol and trace gas distributions and their variability on time scales of minutes to days. Therefore, the distributions are sensitive to circulations on the meso and local scales. On such temporal and spatial scales interactions between short timescale disturbances, such as urban, land and sea -breeze circulations, frontal circulations, cloud and precipitation development and flow bifurcations cannot be neglected, hence, the need for online models. Through changes in the surface radiation budget and condensation/evaporation processes clouds and precipitation play a major role in shaping the chemical weather. As described in the introduction several pathways exist for aerosol-meteorology feedbacks, and their importance in predicting the variations in aerosol and trace gas fields are largely unknown. The aerosol indirect effects acts through clouds and force[1] radiatively local and mesoscale circulations, hence, they may be important for chemical weather. This view is justified and investigated further in this chapter, in order to show that specific meteorological situations may exist where the hypothesis of this study is correct. The implementation of the first and second aerosol indirect effects in Enviro-HIRLAM was considered in chapter 3.9.

In the first part of this chapter the theoretical and observational basis for the aerosol indirect effects are considered and in the second part experiments on the importance of the aerosol feedbacks for trace gas distributions are presented. In order to constrain the investigation sufficiently only warm phase clouds are considered and the time scales in consideration, range from minutes to one day.

Current understanding of aerosol indirect effects

The premise of the aerosol indirect effects is an increase in CCN concentration and a decrease in the effective radius of the cloud droplets as the aerosol number concentration increase. Hence, activation of the aerosols is coupled to the aerosol number concentration, the water vapor field and to the properties of the CCN. The classical approach to aerosol activation is based on Köhler theory. Clouds form when air masses are subjected to isobaric or adiabatic cooling and hygroscopic aerosols experience supersaturations which are large enough to cause activation. Assuming that the aerosols contain a readily dissolvable solute, the saturation (S) relative to a flat pure water surface becomes:

$$\text{Ln}S = \frac{A}{D} - \frac{B}{D^3} \tag{7.1}$$

where $A = 4M_w\sigma_w/(RT\rho_w)$ is the Kelvin term, with M_w the molecular weight of water, ρ_w the density of water, σ_w the surface tension of the droplet, R the gas constant, T the temperature and D the diameter. The $B = 6n_sM_w/(\pi\rho_w)$ term represents the effect of the solute with n_s the solute moles. The derivation of equation 7.1 assumes equilibrium between the aerosol and ambient saturation fields. However, for sufficiently large aerosol load non-equilibrium situations may arise and the mass transfer from the ambient environment to the aerosols is limited [163, 39]. Therefore, classical Köhler theory may not be directly applicable in urban environments where aerosol concentrations are high. The derivation also assumes that the solute is completely soluble, however, in the real atmosphere aerosols often consist of partly- or in-soluble substances. Also the effects of trace gases dissolving in the aerosols, aerosol composition and mixing state on S are not included. These effects have been incorporated in a modified Köhler theory [123, 126], however, for the

---

[1]Following the IPCC definition of a radiative forcing; strictly speaking, the second indirect effect may not be categorized as a radiative forcing.

illustrative purposes here, the classical expression suffice. The critical supersaturation (S_c) of an aerosol may be evaluated from equation 7.1 and depends on its dry diameter (d_s) as: Ln $S_c = $ k $d_s^{-3/2}$, where k depends on M_w, ρ_w, σ_w, R, T, the solute molecular weight and density, as well as the number of ions resulting from the dissolution of a solute molecule. If the ambient super saturation is greater than S_c the aerosol will be in an unstable equilibrium and grow spontaneously until the ambient supersaturation is sufficiently lowered. From the above it is clear that the aerosol saturation level is strongly dependent on aerosol size. A smaller droplet has a higher critical saturation level, hence, larger aerosols activate sooner than smaller aerosols. On the other hand the growth rate by mass transfer of water, from the environment to the droplet, is inversely proportional to the droplet diameter and a smaller droplet will grow faster than a large one and will evetually catch up in size [205].

The net effect of adding more aerosol in the size range suitable for activation may be examined by using a one-dimensional cloud model. Using an adiabatic Lagrangian parcel model which includes detailed cloud microphysics describing aerosol growth, activation and condensation, the effect of increasing the initial aerosol concentration was considered. The model was designed in the late 1970's and supplied by [60]. Aerosols are represented by 55 size classes of equal width describing the diameters in the range 1 to 25 μm and by five solubility classes, specified as the mass fraction of soluble material (here specified as 0.4, 0.6, 0.75, 0.85, 0.05, where 0 corresponds to totally soluble and 1 to totally insoluble), resulting in 275 different categories of aerosols. The model considers a steady up-draught, w, and solves the coupled differential equations for condensational growth including equation 7.1, supersaturation, mass conservation, temperature and pressure. As an illustration of the effect of increasing the aerosol loading consider an up-draught velocity of $w = 1$ m s^{-1}, a cloud base temperature and pressure of $20°$C and 890 hPa respectively. The initial aerosol distribution is displayed in figure 7.1 and is adapted from a maritime data set. An aerosol factor of one corresponds to clean marine conditions as depicted in the figure, whereas a factor of two corresponds to increasing the concentration in all bins by a factor of two.

Figure 7.1 displays the response of the cloud droplet number concentration and cloud droplet effective radius to changes in the aerosol loading. As was expected the number concentration increases while the effective radius decreases for an increasing aerosol load. The responses to changes in aerosol concentration are greatest for clean clouds. Condensation acts as a sink for S and as the CCN load increase, S is gradually lowered inhibiting further condensation. The cloud liquid water content remains approximately at 0.2 g m^{-3} in all simulations since, w and cloud base temperature remain fixed. The dispersion of the cloud droplet spectrum (σ_p^2/r_{mean}, where r_{mean} is the mean droplet radius) increase from about 0.05 to 0.35 as the aerosol concentration increase due to the increase in effective radius. Cloud models, as illustrated above, generally led to an increase in droplet number concentration for an increasing aerosol concentration [170] and a large number of observations confirm that the cloud droplet concentration increase and the effective radius decrease with increasing aerosol loading, e.g. [52, 234, 89, 186, 20, 224, 115, 82, 237].

The first aerosol indirect effect

The first aerosol indirect effect (also denoted the Twomey effect) was first suggested by [225] and refers to enhanced reflection from clouds which have smaller droplets for fixed LWP. The increase in cloud albedo (A_{cloud}) due to a decrease in effective radius may be understood in terms of basic cloud radiative properties. These does not depend on the detailed microphysics of the clouds but on bulk properties such as the optical thickness, single scattering albedo and asymmetry factor and in particular the cloud albedo mainly depends on cloud optical depth. Following [205], $A_{cloud} = \tau/(\tau + 7.7)$ is found for droplets with radii much greater than the wavelength of visible light. The
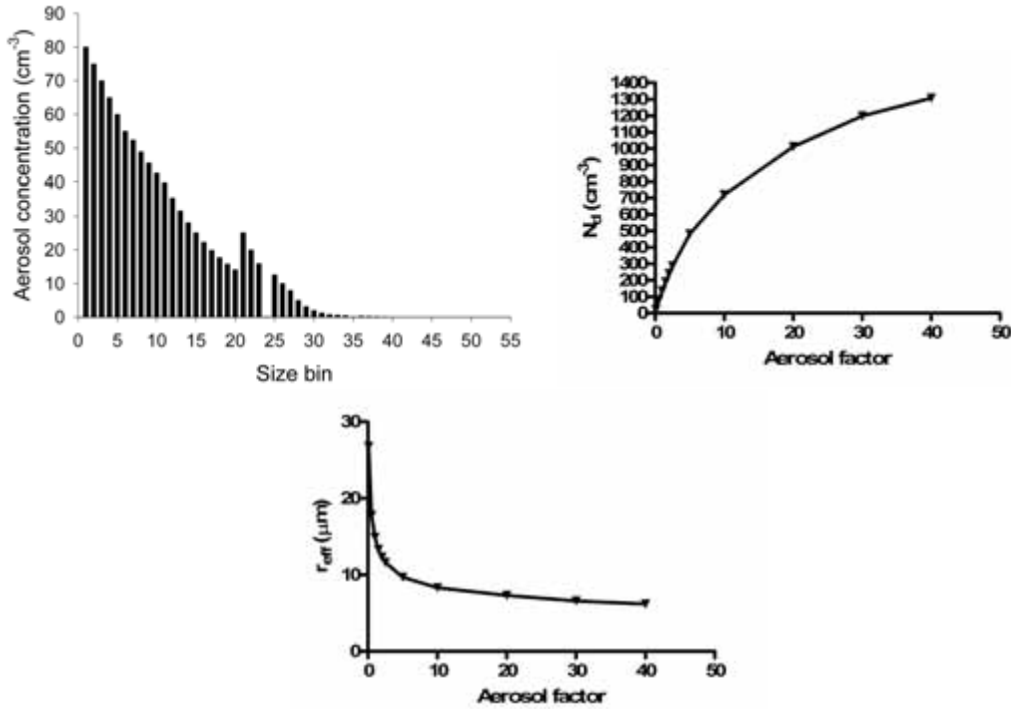
Figure 7.1: Top left: Initial aerosol number concentration for each size bin regardless of solubility, for an aerosol factor of one. An aerosol factor of 0.5 corresponds to a very clean case while a factor of 40 is a very polluted case. The right hand plot shows the cloud droplet number concentration as a function of aerosol loading. Lower plot: Cloud droplet effective radius as a function of aerosol loading.

optical thickness (τ) of a cloud is defined as the integral over the extinction coefficient in the direction of light propagation. In the Mie regime the extinction coefficient due to scattering and absorption of the cloud droplets is given as:

$$b_{ext}(\lambda) = \frac{\pi}{4} \int_0^{D^{max}} D^2 Q_{ext}(m, \alpha) n(D) dD \qquad (7.2)$$

where the refractive index m of all droplets is assumed identical, $n(D)$ is the size distribution, $\alpha = \pi D/\lambda$, λ is the wave length of the incident light, Q_{ext} is the extinction cross section, N is the droplet number concentration, D is the droplet diameter and D^{max} is the largest diameter in the droplet population. Following [205] a monodisperse cloud with droplet number concentration N and effective radius R_{eff} is considered. For visible wavelengths and for spherical droplets with diameters $D \approx 20$ μm, $Q_{ext}(2\pi r_{eff}/\lambda) \approx 2$. If the depth of the cloud is assumed to be h the optical depth is defined as $\tau = b_{ext}$h which then may be reduced to $\tau = 2\pi r_{eff}^2$Nh under the above assumptions. Using equation 5.5 it is found:

$$\tau = \frac{3LWP}{2r_{eff}\rho_w} \qquad (7.3)$$

where LWP is the liquid water path of the cloud. Hence, the optical depth, and thereby the albedo, of the cloud depends on its LWP and the effective radius of the cloud droplets. As r_{eff} decrease the optical depth increase leading to an increase in A_{cloud}.

The first aerosol indirect effect has received much attention due to its relevance for climate. Changes in A_{cloud} due to anthropogenic aerosols are expected to be of greatest importance for low clouds such as stratocumulus, which exerts a strong influence on the global shortwave radiation budget. Such

clouds radiate in the longwave end of the spectrum at the same temperature as the underlying surface and do, therefore, not exert a strong influence on the longwave budget. High clouds such as cirrus clouds, however, mainly affects the outgoing longwave radiation. Deep convective clouds do not occupy a large fraction of Earth's surface and are optically thick, leading to a small first aerosol indirect effect for this cloud type. They are, however, prone to modification through the second aerosol indirect effect. Due to their potential climatic importance there have been a large amount measurement campaigns focusing on these effects and it is supported by substantial observational evidence [167, 214, 132]. In situ measurements of ship tracks in stratocumulus clouds were amongst the first to document the effect [41, 61], but also remote sensing [174, 59, 83, 30, 113] and airborne measurements [87, 27] have been carried out.

The second aerosol indirect effect

The second aerosol indirect effect (also denoted the lifetime effect) was proposed by [2] and states that the suppression of drizzle in shallow maritime clouds (stratocumulus and fair weather cumulus), due to an increase in aerosol concentration, leads to increased LWP, cloud fraction and cloud lifetime and thereby act as an additional cloud albedo enhancement, affecting the surface radiative balance. Marine stratocumulus is of particular importance due to its persistence and large spatial coverage which implies they are of relevance in the global radiative balance. Furthermore, they contain only a low number of CCN and are therefore more sensitive to changes in aerosol loading. Therefore, most investigations have focussed on stratocumulus layers.

Suppression of precipitation in polluted clouds was first suggested by [235] who hypothesized that aerosol resulting from biomass burning suppressed rainfall. The suppression effect is well documented in observations [62, 87, 93] and current large eddy simulations (LES) including detailed microphysics supports that precipitation in stratocumulus and cumulus clouds is suppressed by the addition of aerosols [244, 105]. This effect seems much better documented than the influence on cloud lifetime, LWP or cloud fraction. As will be discussed in this chapter, recent results indicates that the above picture of increasing cloud fraction, LWP and lifetime is much too simplified. Once droplets have formed in a cloud they will either keep growing until a stable equilibrium is reached, evaporate or rain out, depending mainly on the ambient conditions. Growth proceeds by condensation. However, at around $10 \ \mu$m other processes start to become important [192]. These include collision and coalescence of the droplets. Droplets may collide because different sized droplets have different terminal fall speeds. Consider the collision between a large droplet of radius R and a smaller droplet of radius r. The importance of a collision depends on r/R and gR^3/ν^2 where ν is the kinematic viscosity and g is the gravitational acceleration. The collision efficiency is small if r/R is small and is without importance for $R < 10 \ \mu$m. Coalescence happens when two droplets collide in such a way that the water surfaces come into contact and the surface is destroyed over the area of contact. As the droplets coalesce a new larger droplet is formed. This process takes place in the size range of r $= 10 \ \mu$m to $100 \ \mu$m. As droplets become larger than approximately $100 \ \mu$m rain may be initiated.

Rain is produced by the collision-coalescence processes and not by condensational growth. The basic droplet size distribution is set up by condensation. The distribution then evolves through random collisions and at some point the coalesced droplets cannot be held against the up-draught velocity and starts falling. The droplet concentration field is highly variable, even within a well mixed cloud, and rain initiates as a few droplets fall through a local region of high concentration, and thereby experience a larger than usual number of collisions with smaller droplets. Hence, rain is initiated by statistical effects and then governed by collision-coalescence. A drizzle threshold at an effective radius around $15 \ \mu$m seems to exists for stratus clouds [67], hence, if the effective radius

drops below the threshold there will be no drizzling.

The premise of the second aerosol indirect effect is that as the effective radius decrease less droplets will be within the collision-coalescence size range and drizzling will be suppressed. Drizzle acts to remove cloud water, CCN and aerosols and may act to stabilize the subcloud layer. The stabilization occurs as drizzle evaporates and cool the boundary layer, which inhibits vertical mixing and promotes decoupling of the cloud layer [164]. Hence, suppression of drizzle should lead to an increase in LWP, cloud cover and cloud lifetime. An increase in LWP will then according to equation 7.3 lead to a further increase in cloud albedo.

Recent LES simulations have shown that LWP, cloud cover and cloud lifetime are not always coupled in the way envisaged by [2]. Clouds are a dynamical phenomena and the interaction between microphysics and dynamics may be of great importance. Recent studies using LES models show that suppression of heavy drizzling, due to increases in the aerosol load, induces a larger LWP [210] in line with the hypothesis of the second indirect effect. As heavy drizzle reaches the surface and evaporates it leads to surface cooling and stabilization of the subcloud layer over land. Suppression of drizzle leads to stronger plumes, carrying more moisture, into the stratocumulus layer [171].

For lightly drizzling stratocumulus evaporation of the drizzle drops, just below cloud base, may cause destabilization of the cloud layer. Suppression of the drizzle leads to a more stable cloud layer and cumulus plumes carrying moisture into the layer are suppressed [104]. If humidity above the cloud layer is low more vigorous entrainment may lead to a decrease in LWP [57, 137]. Furthermore, such simulations suggest that the suppression of rain-out of the cloud does not always lead to increased cloud lifetime. When simulating the effects of aerosol on warm trade cumulus and warm convective clouds found that cloud fraction decreased in response to increased aerosol concentration [244, 245, 105]. They concluded that a balance between suppression of rain through the second aerosol indirect effect and more effective evaporation of small droplets exist. The rate of change due to droplet evaporation is governed by:

$$\frac{dr}{dt} \propto \frac{S}{r}$$

For high aerosol loading and correspondingly small r_{eff} the evaporation is dominating the suppression of rain, leading to shorter cloud lifetime, while for low aerosol loading cloud lifetime increases due to the lifetime effect. It should be noted that this result was obtained for small cumulus clouds of order 100 m. The lifetime effect is inherently difficult to observe and to my knowledge no direct observations of the cloud lifetime has yet been made. LWP has been observed to both increase, decrease or remain unaffected by the presence of anthropogenic aerosols [180, 42, 84, 61, 185, 116, 4].

Urban areas are major emitters of anthropogenic aerosols and affect cloud properties both in the vicinity of the urban area and far removed from it [129, 144]; [193] reported a complete shut off of precipitation from clouds with cloud top temperatures about $-10°C$. Urban areas have also been reported to increase precipitation an effect which is mainly due to the dynamics of the urban heat island which dominates the microphysical effect of an increased fraction of large CCN [88, 206, 156]. However, results from LES simulations indicate that polluted clouds are susceptible to precipitation enhancement by introduction of giant nuclei while clean clouds remain unaffected [58]. A CCN around 2 μm rapidly evolves into a collector drop of 20 μm thereby enhancing the collision-coalescence process.

It is often assumed that the lifetime effect applies for all cloud types, however, it was basically hypothesized for low boundary layer clouds with a relatively low concentration of cloud droplets.

Other types of clouds, including deep cumulus clouds, have significantly different life cycles and their maintenance are less dependent on drizzle. Conceptually, a decrease in effective radius of the droplets in a cumulus cloud, and the corresponding increase in evaporation leads to more vigorous entrainment of ambient air and correspondingly suppressed precipitation. Invigoration of deep convective rain clouds with cloud base temperature above 15°C, due to an increased anthropogenic aerosol load, has been observed by several authors, e.g. [240, 133, 14]. Deep convective clouds, usually extents above the zero isotherm and must be quantified as mixed phase clouds. In such clouds invigoration due to a decrease in effective radius may results from ice phase microphysics [194].

Aerosol-cloud feedbacks

Aerosol and trace gas distributions (and therefore the chemical weather) is mainly controlled by emissions, mixing strength, wind and removal processes. From the above discussion it follows that the aerosol indirect effects have the potential to modify all these processes, disregarding the emissions of anthropogenic species. Hence, the question of how important the indirect effects are in controlling the chemical weather is a valid one. The first indirect effect may be of particular importance if clouds are optically thin, while the second indirect effect is expected to be of importance for situations with light rain, which is more easily suppressed. Meteorological situations with a strong large scale forcing (strong synoptic wind) or heavy precipitation may simply remove the effects. Hence, for continental areas where the anthropogenic aerosol fraction is large, it is expected that the aerosol indirect effects may be of importance if the polluted region contains convective activity and light rain or drizzle.

The CCN concentrations are to some extent controlled by the aerosol-cloud feedbacks. This issue was considered by [7] who used a simple model of a cloud topped boundary layer and found two stable CCN concentration regimes, corresponding to a low concentration maritime regime and a high concentration continental regime. The maritime regime was characterized by low CCN concentrations maintained by a balance between removal by drizzle and marine sources, while the continental regime was characterized by suppressed drizzle and larger cloud albedo. Conceptually the feedbacks may act in two ways. As precipitation is suppressed, the changes in circulations may lead to a dynamical re-distribution of the aerosols and gases. This also includes changes in wet deposition due to modification of the precipitation and changes in dry deposition due to modified stability. The changes in meteorology may also lead to changes in chemistry. Cloud cover may efficiently suppress photolysis and modify surface temperature, leading to changes in chemical reaction rates. The next chapter is devoted to studying the importance of the aerosol indirect effects on trace gas distributions in a particular meteorological case.

Summary and conclusion

Increasing the anthropogenic aerosol load in the atmosphere leads to an increase in cloud droplet number concentrations and a decrease in droplet effective radius. This has been established through both observational and modeling studies. It is likewise well established that a decrease in effective radius leads to an increase in cloud albedo. A decrease in effective radius has also been observed to cause suppression of drizzle in stratocumulus clouds but the effects on LWP, cloud fractions and cloud lifetime may both lead to a positive (increase in cloud fraction, lifetime and LWP and negative second indirect effect, depending on cloud type and the ambient meteorological conditions, through aerosol/cloud microphysics-dynamics feedbacks. Such feedbacks may affect the processes most important in controlling aerosol and trace gas distributions. Clouds acts as both sources and sinks for aerosols and the feedbacks between aerosols and clouds affect the processes which are most important for aerosol and trace gas distributions. Hence, the chemical weather (timescales of

minutes to days) may in some meteorological situations be influenced by such feedbacks.

The second aerosol indirect effect in idealized settings

Before using the parameterization of the second indirect effect in the full three-dimensional model it is important to investigate its properties in a more controlled environment (see chapter 2). Therefore, before using it in the full three-dimensional model it was tested in a one-dimensional version of Enviro-HIRLAM. This procedure serves two purposes; to find out how appropriate it represents the second indirect aerosol effect, and investigate the dynamics of the feedbacks, i.e. what response is expected from the three-dimensional model. The former purpose is achieved by comparing the one-dimensional results with those from the microphysically detailed cloud models (LES model) presented in the previous chapter.

The parameterization of the second indirect effect was described in chapter 3. It is based on the autoconversion formula by [188] and is dependent on the number concentration of activated aerosols (see equation 5). In order to examine the response of the parameterization to changes in CCN concentration and to preliminary investigate the effect of rain suppression in a controlled set-up a one-dimensional version of Enviro-HIRLAM was constructed based on a pre-existing one-dimensional version of HIRLAM. In a sensitivity study the CCN concentration was varied between 10^2 cm^{-3} and $5 \cdot 10^3$ cm^{-3} and the response of the model atmosphere, when going from clean to polluted conditions, was analyzed. The meteorological case considered corresponds to a convectively unstable warm and moist boundary layer.

The model code is identical to that used in the three-dimensional experiments except for the dynamics which is simplified, but includes the main terms including the pressure gradient term, the Coriolis term and frictional effects. Horizontal and vertical advection can be explicitly specified. In these simulations 80 levels was used with 40 below 2000 m in the low troposphere. The initial conditions are specified with a lapse rate of 9 K/km and a relative humidity of 85% in the first three kilometers from the surface. Above three kilometers the atmosphere is stable with a relative humidity of 20% (figure 7.2 bottom panel). To simulate an idealized warm (tropical) atmosphere and to trigger convection the lowest model level was fixed (initially) at 27°C and the sea surface temperature was five degrees higher at 32°C. To simulate a case of weak large scale forcing, geostrophic wind was fixed at 10 m/s, accounting for weak advection. No chemistry or aerosol dynamics is specified and the CCN concentration values are kept constant in time during the simulations without vertical variation. The model can evolve freely due to the physical processes, but the surface temperature remains fixed (fluxes of, e.g. heat and moisture are not fixed). The simulations differ only with respect to the value of the CCN concentration and model is integrated out to 24 hours. The first hour may be regarded as spin-up.

The accumulated precipitation decreases as the CCN concentration increase and for the very polluted case with a CCN concentration of $5 \cdot 10^3$ cm^{-3} it almost shut off completely (left hand plot in figure 7.2). This behaviour is controlled by the value of the critical droplet size in equation 5. The value of $r_0 = 5 \ \mu$m is taken from [188] and is found by tuning the autoconversion parameterization against the real atmosphere. In principle a more appropriate value could exist for very polluted clouds; this issue has not been investigated further. For the other values of the CCN concentration the accumulated precipitation varies between approximately 6 and 2.5 mm when increasing the CCN concentration. LWP increase with increasing CCN concentration as expected from the hypothesis of the second indirect effect (figure 7.2 top panel right hand figure). The LWP contains fluctuations due to numerics and statistical effects of the convection. For a very large pollution load a steady state is not reached. The accumulated moisture flux from the surface to the atmosphere varies between 18
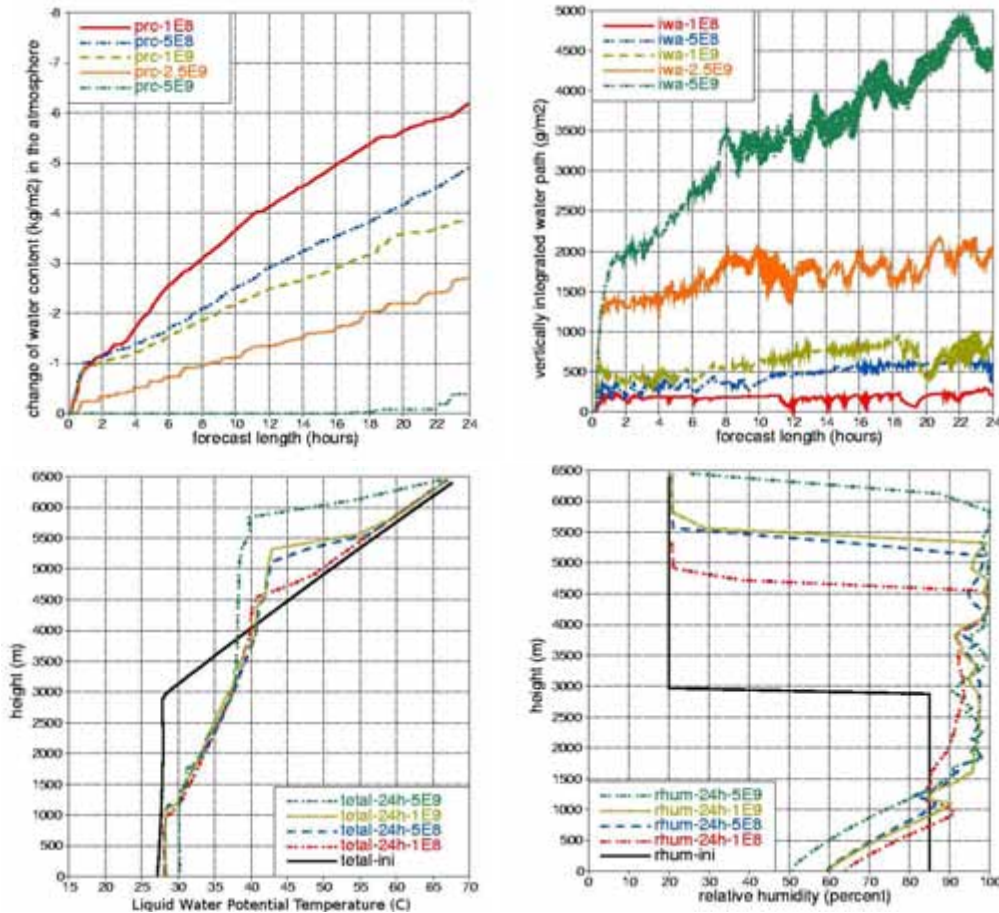
Figure 7.2: Top panel: Left hand plot, precipitation release versus time, negative values indicate removal from the atmosphere. Right hand plot, LWP versus time. Bottom panel: Left hand side, liquid water potential temperature (C) as function of height (m). Right hand side, relative humidity (%) as function of height (m). The black line corresponds to the initial conditions. The color code reflects the CCN concentration, red 10^8 m^{-3}, blue $5 \cdot 10^8$ m^{-3}, yellow 10^9 m^{-3}, orange $2.5 \cdot 10^9$ m^{-3} and green $5 \cdot 10^9$ m^{-3}.

and 22 mm when increasing the CCN concentration. The excess moisture (the part not returned to the surface as convective precipitation) raises the relative humidity (right hand plot in figure 7.2) at high levels, due to detrainment from the cloud top. In the boundary layer the suppression of precipitation leads to less evaporation and therefore a decrease in relative humidity. The middle plot on figure 7.2 displays the liquid water potential temperature (θ_l) as a function of height. Convection sets up an unsaturated well mixed boundary layer which is 1-1.5 km thick and the decrease in boundary layer evaporation leads to an increase in θ_l of a few degrees as the CCN concentration increase. Above the boundary layer the initial stable layer is eroded by convective overturning and θ_l remains approximately constant up to 3.5 km as the CCN concentration increase. Hence, a 2 km well mixed convective cloud layer is present above the boundary layer. The cloud layer extents further up and cloud height increase with CCN concentration. The increase in cloud water leads to more vigorous convection. Above the well mixed cloud layer cloud top radiative cooling and entrainment maintains a circulation giving rise to a θ_l which is almost constant with height. This part of the cloud is less coupled to the surface and, as ambient air is entrained, condensation leads to heating of the cloud layer. Therefore the structure of this layer may be strongly affected by the constant value of the CCN concentration with height. Another drawback of these simulations is that the effect of subsidence is not included. Strong subsidence could lead to large changes in the cloud structure and dynamics. In the stable layer above the cloud relative humidity decreases rapidly with

height and at a given height it increases rapidly with CCN concentration.

These idealized simulations compare well with the findings reported in the previous chapter (mainly for stratocumulus) and with the basic hypothesis of the second indirect effect. Increased CCN concentration leads to destabilization of the sub-cloud layer and more vigorous overturning. The suppression of rain leads to increased LWP, however, the effect on cloud lifetime and cloud fraction has not been considered. For reasonable values of the CCN concentration the parameterization of the second indirect effect seems to reproduce the low pollution case described above [244, 245, 105]. It should be noted that the cloud microphysics may be too simplified to account for the correspondng high pollution scenario. In the next chapter the parameterization of the second indirect effect is used in Enviro-HIRLAM together with a more precise description of aerosol dynamcis and activation.

Sulfate aerosol–meteorology feedbacks on short time scales in a convective case

This chapter has been submitted for publication as [122]

Abstract

The time scales of aerosol indirect effects render them potentially important for the prediction of local and regional scale air quality and weather forecasting. Suppression of rainout and albedo enhancement in convective clouds due increased number concentration of anthropogenic aerosols, may lead to changes in cloud cover, radiation and temperature, and thereby, to changes in local and regional circulations. In addition to changes in wet removal the aerosol and trace gas distributions may be affected directly by changes in circulation or through chemical transformations which are dependent on cloud cover and temperature. In this study representations of the first and second aerosol indirect effects were implemented in the online coupled model Enviro-HIRLAM. We considered a convective case with low precipitation and compared simulations with and without feedbacks to measurements of two-meter temperature and sulfate aerosol mass concentration. The influence of the aerosol indirect effects on the distribution of NO_2 was investigated. The model performed satisfactory when compared to measurements and the simulations including the aerosol indirect effects showed better statistical scores than the reference simulation. It was shown that the aerosol indirect effects exerted an important influence on the distribution of NO_2 through changes in dynamics rather than changes in chemistry. The second aerosol indirect effect dominated the first effect and its influence on two-meter temperature was stronger than the direct effect derived from other studies. Non-linearity was very important and the effects were not additive.

Introduction

Hydrophilic aerosols are a necessary condition for cloud formation. An increased load of small aerosols leads to an increase in cloud droplet number concentration, a decrease in cloud droplet effective radius, suppression of rain and increased brightness of warm clouds (the first indirect effect [225]). The second indirect effect states that suppression of rain leads to increased liquid water path, cloud fraction and cloud lifetime of stratocumulus clouds [2]. The time scales of the indirect effects are the same as those of clouds, ranging from minutes to hours and therefore they may feed back onto the aerosol populations on short time scales, changing both composition, deposition and dispersion. Only very few studies investigate such feedbacks (e.g. [253, 232]) and often the focus is on the impact on meteorology rather than the impact on chemical species. Aerosol-cloud interactions have traditionally been modeled in large eddy simulations which includes detailed cloud microphysics, but lack sufficient domain size to represent dynamical processes. In this study a short-range chemical weather model with a modified bulk cloud microphysics scheme to represent

the aerosol indirect effects was used.

Suppression of rain in convective clouds may modify the convective available potential energy leading to changes in small scale circulation patterns [193]. In a study of the combined influence of direct radiative effects of gases and aerosols and aerosol indirect effects, [35] found that cloud properties were quite sensitive to changes in anthropogenic aerosol number concentrations. Removing stack emissions led to large changes in cloud formation, radiative properties of the clouds and in precipitation, indicating that feedbacks are of great importance in local and regional weather. Specie concentration fields may be modified not only through dynamical effects, such as increased convection or modified boundary layer stability, but also through direct changes in chemical transformations due to, e.g. changes in actinic fluxes or temperature and therefore even small changes in meteorological fields may be of importance.

Meteorological and air-pollution models are reaching high resolution (below 5 km) and explicitly resolve much more variability than was previously parameterized. In order to produce accurate air pollution forecasts on these scales it is of importance to investigate the effects of the feedbacks between air pollution and meteorology.

The purpose of this study is to investigate the importance of the aerosol indirect effects on NO_2 concentration levels. Section 2 contains the methodology used, section 3 the model description, section 4 the simulation set-up, section 5 a discussion of the results and section 6 contains the conclusions.

Methodology

In order to study the influence of aerosol indirect effects on the NO_2 concentration levels, parameterized versions of the first and second indirect effects were implemented in the online coupled chemical weather model Enviro-HIRLAM [121]. The model contains representations of meteorological dynamics and physics, gas-phase chemistry and aerosol and cloud microphysics. Enviro-HIRLAM was used in a case study with convective activity, low precipitation and normal pollution levels. Simulations containing the first, second and both indirect effects (1IE, 2IE and 12IE respectively) were compared to a reference simulation containing no feedbacks (denoted REF) as well as to measurements of PM2.5 and two-meter temperature (T_{2m}).

Model description

Enviro-HIRLAM consists of the HIRLAM (High Resolution Limited Area Model) mesoscale short-range numerical weather predictio n (NWP) model along with gas-phase chemistry, aerosol microphysics and dynamics. For a more detailed description of HIRLAM the reader is referred to the documentation [226]. The chemical species are treated on the HIRLAM grid using the native parameterizations for convection [198] and vertical diffusion [48]. Advection is done using the scheme by [22, 23], while dry deposition follows [236] and wet deposition follows [205, 9]. The NWP-Chem gas-phase chemistry scheme [121] is based on the quasi steady state approximation [86]. The chemistry and aerosol schemes includes 24 advected species including NO_2, SO_2, HNO_3, O_3 and volatile organic compounds (VOC's). Using the simplified version of the chemistry solver there are four photolysis reactions and 17 gas-phase reactions, including NO_2 and O_3 chemistry, oxidation of SO_2 and photo-oxidation of VOC to peroxy radicals.

The gas-liquid phase partitioning in wet aerosols is represented using the analytical equilibrium iteration method [99]. Aerosol dynamics is described in a modal model, using two log-normal modes representing nucleation mode (radius up to $0.01 \mu m$) and accumulation mode (radius up to $0.1 \mu m$). Inter and intra-mode coagulation, condensation an d homogeneous nucleation [123] are represented and the accumulation mode aerosols may act as cloud nuclei. For the se experiments aerosol consists of H_2O, SO_4^{2-}, SO_3^{2-}, HSO_4^-, HSO_3^-, hence, the influence of NO_3^- , NH_4^+ and the
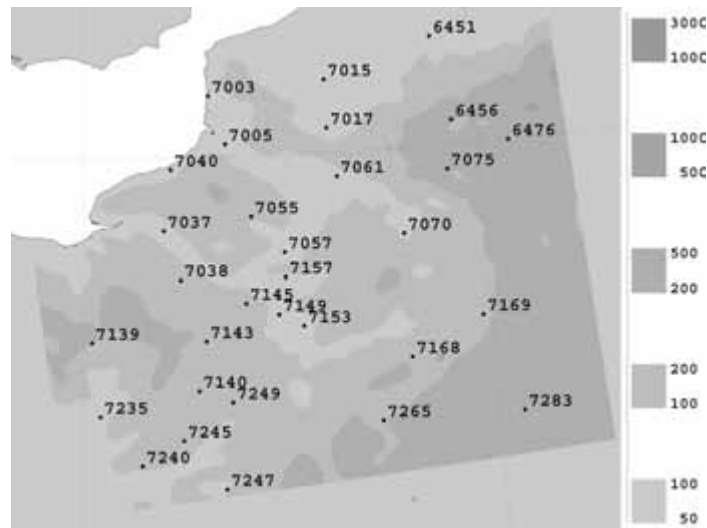
Figure 7.3: Modelling domain, displayed as surface geopotential height (m), including meteorological measurement stations used in the T_{2m} comparison.

organic fraction has been neglected.

A fraction of the accumulation mode sulfate aerosol may activate and act as cloud condensation nuclei. The aerosol number concentration is related to the cloud droplet number concentration using the parameterization by [26]. The Autoconversion formulation follows [188] and is dependent on the effective radius of the cloud droplets. The same holds true for the cloud radiative properties which follow [243]. By pertubing the natural background cloud droplet number concentration with the anthropogenic fraction the effective radius decreases affecting both autoconversion and the radiative properties of the clouds. As part of this work this approach was tested in a one-dimensional idealized test case and shown to produce results which are in line with the hypothesis of the second aerosol indirect effect, i.e. rain is suppressed and the liquid water path increases.

Simulation set-up

The effects were investigated over a 24 hour period during summer (30 June 2005 to 1 July 2005) on a domain, including Paris, extending 665 km × 445 km (longitude × latitude) in northern France (Fig. 7.3). The horizontal resolution was $0.05° \times 0.05°$ while 40 levels were used with 30 levels within the troposphere and the top level at approximately 10 hPa. The chemical spin-up was 24 hours, hence, the model was initialized at 00 UTC 29 June 2005 and the integrated until 00 UTC 1 July 2005 and only the results from the last 24 hours were considered. The meteorological spin-up is much shorter and aided by digital filter initilization.

Hourly boundaries and meteorological initial conditions were interpolated from the DMI-HIRLAM-S05 model, which is an operational weather forecast model at the Danish Meteorological institute, with $0.05° \times 0.05°$ degree resolution and which includes surface and upper air data assimilation. Inflow of chemical species was not considered and the chemical species were relaxed towards background levels in a boundary zone surrounding the modeling domain. Initial conditions for NO_2, O_3, HNO_3 and SO_2 were taken from the New England Air Quality Experiment [117], while the rest of the species are set to climatic values [78]. Emissions are taken from the GEMS-TNO emission inventory [231], with resolution ($0.125°$ longitude $\times 0.0625°$ latitude) and preprocessed to the model grid and read during run-time.

Synoptic situation

The synoptic situation during the simulation period was characterized by convective unstable air and cloudiness. On the 28 and 29 June 2005 a low pressure system, situated north-west of France, advanced towards the east. Heavy thunder showers were seen over the central and southern part of France. During 30 June a small low pressure system traversed the northern/north-western part of France resulting in continuous rain with precipitation up to 10 mm over the north-western part. The modeling domain was dominated by unstable, slightly cooler (as compared to the previous days) air with winds from a westerly direction and experienced small amounts of rain (about 5 mm). Anemometer level wind speeds were around 5 m/s during daytime and upper level winds were around 25 m/s (at 600 hPa).

Results and discussion

For the purpose of this study it is of importance to evaluate the model against measurements of T_{2m} and aerosol concentrations. There are 41 standard WMO (World Meteorological Organization) ground based stations available in the modeling domain for the temperature comparison. However, some of these had to be excluded due to their proximity to the boundary zone of the modeling domain and some contained too few measurements (less than one measurement every six hours). Therefore, the number of meteorological measurement stations used for the temperature statistics was reduced to 31, with data available every three hours at UTC terms (the location of the stations is displayed in Fig. 7.3).

The statistical quantities used to compare the REF and 12IE simulations are the linear correlation (R), the standard deviation (σ), the standard error of the mean (sem), the bias ($bias$) and the variance (var). These quantities are here defined as: $\sigma = (\sum_{i=1}^{N}(\psi_i - \overline{\psi})^2/N)^{1/2}$, where N is the sample size and ψ is the entity being sampled, $var = \sigma^2$, $sem = \sigma/\sqrt{N}$, $bias = \sum_{i=1}^{N}(\psi_i^m - \psi^p)/N$ and $R = \sum_{i=1}^{N}(\psi_i^m - \overline{\psi^m})(\psi_i^p - \overline{\psi^p})/\sqrt{\sum_{i=1}^{N}(\psi_i^m - \overline{\psi^m})^2 \sum_{i=1}^{N}(\psi_i^p - \overline{\psi^p})^2}$, where p represents predicted and m measured values.

Comparing to T_{2m} measurements
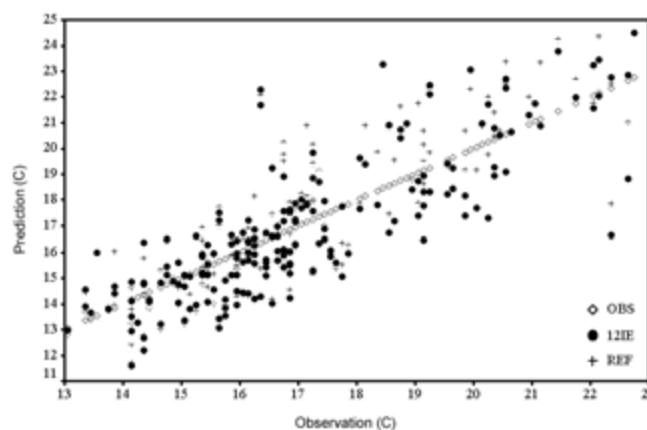
Figure 7.4: Global T_{2m} (C) scatter plot for REF and 12IE. Global statistical scores for the REF simulation is $sem = 0.11$, BIAS$= -0.17$, $var = 2.47$ and $\sigma = 1.57$, while the scores for the 12IE simulation is $sem = 0.11$, BIAS$= 0.14$, $var = 2.38$ and $\sigma = 1.54$.

For the global statistical scores (including all stations at all times) it was found found that the $bias$, σ and var decreased (Fig. 7.4) while the sem remained unaffected. The negative bias ($-0.17°C$) in the REF simulation was changed to a positive bias ($0.14°C$) in the 12IE simulation. The largest decrease

in bias was found during day and evening -time. The bias varied between $-0.67°C$ and $0.67°C$ in the 12IE simulation and between $-1.58°C$ and $0.81°C$ in the REF simulation. The global correlation decreased by 0.03 when going from the REF to the 12IE simulations. In general the inclusion of the first and second indirect effects led to decreased temperature during daytime and slightly increased temperature during nighttime (Fig. 7.5a), at stations where cloud cover changed. Figure 7.5a displays representative examples of stations located near such areas and near unaffected areas, along with the change from the observations. The sem and σ decreased slightly on most stations (61% out of total) located near cloud cover changes, while they remained unaffected or increased slightly at stations in other parts of the domain. Although, T_{2m} changed by more than $1°C$ between REF and 12IE at some stations sem and σ only experienced small changes. This is due to a general better performance during the day, where the clouds cooled the surface and a slight deterioration of the performance during night where the clouds mainly increased surface temperature. Considering an average over all the stations (Fig. 7.5b) it is found that the 12IE simulation performed slightly better than REF during daytime and was almost unaffected during nighttime.
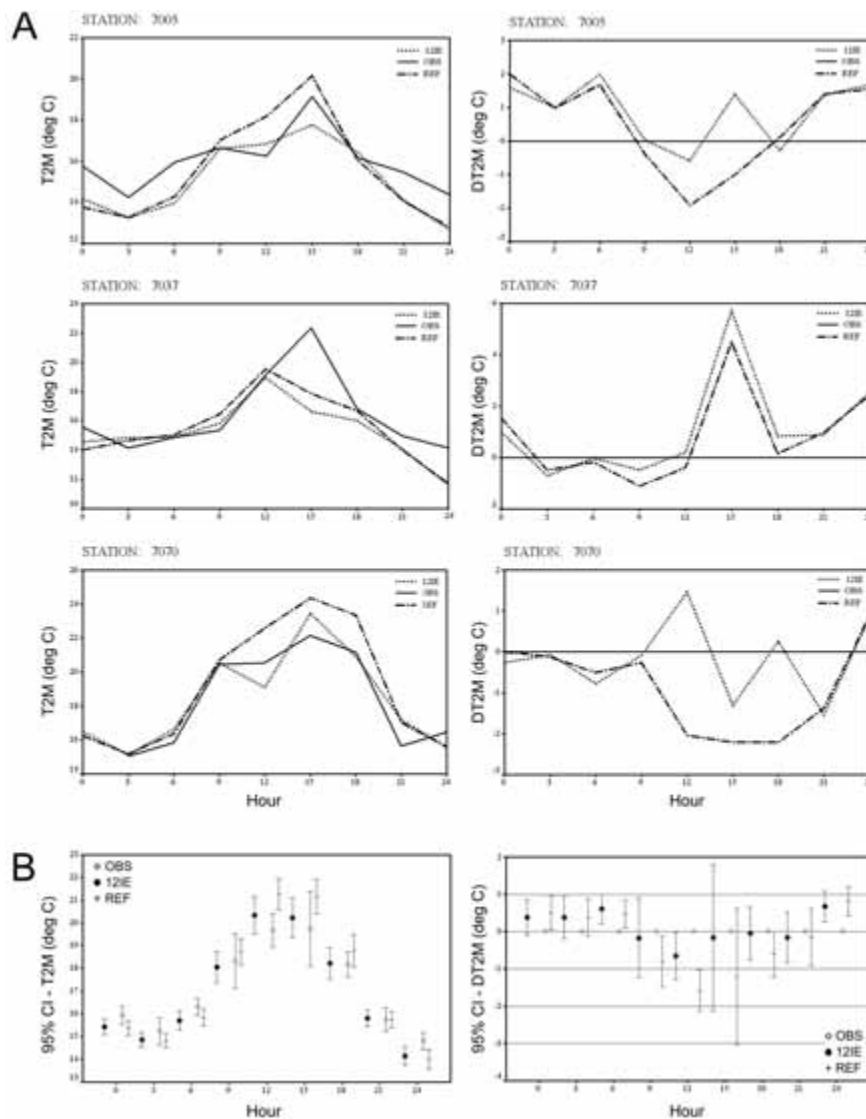

Figure 7.5: A: measured and predicted temporal T_{2m} (C) development at various stations (station id refers to figure 7.3) (right column) and the corresponding deviations between measured and predicted T_{2m} (C). B: Averages over all stations used in the T_{2m} comparison, with 95 % confidence intervals (left) and the corresponding deviations (right).

Comparing to PM2.5 measurements

The predicted total (nuclei plus accumulation mode) mass concentration of SO_4 was compared to observations made by the AIRPARIF air quality network, responsible for air quality survey over the IIe De France region around the Paris agglomeration (www.airparif.asso.fr). Hourly PM2.5 data from five urban and peri-urban stations were used, while the rest of the stations had missing values for this date. Measurements of PM2.5 mass and composition are quite uncertain (up to 50 %) [56]. In particular the volatilization of semi-volatile aerosol components (such as ammonium nitrate and semi-volatile organic material) during measurements leads to underestimation of the the semi-volatile components, resulting in, e.g. too large sulfate fractions. We assumed that approximately 15% of the PM2.5 was sulfate [191] and compared this to the hourly predictions made by the model. An average over the five urban stations along with the deviation from the observations is displayed in figure 7.6. The diurnal cycle is reproduced with maxima and minima corresponding to the observations. A negative bias is clearly seen, in both the REF and 12IE cases, and in the morning hours the deviation reaches 2 μg m^{-3}. The average deviation is -0.97 μg m^{-3} in the REF simulation and -0.87 μg m^{-3} for the 12IE simulation while the average observation, REF and 12IE values are 1.46 μg m^{-3}, 0.48 μg m^{-3} and -0.58 μg m^{-3} respectively. Hence, the 12IE simulations perform slightly better than the REF simulation, keeping the large uncertainty in the sulfate fraction in mind.
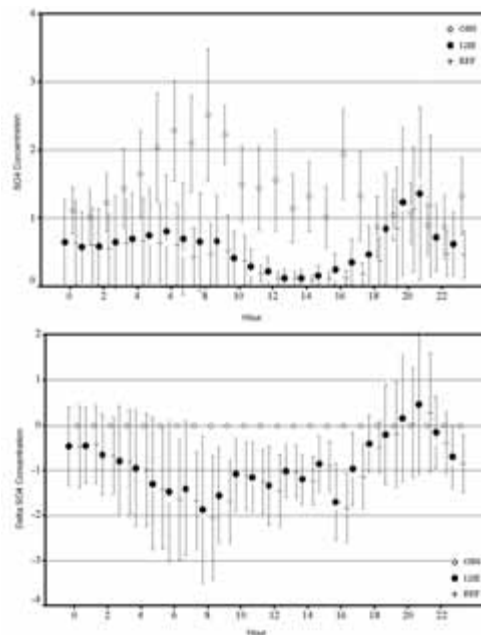
Figure 7.6: Upper figure: Average (over all stations) predicted and measured sulfate mass concentration (μg m^{-3}) versus time. Lower figure: Deviations between predicted and measured concentrations versus time.

Influence of the feedbacks on NO$_2$ concentrations

Close to Paris the spatial structure of the NO$_2$ plumes were mainly dictated by the emission strengths. Following the general wind pattern the plumes extended towards the east with maximum over Paris (Fig. 7.7A and B). Inclusion of the indirect effects led to large changes in NO$_2$ concentration in the lowest model level. In order to determine whether the first or second indirect effect were the main contributor to the effect separate model simulations were made where the first and second indirect effects were likewise excluded (the 2IE and 1IE simulations respectively). From figure 7.7 it is clear that the second indirect effect dominated both during night and day. The 1IE

simulation generated large changes in the NO_2 concentrations, thereby, underlining the nonlinearity of the effects.

Considering the daytime NO_2 maximum increase (49.2° N,2.7° E) (P1) the vertical profile changed, consistently with increased convection, by transporting NO_2 towards the surface (Fig. 7.7I). A corresponding change was found in the boundary layer height. A similar situation existed for the corresponding nighttime point, where strong vertical redistributions of the gases were found. From figure 7.7I it is also clear that the second indirect effect was also dominant in the vertical.

In addition to the dynamical changes induced by the feedbacks, variations in air temperature, relative humidity and cloud cover may directly influence chemical transformations of the NO_2 as well as scavenging by wet aerosols. In order to determine whether the feedback induced concentration changes were primarily of dynamical or chemical origin the NO_2 concentration tendency, at the lowest level, due to dynamical influences (convection, advection, and diffusion) and the tendency due to chemical and aerosol transformations were computed along with the dry deposition velocity. Changes in wet deposition were neglected since precipitation is low and only experienced a slight decrease of 1.5 mm outside the main plume, due to the second indirect effect. The inclusion of feedbacks mainly modified the dry deposition velocity over water and can therefore not explain the changes in the concentration field. The changes in dry deposition velocity is likely to be due to variations in atmospheric stability. Figure 7.8A shows that the dynamical tendency difference (between REF and 12IE) is an order of magnitude larger than the chemical tendency difference both during day and night. Hence, the dynamically induced forcing of the NO_2 concentration, due to feedbacks, was much larger than the forcing induced in chemical and aerosol transformations. The spatial distribution of the dynamical tendency difference correlates with the NO_2 concentration difference both during day and night. Although changes in the chemical transformations were induced by the feedbacks, the NO_2 concentration mainly changed due to dynamical influences.

The temporal development of the dynamical and chemical tendencies, in P1, for the REF and 12IE simulations shows that the change in dynamical tendency is much larger than the change in chemical tendency throughout the 24 hour period (Fig. 7.8E). During the morning hours the REF and 12IE dynamical tendencies are sometimes anti-correlated and changes sign, underlining the importance of the influence of the feedbacks in this particular case. Hence, the dynamical changes induced by the feedbacks drives the maximum daytime increase in NO_2.

The indirect effects gave rise to increased cloud cover (Fig. 7.9A). At individual locations the changes in cloud cover caused large changes in the surface temperature and therefore also in near surface air temperature (Fig. 7.9B). During night the maximum increase in two-meter air temperature was 1.5°C while during daytime the maximum decrease was 5°C. The changes in temperature facilitated the development of a residual circulation acting to redistribute the gases (Fig. 7.9c). The feedbacks tended to decrease the 10-meter wind speed by 4 m/s during night and 5 m/s during daytime. The existence of convergent and divergent regions in the residual circulation suggests increased convective activity. Comparing to studies including the direct aerosol effect [253, 232], it is seen that the temperature signal found here is several degrees larger, underlining the sensitivity of the surface radiation budget to changes in cloud properties. Hence, on these time scales the aerosol indirect effects may be of larger importance than the direct aerosol effects.

Additivity of the feedbacks

The importance of the non-linearity of the feedbacks may be examined further by subtracting the linear (results from adding the NO_2 concentrations from the 1IE and 2IE simulations) from the non-linear signal (NO_2 concentration resulting from simulation including both first and second aerosol indirect effects). The non-linear contribution was substantial (Fig. 7.10) and the order of magnitude was the same as the individual effects. Both during day and night, non-linearity leads to a
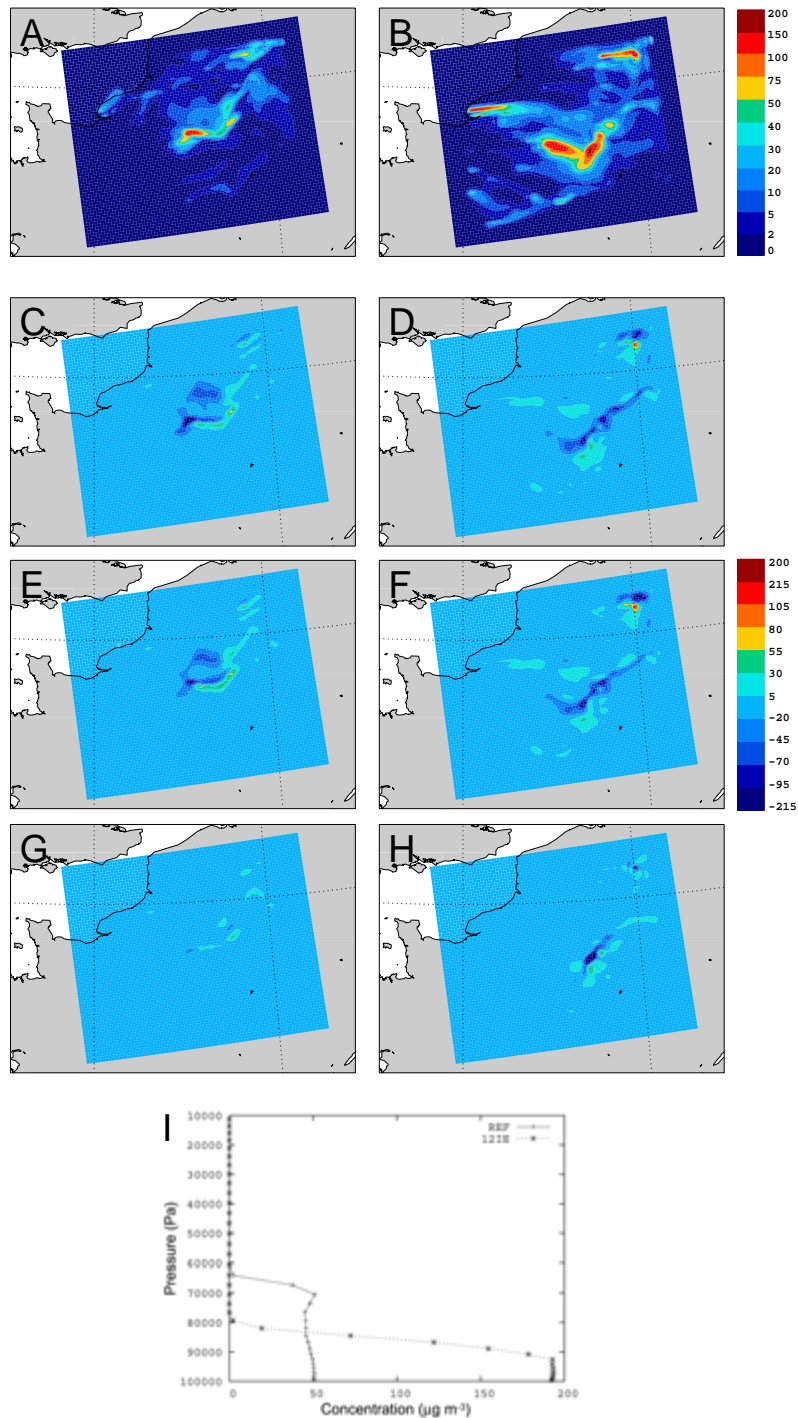
Figure 7.7: A and B shows the NO$_2$ concentration (μg m^{-3}) for the REF simulation, C and D shows the difference (REF-12IE) between REF and 12IE, E and F displays the difference (REF-2IE) between REF and 2IE, G and H displays the diffe rence (REF-1IE) between the REF and 1IE simulations. The left column corresponds to 12 UTC 29 June 2005 while the right column corresponds to 00 UTC 1 July 2005 respectively. I displays the the NO$_2$ concentration as function of pressure in the point P1 P1 (point of maximum daytime increase in NO2 concentration) during day (12 UTC 29 June 2005).

large (as compared with Fig. 7.7A and B) decrease of the NO$_2$ concentration. During night the maximum decrease was $235\ \mu$g m^{-3} while during daytime it was $180\ \mu$g m^{-3}. These findings underline the non-linearity of the convective and precipitative processes and indeed part of the NO$_2$ concentration changes observed could be due to such nonlinear changes in convection. Hence, in this case, it is of great importance to not constrain the non-linear degrees of freedom too much when

Figure 7.8: A and B displays the day (12 UTC 29 June 2005) and night (00 UTC 1 July 2005) -time dynamical tendency, whi le C and D shows the corresponding 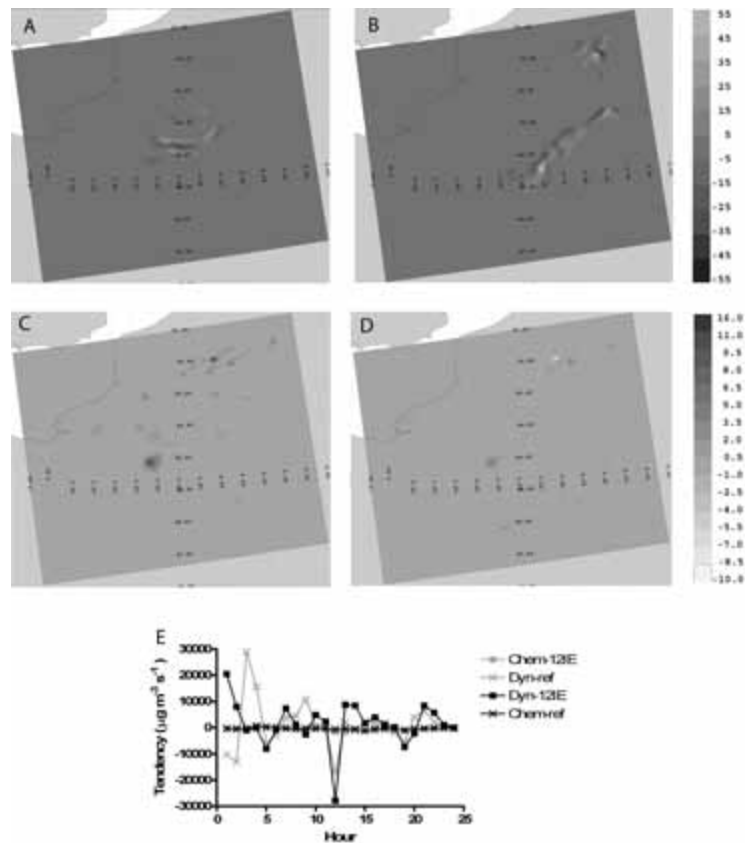chemical tendency. Plot E displays the temporal development of the dynamical and chemical tendencies for REF (Dyn-ref, Chem-ref) and 12IE (Dyn-12IE, Chem-12IE at the point P1 P1 (point of maximum daytime increase in NO2 concentration).

simulating aerosol-meteorology feedbacks. Models employing prescribed aerosol fields, may therefore exaggerate the indirect effects because they resrict some important degrees of freedom. The large nonlinear component underlines the importance of doing many case studies varying the meteorological and pollution conditions. Further studies are planned for the future.

This study considers warm-phase clouds only. It is possible that the inclusion of feedbacks through the ice-phase could act to decrease the signal found here. For instance, when aerosols are transported into supersaturated environments above the 0-isotherm they may lead to increased precipitation instead of a decrease. This could act to deplete the aerosols via wet scavenging. During this study very little precipitation was present and the effect of including the ice-phase is presently not clear.

Conclusion

Two-way aerosol-meteorology feedbacks, mediated through the first and second aerosol indirect effects, had important influences on the NO_2 concentration near the surface in a case with convective cloud cover and little precipitation. The change in NO_2 concentration was of order $100 \; \mu g \; m^{-3}$ during day and night. The first indirect effect seemed to be of considerably less importance than the second indirect effect which dominated in all respects. The concentration changes were mainly induced by dynamical changes in the dispersion of the species. The second indirect effect led to increased cloud cover and thereby in large changes in surface and air temperature. The induced residual circulation acted to redistribute the species both horizontally and vertically. Comparison of the model temperature and aerosol mass concentration against measurements showed that the
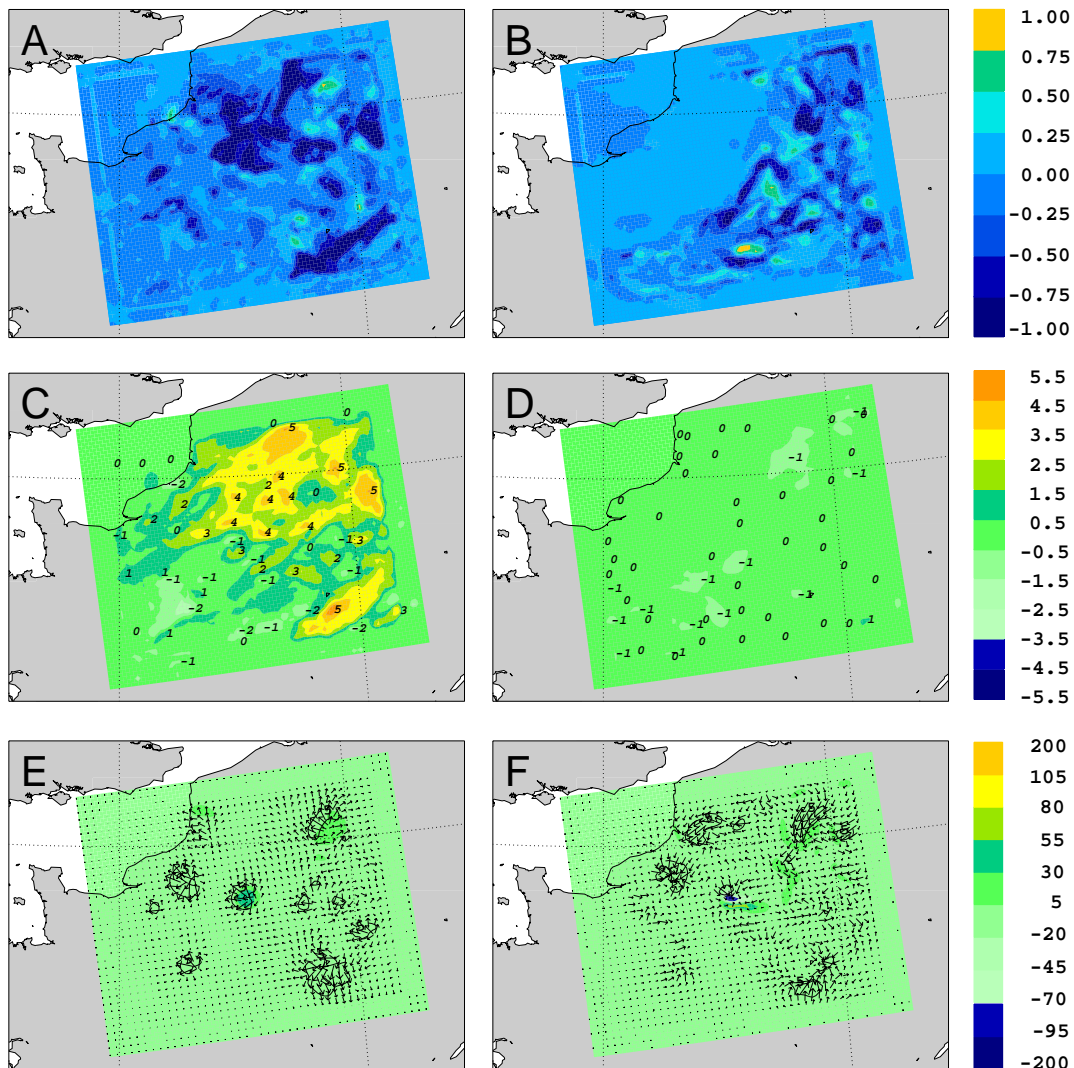
Figure 7.9: A and B: Day (12 UTC 29 June 2005) and night (00 UTC 1 July 2005) -time changes in cloud cover between REF and 12IE (REF-12IE). C and D: Corresponding day and night -time changes in T_{2m} (C) (numbers indicate local maxima). E and F: Residual circulation in the form of wind arrows at 850 hPa and 710 hPa superimposed on the corresponding changes in NO2 concentration (REF-12IE) (μg m^{-3}).

reference simulation performed satisfactorily and the overall performance improved slightly when the first and second indirect effects were included.

Non-linearity of the interaction between the aerosols and meteorology is important and acts to decrease the effect of the feedbacks on the NO_2. Therefore, models with prescribed aerosol fields may exaggerate the effects of the feedbacks. The study considered here consisted of a single meteorological case and therefore, no general conclusions should be drawn, especially in light of the non-linearity of the effect. Therefore, more case studies, in other meteorological situations, are required in order to fully understand the influence of these feedbacks on pollutant dispersion and transformations.

Summary and conclusions

The first indirect aerosol effect seems to be well understood in terms of both modeling and observations. The second indirect aerosol effect is difficult to observe directly and recent results from LES simulations show that it may be more complex than originally hypothesized. As the effective droplet radius become smaller (high pollution load) the droplets evaporate more easily
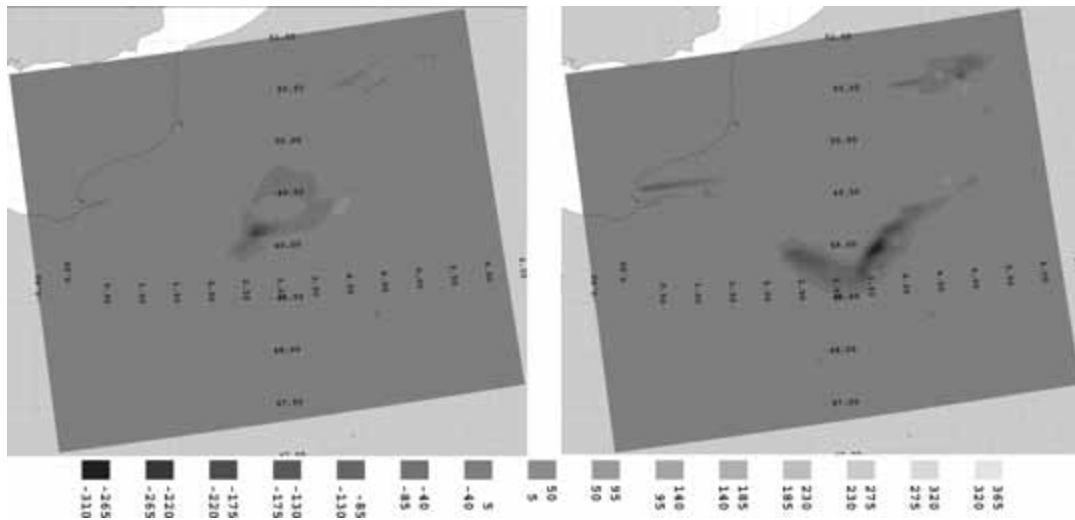
Figure 7.10: Day (12 UTC 29 June 2005) (left) and night (00 UTC 1 July 2005) (right) -time nonlinear part of the NO_2 concentration field (μg m^{-3}).

leading to shorter cloud lifetime while for low pollution load the situation is reversed.

Using a one-dimensional version of Enviro-HIRLAM in an idealized test case, it was shown that the parameterization of the second indirect effect reproduces the low pollution regime, leading to increased LWP. For high pollution load precipitation may be shut off and it was concluded that the parameterization is appropriate for low pollution levels.

In the full three-dimensional simulations the inclusion of the first and second indirect aerosol effects led to marginally better correspondence with observations of T_{2m} and aerosol mass concentration, in a case with convective activity and light rain. The effect of the feedbacks on the NO_2 concentration near the surface was substantial and the second indirect effect dominated the first at all times. The feedbacks led to a dynamical redistribution of NO_2 rather than changes in photolysis rates or chemical reaction rates. Nonlinearity played an important role in dampening the effect of the feedbacks and the first and second indirect aerosol effects were not additive.

General discussion and conclusion

The main hypothesis of this study is that *the aerosol indirect effects may exert an important influence on the distribution of aerosols and trace gases on short time scales*. In order to test the hypothesis, two objectives were defined. The main objective has been to develop a model which is able to simulate the aerosol indirect effects and the secondary objective has been to employ the model in a case study of the influence of the aerosol indirect effects on trace gas distributions. The HIRLAM model was used as a base for the new Enviro-HIRLAM online coupled chemical weather model. Several issues made usage of an online coupled model important. An offline model does not permit feedbacks between aerosols and meteorology because the timescales of the coupling would be too great (notice that in the definition applied here, usage of a very short coupling interval would lead to an online access model, which, although cumbersome, could include feedbacks). In addition, usage of an offline model is inappropriate because the time scales of the feedbacks are of the order minutes to an hour whereas the coupling interval in an offline model is typically one to three hours. Using an online coupled model removes post processing of the input fields (temporal and spatial interpolation), it does not apply an 'artificial' cut-off in the variability of the meteorological fields and it is possible to avoid inconsistencies. The last point is not trivial, even in online models. Dynamical cores often employ semi-implicit methodology and the model mass field is often a solution to an elliptic equation. Consistency of the tracer fields within this numerical set-up is challenging due to the numerics of the elliptic solvers (e.g. the Helmholtz solver in Enviro-HIRLAM). Furthermore, strict conservation of species mass does not automatically imply conservation of relative concentration fields, i.e. the ratio of species concentrations. Nonlinearity of the numerical schemes and the chemical equations may enhance errors if the concentration ratios are changing due to the numerical solution schemes. This effect, however, is believed to be of minor importance as compared to conservation of mass.

The effect of the coupling interval was investigated, in a simulation of the ETEX-1 release, by using the model in online access and offline mode, and concentration levels at individual stations were compared to observations. The main conclusion was:

- The meteorological coupling interval in an offline model may prohibitive of its transport and dispersion performance if the tracer is affected by mesoscale systems.

Mesoscale systems include breeze and frontal circulations as well as cloud and precipitation development. Such perturbations in the large scale flow have timescales which are below that of the coupling interval and they are therefore not resolved by the offline models.

Comparing to other online coupled models developed in Europe, Enviro-HIRLAM is the only one containing a representation of the second aerosol indirect effect. It should, however, be noted that the effect is not explicitly resolved (e.g. using a size resolved cloud model), but is based on parameterizations of aerosol activation and cloud properties. The only model in use in Europe containing explicit aerosol-cloud interactions is WRF-CHEM. Investigations using this model supports the basic hypothesis of this study. It can be questioned whether a bulk cloud microphysics scheme can represent the second aerosol indirect effect realistically enough to investigate the effects of varying the load of anthropogenic aerosols. However, in principle the sensitivity of the autoconversion formula could be too sensitive towards variations in the activated fraction of the aerosols. The parameterization of the second aerosol indirect effect was investigated in a one-dimensional version of Enviro-HIRLAM. The main conclusion was:

- The parameterization of the second aerosol indirect effect is applicable for normal pollution loads. In a case with deep tropical convection and precipitation the second aerosol indirect effect leads to more vigorous convection and increased liquid water path as hypothesized in the second aerosol indirect effect. These results are also in line with results from detailed LES simulations.

The model transport, dispersion and deposition capabilities were evaluated in simulations of the ETEX-1 release and the Chernobyl accidental release and compared to measurements of concentration and deposited Cs^{137}, respectively. The main conclusions of these simulations were:

- Enviro-HIRLAM performed satisfactorily in a test of its ability to transport and disperse a passive tracer. It was found that the concentration was overestimated close to the source regions, giving rise to a large global error. This is a consequence of the Eulerian treatment of the source point.

- Enviro-HIRLAM performed satisfactory in a test of its ability to dry and wet deposit Cs^{137}.

Currently, all source points are assumed to be located in the lowest model layer. This assumption, however, is not fulfilled for stacks which may extent further than 30 meters in the vertical direction. The overestimations of the concentration fields near source points may, therefore, partly be removed by including an emission model and by redistributing the emissions corresponding to, e.g. stacks in the vertical. The ability of Enviro-HIRLAM in combination with the NWP-Chem gas-phase chemistry scheme, to predict the concentration of NO_2 was investigated in a single case study, with convective activity and light rain. The main conclusion was:

- Enviro-HIRLAM using NWP-Chem scheme was shown to perform satisfactorily, away from major source points, when comparing predicted and measured NO_2 concentrations. During night the model slightly overpredicted the concentration and during day there was an underprediction.

The full three-dimensional model was used to simulate a particular convective summer case with light precipitation (the same meteorological case as mentioned above) and the influence of the indirect aerosol effects on the distribution of NO_2 was investigated. This simulation also included comparisons between predicted and measured T_{2m} and aerosol mass concentration. The key findings of these simulations were as follows:

- Comparison of T_{2m} and aerosol mass concentration with observations showed satisfactory performance of the model and inclusion of the first and second aerosol indirect effects led to a slight improvement in the performance.

- The feedbacks (through the aerosol indirect effects) led to changes in cloud cover and correspondingly large changes in temperature and wind fields.

- The feedbacks from the first and second aerosol indirect effects led to dynamical redistributions of NO_2 in the lowest model level. The changes were mainly due to increased convective activity.

- The effect of the feedbacks on dynamics was more important than the effect on chemistry.

- The second aerosol indirect effect dominated the first indirect effect.

- The first and second aerosol indirect effects were not additive and nonlinear effects were strongly dampening of the effects on the NO_2 concentration.

The case study presented here supports the main hypothesis of this study. The hypothesis is based on the fact that short time scale cloud feedbacks are already known to be of importance in local and regional circulations [215]. These include cloud-radiation feedbacks. All types of boundary layer clouds block out sunlight and shade the surface, resulting in fewer and weaker thermals, suppressing the growth of the mixed layer. Hence, this is a negative feedback on cloud development and may for some types of clouds cause decoupling from the surface. Another type of negative feedback is based on dynamics. If a cloud withdraws air from the mixed layer it causes suppression of the growth of the mixed layer and fewer thermals reach lifting condensation level. Other types of feedbacks (including positive ones) exist as well and the aerosol indirect effects are inducing changes in an existing feedback system and are therefore feeding back upon the aerosol distributions. However, general conclusions cannot be drawn from a single case study. Assuming that the hypothesis is correct, the interaction between weather and air pollution is stronger than previously assumed. This is mainly because pollutants such as gases and particles are global in nature and cannot be neglected. Currently, the aerosol number concentration over continental areas is one to two orders of magnitude larger than over marine areas. Hence, there is a significant impact on weather through changes in clouds, precipitation and the surface radiative balance.

As described previously in the introduction [232] found strong modifications of the shortwave radiation balance due to the aerosol direct effect. In this case mineral dust from desert sand storms acted as low clouds and blocked out sunlight. The radiative balance is very sensitive to changes in cloud cover. Feedbacks due to the aerosol direct effect have also been considered with WRF-CHEM [253], in this case over Texas where the aerosol concentration and composition is much different. Temperature changes below $1°C$, were found when comparing simulations with and without feedbacks, were found. The surface PM2.5 concentration was about $20 \ \mu g \ m^{-3}$ during most of the day and hence corresponded to a relatively high concentration. These simulations are not directly comparable to the simulations presented in this study but it is likely that the aerosol indirect effects will be of greater importance to weather and pollutant dispersal in certain meteorological cases, far away from sand storms. Such cases may include light rain, convective instability and low large scale forcing.

The aerosol indirect effects are of particular importance in climate modeling since the estimated global radiative forcing due to the aerosol indirect effects is about -0.5 Wm^{-2} thereby, these effects may counteract part of the warming due to the increase in greenhouse gases. The nonlinearity of the effects is consistent with climate studies showing that the sum of the radiative forcings adhering to the aerosol indirect effects is greater than the forcing from the combined effect [197]. Most current climate models applies imposed aerosol fields from offline CTM's and therefore do not include such feedbacks. This is mainly due to computational issues since high spatial resolution and cloud microphysics are computationally demanding. The results presented here show that it is possible to represent at least some aspects of the aerosol indirect effects using a simplified parameterization. Given the long time scales simulated with climate models and the nonlinearity of the chemical reactions it is likely that aerosol-cloud feedbacks will be of importance in climate modeling. The GATOR model has been used in a regional climate simulation to assess the aerosol direct, semi-direct and aerosol indirect effects in a one-month simulation nesting from a global domain ($4°$ $\times 5°$) to a domain covering parts of California ($0.045° \times 0.05°$). A reference simulation without aerosol feedbacks was compared to simulations including the feedbacks. Strong monthly and domain averaged feedbacks on the aerosol number concentration were found. The feedbacks acted to increase the near-surface number concentration of particles larger than 1 nm by 56% during

February and 43% during August. Near-surface aerosol liquid water content increased by 40% in February and 47% in August due to the feedbacks [103]. Although not directly applicable to the simulations presented here, it demonstrates that the feedbacks may be of importance to the distribution of aerosol and trace gas fields, also over longer time scales.

Feedbacks on short time scales have not previously been investigated in detail and a classification is currently lacking. A classification of aerosol-meteorology feedbacks could be based on the chain of processes relating the aerosols and meteorological fields: The presence of anthropogenic aerosols in the atmosphere leads to changes in the radiative balance, directly or through interactions with clouds, and to changes in condensation/evaporation processes. These changes can have two effects with respect to the aerosols: Either circulation changes are induced (dynamical or physical effect), which act to re-distribute the aerosols (including increased/decreases deposition), or chemistry is changed, modifying aerosol chemistry and equilibration. Changes in gas-phase and aerosol chemistry may be induced by changes in cloud cover, affecting the actinic fluxes, and leading to changes in photolysis rates or changes in chemical reaction rates due to temperature changes. Hence, two types of feedbacks may be introduced; those working through dynamical or physical effects and those acting through chemical effects.

Outlook

Using Enviro-HIRLAM as an air-quality model, focusing on ozone forecasting, will be considered and long term evaluation of its predictive skill will be carried out. Several research issues are planned: The general topic of aerosol-meteorology feedbacks and its consequences for weather and trace gas distributions will be examined in more detail. In particular the properties of the parameterization of the second aerosol indirect effect will be considered further in the one-dimensional set-up and then applied in the climate model HIRHAM [147] used at the Danish Climate Center for climate projections. A more detailed condensation scheme based on modified Köhler theory will be implemented in order to examine the effects of organics on the aerosol indirect effects. Feedbacks through the aerosol direct effect and gaseous absorption will also be considered. This work will be done in the context of various projects in which Enviro-HIRLAM is already in use. MEGAPOLI (Megacities: Emissions, urban, regional and Global Atmospheric POLlution and climate effects, and Integrated tools for assessment and mitigation) is a FP7 European Commission project (www.megapoli.dmi.dk) considering the effect of megacity pollution on local, regional and global weather and climate. The CEEH (Center for Energy Environment and Health) project seeks to economically optimize the use of energy systems in Denmark, accounting for externalities. During this study an Enviro-HIRLAM version for pollen prediction has also been developed (results not shown). This version consists of online coupled passive pollen transport, dispersion and deposition and an emission module for birch pollen, developed in collaboration with the Finish Meteorological Institute. The model is currently being tested and is expected to become operational for the 2009 pollen season. Similarly, an urbanized version including the effects of urban roughness, heat fluxes and urban albedo changes has been developed and is currently being tested (results not shown).

Several research groups are now involved in further developments of Enviro-HIRLAM. These include the University of Copenhagen (implementation of a new mass conserving consistent dynamical core), University of Tartu (aerosol-radiation feedbacks), Russian State and Hydro-Meteorological University (gas-radiation feedbacks, deposition), Tomsk State University (obstacle-resolved modeling with Enviro-HIRLAM), Belgium Royal Meteorological Institute (urban aerosol), Vilnius University (urbanization), and Odessa State Environmental University (boundary layer parameterizations and validation). In addition the HIRLAM consortium has opened a chemistry branch which is going to feature Enviro-HIRLAM with the NWP-Chem scheme as a baseline system. Hence, all HIRLAM member institutions may download, use and further develop

the model (non-HIRLAM member institutions are acquired to sign an agreement). The NWP-Chem scheme is being continuously developed and new versions will be implemented and tested in the context of the HIRLAM chemical branch.

Summary

The continental regions of the Earth are heavily polluted by aerosols in the size range important for cloud and precipitation development. These are mainly formed through secondary gas-to-particle conversion processes in the plumes of major urban areas. As clouds form in polluted air masses the hygroscopic aerosols will compete for the available water vapor, leading to the formation of more numerous but smaller cloud droplets for the same liquid water content. This in turn leads to increased cloud albedo and the suppression of rain and drizzle in warm clouds, and subsequent changes in cloud liquid water path, cloud fraction and cloud lifetime. These effects are denoted the first and second aerosol indirect effects and their influence on global climate is currently receiving much attention. However, recent results from large eddy simulations, including detailed representations of cloud microphysics, indicate that feedbacks between cloud dynamics and microphysics is of great importance in shaping the response to an increase in cloud droplet number concentration. The suppression of drizzle in stratocumulus and of rain in cumulus clouds may lead to more vigorous convection. However, since smaller droplets evaporate more easily than larger droplets, a large pollution load can also lead to a shortening of cloud lifetime. In either case the dynamical changes may be of importance to the distribution of aerosols and trace gases on short timescales (hours to days) as well as on climatic timescales. The aerosol and trace gas distributions may be affected by changes in wind, mixing strength, boundary layer stability or rainout. As cloud cover changes, the actinic fluxes are modified leading to modifications in photolysis rates, and temperature changes may lead to variations in chemical reaction rates affecting both trace gases and aerosols. In order to investigate the importance of such feedbacks on the trace gas distributions, a chemical weather model using a bulk cloud microphysics scheme and coupled aerosols and clouds through parameterizations of the first and second aerosol indirect effects was used. The model is based on a short-range numerical weather prediction model and with regards to spatial and temporal resolution it fits between climate and LES models. Meteorological dynamics and physics is represented and the evolution of the size-resolved aerosol number and mass concentrations were added, accounting for primary and secondary aerosol emissions, growth by condensation and coagulation, dry and wet deposition and gas-liquid phase equilibration. Trace gas chemistry is represented in a new chemistry scheme accounting for the processes of most importance for the evolution of the aerosol fields.

The model was tested for its ability to transport and disperse a passive tracer by simulating the release during the first European Tracer Experiment (ETEX-1) and comparing the modeled mass concentrations to measurements. Performance was good but an overestimation of the concentration close to the source led to a positive bias. Aerosol deposition was tested in a simulation of the accidental release of Cs^{137} during the Chernobyl accident. The model performed satisfactorily. The choice of an online model instead of an offline model was investigated by running the model in offline and online mode in a simulation of ETEX-1 and comparing the concentration fields at different stations. It was found that offline models are susceptible to large errors if the plume is affected by mesoscale eddies which have short timescales. The variability cannot be resolved by the coupling interval in an offline model. In a one-dimensional version the parameterization of the second indirect effect was considered in detail and it was found that increasing the pollution load led to increased cloud droplet number concentration, suppression of rainout and increased liquid water path, in line with the hypothesis of the aerosol second indirect effect. Whether the simplified parameterization can simulate some of the other properties found by detailed LES models is currently not known.

In a convective case, with light rain, the ability of the model to predict the mass concentration of sulfate aerosols was tested and found to be satisfactory. When comparing simulations with and without the aerosol indirect effects, it was found that two-meter temperature was predicted marginally better when the indirect effects were included. The mass concentration of NO_2 (and other trace gases) was heavily modified by the feedbacks. This modification was solely due to dynamical changes and not through the chemistry mechanism suggested above. When both the first and second indirect effects were included the first effect was without influence. The second aerosol indirect effect led to increased cloud cover in some areas of the modeling domain, and, correspondingly, to large changes in air temperature. A residual circulation with several convective cells redistributed the trace gases leading to large changes in concentration levels.

This work suggests that the aerosol-cloud feedbacks mediated through the aerosol indirect effects may be of importance for the distribution of aerosols and gases in cases with convective instability, light rain and normal pollution load. The study also emphasizes the need for online models in modeling cloud-aerosol interactions and aerosol and trace gas distributions.

References

[1]   AirBase - the European Air quality dataBase. European Topic Centre on Air and Climate Change: http://air-climate.eionet.europa.eu/databases/airbase.

[2]   Albrecht, B., 1989. Aerosols, Cloud Microphysics, and Fractional Cloudiness. Science, 245, 1227-1230.

[3]   Anderson, L., T., Charlson, J., R., Winker, M., D., Ogren, A., J., Holmen, K., 2003. Mesoscale Variations of Tropospheric Aerosols. J. Atm. Sci., 60, 119-136.

[4]   Andreae, M., O., Rosenfeld, D., Artaxo, P., Costa, A., A., Frank, G., P., Longo, K., M., Silva-Dias, M., A., F., 2004. Smoking Rain Clouds over the Amazon. Science, 303, 1337 - 1342.

[5]   Arteta, J., Cautenet, S., Taghavi, M., Audiffen, M., 2006. Impact of two chemistry mechanisms fully coupled with mesoscale model on the atmospheric pollutants distribution. Atmospheric Environment, 40, 7983-8001.

[6]   Atkinson, R., 1990. Gas-phase tropospheric chemistry of organic compounds: a review. Atm. Env. 24A, 1-41.

[7]   Baker, M., B., Charlson. R., J., 1990. Bistability of CCN concentrations and thermodynamics in the cloud-topped boundary layer. Nature 345, 142-145.

[8]   Baklanov, A., 2008. Personal communication.

[9]   Baklanov, A., Sørensen, J., 2001, Parameterisation of Radionuclide Deposition in Atmospheric Long-Range Transport Modelling, Phys. Chem. Earth. (B), 26, 787-799.

[10]   Baklanov, A., 2008: Integrated Meteorology and Atmospheric Chemical Transport Modelling: Perspectives and Strategy for HIRLAM/HARMONIE. HIRLAM Newsletter, 53, pp. 68-78.

[11]   Baklanov, A., Fay, B., Kaminsky, J., Sokhi, R., 2008. Overview of Existing Integrated (Off-line and On -line) Mesoscale Meteorological and Chemical Transport Modelling Systems In Europe. GAW report No. 177. Joint report of COST action 728 and GURME (www.cost728.org).

[12]   Baklanov, A., Korsholm, U. S., 2008. On-line Integrated Meteorological and Chemical Transport Modelling: Advantages and Prospectives. Air Pollution Modeling and its Applications XIX, NATO Science for Peace and Security Series - C: Environmental Security. [Borrego, C., Miranda, I. A. (eds.)], Springer.

[13]   Baklanov, A., Korsholm, U. S., Mahura, A., Petersen, C., Gross, A., 2008. ENVIRO-HIRLAM: on-line coupled modelling of urban meteorology and air pollution. Adv. Sci. Res., 2, 41-46.

[14]   Bell T. L., Rosenfeld, D., Kim, K.,-M., Yoo, J., -M., Lee, M., -I., Hahnenberger, M., 2008. Midweek increase in U.S. summer rain and storm heights suggests air pollution invigorates rainstorms. J. Geophys. Res., 113, doi:10.1029/2007JD008623.

[15]   Berge, E., Kristjansson, J., 1992. Numerical weather simulations with different formulations for the advection of humidity and cloud water. Mon. Wea. Rev., 120, 205-223.

[16] Berge, E., 1993. Coupling of wet scavenging of sulphur to clouds in a numerical weather prediction model. Tellus, 45B, 1-22.

[17] Bermejo, R., Conde, J. 2002. A conservative quasi-monotone semi-Lagrangian scheme. Mon. Wea. Rev., 130, 423-230.

[18] Binkowski, F., 1999, Aerosols in Models-3 CMAQ. In: Science algorithms of the EPA Models-3 community multiscale air quality (CMAQ) modeling system. EPA/600/R-99/030. 14.1-14.6.

[19] Black, T. L., 1994: The new NMC mesoscale Eta Model: Description and forecast examples. Weather Forecasting, 9, 265-278.

[20] Boers, R., Acarreta, J., and Gras, J., 2006. Satellite monitoring of the first indirect aerosol effect:Retrieval of the droplet concentration of water clouds. J. Geophys. Res., 111, doi:10.1029/2005JD006838.

[21] Bondietti, E, A., Papastefanou, C., 1993. Estimates of residence times of Sulfate aerosols in ambient air. Science of the total environment, 136, pp. 15-31

[22] Bott, A., 1989a. A positive definite advection scheme obtained by non-linear renormalization of the advective fluxes. Monthly Weather Review, 117, 1006-1015.

[23] Bott, A., 1989b. Reply. Monthly Weather Review. 117, 2633-2636.

[24] Bott, A., 1992. Monotone flux limitation in the area preserving flux-form advection algorithm. Mon. Wea. Rev., 120, 2592-2602.

[25] Bott, A., 1993. The monotone area preserving flux-form advection algorithm: Reducing the time-splitting error in two dimensional flow fields. Mon. Wea. Rev., 121, 2637-2641.

[26] Boucher, O., Lohmanmn, U., 1995. The sulfate-CCN-cloud albedo effect, a sensitivity study with two general circulation models. Tellus, 47B, 281-300.

[27] Brenguier, J., -L., Pawloska, L., Schüller, L., Preusker, R., Fischer, J., 2000. Radiative properties of boundary layer clouds: Droplet effective radius versus number concentration. J. Atmos. Sci., 57, 807-821.

[28] Brost, R. A., Haagenson, P. L. and Kuo Y.-H., 1988. Eulerian simulation of tracer distribution during CAPTEX. Journal of Applied Meteorology, 27, 579-593.

[29] Brown, P., Collier A., Grant, K., Hindmarsh, A., Lee, S., Serban, R., Woodward, C., 2 006. SUite of Nonlinear and DIfferential/ALgebraic equation Solvers, https://computation.llnl.gov/casc/sundials/main.html.

[30] Bréon, F., -M., Tanré, D., Generoso, S., 2002. Aerosol effect on cloud droplet size monitored from satelitte. Science, 295, 834-838.

[31] Byun, D., W., 1999a. Dynamically consistent formulations in meteorological and air quality models for multiscale atmospheric studies. Part I. Geoverning equations in a generalized coordinate system. J. Atm. Sci., 56, 3789-3807.

[32] Byun, D., W., 1999b. Dynamically consistent formulations in meteorological and air quality models for multiscale atmospheric studies. Part II: Mass conservation issues. J. Atm. Sci., 56, 3808-3820.

[33] Carissimo, B., Dupont, E., Musson-Genon, L., Lacour, S., Foudhil, H., Milliez, M., Albriet, B., Damael, E., 2004. Local scale atmospheric simulations with the Mercure-Saturne model (http://cerea.enpc.fr/fich/mercure/mercure_anglais_web.html).

[34] Carter, W., 1990. A detailed mechanism for the gas-phase atmospheric reactions of organic compounds. Atm. Env., 22A, 481-518.

[35] Chapman, E., G., Gustafson, W., I., Easter, Jr., R., C., Barnard, J., C., Ghan, S., J., Pekour, M., S., Fast, J. D., 2008. Coupling aerosol-cloud-radiative processes in the WRF-Chem model: investigating the radiative impact of elevated point sources. Atmos. Chem. Phys. Disc., 8, 14765-14817.

[36] Chenevez, J., 2000. Advection experiments with DMI-HIRLAM-TRACER. Danish Meteorological Institute, Scientific Report, 00-05, http://www.dmi.dk/dmi/index/viden/dmi-publikationer/videnskabeligerapporter.htm.

[37] Chenevez, J., Baklanov, A. and Sorensen, J. H., 2004. Pollutant transport schemes integrated in a numerical weather prediction model: model description and verification results. Meteorological Applications, 11, 265-275.

[38] Chlond, A., 1994. Locally modified version of Bott's advection scheme. Mon. Wea. Rev., 122, 111-125.

[39] Chuang, P., Y., Charlson, R., J., Seinfeld, J., H., 1997. Kinetic limitation on droplet formation on clouds. Nature, 390, 594-596.

[40] Ciarlet, P., G., Teman, R., Tribbia, J., 2009. Handbook of numerical analysis. Special volume: Computational methods for the atmosphere and the ocean. Volume XIV, North-Holland.

[41] Coakley, J., A., Bernstein, J., R., Durkee, P., A., 1987. Effect of ship track effluents on cloud reflectivity. Science, 327. 1020-1021.

[42] Coakley, J., A., Walsh, C., D., 2002. Limits to the aerosol indirect radiative effect derived from observations of ship tracks. J. Atmos. Sci., 59, 668-680.

[43] Colbeck, I., 1998. Physical and Chemical Properties of Aerosols. 1st Ed. Thomson Science, Blackie Academic & Professional.

[44] Colella, P., Woodward, P. R., 1984. The Piecewise Parabolic Method (PPM) for gas-dynamical simulations. J. Comp. Phys., 54, 174-201.

[45] Costa, A., A., Sampaio, A., J., C., 1997. Bott's area-preserving flux-form advection algorithm: Extension to higher orders and additional tests. Mon. Wea. Rev., 125, 1983-1989.

[46] Coté, J., Gravel, S., Méthot, A., Patoine, A., Roch, M., Staniforth, A., 1998a. The operational CMC MRB Global Environmental Multiscale (GEM) model: part I - Design considerations and formulation. Mon. Wea. Rev., 126, 1373-1395.

[47] Crassier, V., Suhre, K., Tulet, P., Rosset, R., 2000. Development of a reduced chemical scheme for use in mesoscale meteorological models. Atm. Env., 34, 2633-2644.

[48] Cuxart, J., Bougeaults, P. and Redelsberger, J., L., 2000. A turbulence scheme allowing for mesoscale and large-eddy simulations. Quarterly Journal of the Royal Meteorological Society, 126, 1-30.

[49] De Cort, M., Dubois, G., Fridman, Sh. D., Germenchuk, M., G., Izrael, Yu., A., Janssens, A., Jones, A., R., Kelly, G., N., Kvasnikova, E., V., Matveenko, I, I, Nazarov, I., N., Pokumeiko, Yu., M., Sitak, V., A., Stukin, E., D., Tabachny, L., Ya., Tsaturov, Yu., S., 1998. Atlas of Caesium Deposition on Europe after the Chernobyl Accident, EUR report nr. 16733, Office for Official Publications of the European Communities, Luxembourg, Plate 1.

[50] Desiato, F., Anfossi, D., Castelli, S., T., Ferrero, E., Tinarelli, G., 1998. The Role of Wind Field, Mixing Height And Horizontal Diffusivity Investigated Through Two Lagrangian Particle Models, Atmospheric Environment, 32 (24), 4157-4165.

[51] Devell, L., Guntay, S., Powers, D. A., 1995. The Chernobyl Reactor Accident Source Term: Development of a Consensus View. Paris CSNI report, OECD/NEA.

[52] Eagan, R., C., Hobbs, P., V., Radke, L., F., 1974. Measurements of cloud condensation nuclei and cloud droplet size distributions in the vicinity of forest fires. J. Appl. Meteor., 13, 553-557.

[53] Easter, R., C., 1993. Two modified versions of Bott's positive definite numerical advection scheme. Mon. Wea. Rev., 121, 297-304.

[54] Ekman, A., 2000. Implementation of an atmospheric sulfur scheme in the HIRLAM regional weather forecast model. Report, CM-96, International Meteorological Institute in Stockholm, Department of Meteorology, University of Stockholm.

[55] Fast, J. D., Gustafson, Jr., W. I., Easter, R. C., Zaveri, R. A., Barnard, J. C., Chapman, E. G., Grell, G. A., 2006. Evolution of ozone, particulates, and aerosol direct forcing in an urban area using a new fully-coupled meteorology, chemistry and aerosol model. J. Geophys. Res., 111, D21305, doi: 10.1029:2005JD006721.

[56] Favez, O., Cachier, H., Sciare, J., Moullec, Le, Y., 2007. Characterization and contribution to $PM_{2.5}$ of semi-volatile aerosols in Paris (France). Atm. Env., 41, 7969-7976.

[57] Feingold, G., Stevens, B., Cotton, W., R., Frisch,, A., S., 1996. The relationship between drop in-cloud residence time and drizzle production in numerically simulated stratocumulus clouds. J. Atmos. Sci., 53, 1108-1122.

[58] Feingold, G., Cotton, W., R., Kreidenweis, S., M., Davis, J., T., 1999. Impact of giant condensation nuclei on drizzle formation in marine stratocumulus: Implications for cloud radiative properties. J. Atmos. Sci., 56, 4100-4117.

[59] Feingold, G., Eberhard, W., L., Veron, D., E., Previdi, M., 2003. First measurements of the Twomey indirect effect using ground-based remote sensors. Geophys. Res. Lett., 30, doi: 10.1029/2002GL016633.

[60] Feingold, G., 2008. NOAA Earth System Research Laboratory, *Personal communication*.

[61] Ferek, R., J., Hegg, D., A., Hobbs, P., V., Durkee, P., A., Nielsen, k., 1998. Measurements of ship induced tracks in clouds off the Washington coast. J. Geophys. Res., 103, 23199-23206.

[62] Ferek, R., J., Garrett, T., Hobbs, P., V., Strader, S., Johnson, D., Taylor, J., P., Nielsen, K., Ackerman, A., S., Kogan, Y., Liu, Q., Albrecht, A., Babb, D., 2000. Drizzle suppression in ship tracks. J. Atmos. Sci., 57, 2707-2728.

[63] Forster, P. V., Ramaswamy, V., Artaxo, P., Berntsen, T., Betts, R., Fahey, D. W., Haywood, J., Lean, J., Lowe, D. C., Myhre, G., Nganga, J., Prinn, R., Raga, G., Schulz, M., Van Dorland, R., 2007. Changes in Atmospheric Constituents and in Radiative Forcing. *In: Climate Change 2007: The Physical Science Basis. Contribution of Working Group I to the Fourth Assessment Report of the Intergovernmental Panel on Climate Change*[Solomon, S., Qin, D., Manning, M., Chen, Z., Marquis, M., Averyt, K. B., Tignor, M., Miller, H. L. (eds.)] Cambridge University Press, Cambridge, United Kingdom and New York, NY, USA.

[64] Ganev, K., Dimitrova, R., Syrakov, D., Zerefos, C., 2003. Accounting for the Mesoscale Effects on the Air Pollution in Some Cases of Large Sulfur Pollution in Bulgaria or Northern Greece. Environmental Fluid Mechanics, 3, 41-53.

[65] Geiger, H., Barnes, I., Benjan, I., Benter, T., Splitter, M., 2003. The tropospheric degradation of Isoprene: an updated module for the regional chemistry mechanism. Atm. Env., 37, 1503-1519.

[66] GEMS: The Global and regional Earth-system (Atmosphere) Monitoring using Satellite and in-situ data EU project. Web site: http://gems.ecmwf.int/d/products/raq/verification/plot_RAQ_mean_scores/

[67] Gerber, H., 1996. Microphysics of marine stratocumulus clouds with two drizzle modes. J. Atmos. Sci., 53, 1649-1662.

[68] Gery, M., W., Whitten, G., Z., Killus, J. P., Dodge, M. C., 1989. A photochemical kinetics mechanism for urban and regional scale computer modelling. J. Geophys. Res., 94, 925-956.

[69] Ghan, S. J., Schwartz, S. E., 2007. Aerosol properties and processes, a path from field and laboratory measurements to global climate models. B. Am. Meteorol. Soc., 88(7), 1059-1083.

[70] Gong, S. L., Huang, P., Zhao, T. L., Sahsuvar, L., Barrie, L. A., Kaminski, J. W., Li, Y. F., Niu, T., 2007. GEM/POPs: a global 3-D dynamic model for semi-volatile persistent organic pollutants - 1. Model description and evaluations. Atmos. Chem. Phys., 7, 4001-4013.

[71] Graziani, G., Klug, W. and Mosca, S., 1998: Real-time long-range dispersion model evaluation of the ETEX first release, EUR 17754 EN. Office for official publications of the European Communities, Luxembourg. ISBN 92-828-3657-6.

[72] Grell, G., Emeis, S-., Stockwell, W.R., Schoenemeyer, T., Forkel, R., Michalakes, J., Knoche, R., Seidl, W., 1999. Application of a multiscale, coupled MM5/Chemistry model to the complex terrain of the VOTALP Valley Campaign. Atm. Env., 34, 1435-1453.

[73] Grell, G. A., Emeis, S., Stockwell, W. R., Schoenemeyer, T., Forkel, R., Michalakes, J., Knoche, R., Seidl, W., 2000. Application of a multiscale, coupled MM5/chemistry model to the complex terrain of the VOTALP valley campaign. Atmos, Env., 34, 1435-1453.

[74] Grell, G., Devenyi, D., 2002. A generalized approach to parameterizing convection combining ensemble and data assimilation techniques. Geophys. Res. Let., 29, 14, doi: 10.1029/2002GL015311

[75] Grell, A., G., Knoche, R., Peckham, E., S., McKeen, A., S., 2004. Online versus offline air quality modeling on cloud-resolving scales. Geophysical Research Letters, 31, L16117

[76] Grell, A., G., Peckham, S. E., Schmitz, R., McKeen, S. A., Frost, G., Skamarock, W. C., Eder, B., 2005. Fully coupled "online" chemistry within the WRF model. Atmos. Env., 39, 6957-6975.

[77] Gross, A., Baklanov, A., 2004. Modelling the influence of dimethyl sulphid on the aerosol production in the marine boundary layer. International Journal of Environment and Pollution, 22, 51-71.

[78] Gross, A., Sørensen, J., H., Stockwell, W., R., 2005. A Multi-Trajectory Chemical-Transport Vectorized Gear Model: 3-D Simulations and Model Validation. J. Atm. Chem., 50, 211-242.

[79] Gross, A, 2008. Danish Meteorological Institute, Research Department. Personal communication.

[80] Gryning, E., S., Batchvarova, E., Schneiter, D., Bessemoulin, P., Berger, H., 1998. Release site during two tracer experiments. Atmospheric Environment, 32 (24), 4123-4137.

[81] Gupta, S., McNider, R. T., Trainer, M., Zamora,R. J., Knupp, K. and Singh, M. P., 1997. Nocturnal wind structure and plume growth rates due to inertial oscillations. Journal of Applied Meteorology, 36, 1050-1063.

[82] Han, Q., Rossow, W., B., Lacis, A., A., 1994. Near-global survay of effective droplet radiiin liquid water clouds using ISCCP data. J. Clim., 7, 465-497.

[83] Han, Q., Rossow, W., B., Chou, j., Welch, R., M., 1998. Global variation of column droplet concentration in low-level clouds. Geophys. Res. Lett., 25, 1419-1422.

[84] Han, Q, Rossow, W., B., Zeng, J., Welch, R., 2002. Three different behaviours of liquid water path of water clouds in aerosol-cloud interactions. J. Atmos. Sci., 59, 726-735.

[85] Haywood, J., Bush, M., Abel, S., Claxton, B., Coe, H., Crosier, J., Harrison, M., Macpherson, B., Naylor, M., Osborne, S., 2008. Prediction of visibility and aerosol within the operational Met Office Unified Model. II: Validation of model performance using observational data. Q. J. R. Meteorol. Soc. 134: 1817-1832.

[86] Hesstvedt, E., Hov, Ø., Isaksen, I., 1978. Quasi-steady-state-approximation in air pollution modelling: comparison of two numerical schemes for oxidant production. Int., J. Chem., Kinet., 10, 971.

[87] Heymsfield, A., J., McFarquhar, G., M., 2001. Microphysics of INDOEX clean and polluted trade cumulus clouds. J. Geophys. Res., 106, 28653-28673.

[88] Hindeman, E., E., Tag, P., M., Silverman, B., A., Hobbs, P., V., 1977. Cloud condensation nuclei from a paper mill. PartII: Calculated effects on rainfall. J. Appl. Meteor., 16, 753-755.

[89] Hobbs, P., V., Garrett, T., J., Ferek, R., J., Strader, S., R., Hegg, D., A., Frick, G., M., Hoppel, W., A., Gasparovic, R., F., Russell, L., M., Johnson, D., W., O'Dowd, C., Durkee, P., A., Nielsen, K., E., Innis, G., 2000. Emissions from Ships with respect to Their Effects on Clouds. Journal of the Atmospheric Sciences, 57, 2570-2590.

[90] Holloway, T., Fiore, A., Hastings, G. M., 2003. Intercontinental Transport of Air Pollution: Will Emerging Science Lead to a New Hemispheric Treaty ?. Environ. Sci. Technol., 37, 4535-4542.

[91] Holmes, N. S., Morawska, L., 2006. A review of dispersion modelling and its application to the dispersion of particles: An overview of different dispersion models available. Atm. Env., 40, 5902-5928.

[92] Holton, R., J., 1992. Introduction to Dynamic Meteorology. Third edition, Academic Press, p. 307.

[93] Hudson, J., G., Yum, S., S., 2001. Marine-continental drizzle contrasts in small cumuli. J. Atmos. Sci., 58, 915-926.

[94] IFS: Integrated Forecasting System, Documentation, 2006. Cy31r1, Part IV, Physical Processes: http://www.ecmwf.int/research/ifsdocs/.

[95] Jacobson, M. Z., Lu, R., Turco, R. P. and Toon, O. B., 1996. Development and application of a new air pollution modeling system-Part I: Gas-phase simulations. Atmospheric Environment, 30, 1939-1963.

[96] Jacobson, M. Z., 1997a. Development and application of a new air pollution modeling system-Part II: Aerosol module structure and design. Atmospheric Environment, 31, 131-144

[97] Jacobson, M. Z., 1997b. Development and application of a new air pollution modeling system-Part III: Aerosol-phase simulations. Atmospheric Environment, 31A, 587-608.

[98] Jacobson, M. Z., 1999. Fundamentals of Atmospheric Modeling. Cambridge University Press.

[99] Jacobson, M. Z. A physically-based treatment of elemental carbon optics: Implications for global direct forcing of aerosols, 2000. Geophys. Res. Lett., 27, 217-220.

[100] Jacobson, M. Z., 2002a. Control of fossil-fuel particulate black carbon plus organic matter, possibly the most effective method of slowing global warming. J. Geophys. Res., 107(D19), 4410, doi: 10.1029/2001JD001376.

[101] Jacobson, M. Z., 2002b. Atmospheric Pollution, History, Science AND Regulation. Cambridge University Press, pp. 339-342.

[102] Jacobson, M. Z., 2006. Effects of absorption by soot inclusions within clouds and precipitation on global climate. J. Phys. Chem., 110, 6860-6873.

[103] Jacobson, M. Z., Kaufmann, Y. J., Rudich, Y., 2007a. Examining feedbacks of aerosols to urban climate with a model that treats 3-D clouds with aerosol inclusions. J. Geophys. Res., 112, D24205, doi: 10.1029/2007JD008922.

[104] Jiang, H., Feingold, G., Cotton, W., R., 2002. Effect of aerosol on warm convective clouds: Aerosol-cloud-dynamical feedbacks resulting from entrainment of aerosol into the marine boundary layer during the Atlantic Stratocumulus Transition Experiment. J. Geophys. Res., 107, 4813, doi: 10.1029/2001JD001502.

[105] Jiang, H., Xue, H., Teller, A., Feingold, G., Levin, Z., 2006. Aerosol effects on the lifetime of shallow cumulus. Geophys. Res. Lett., 33, doi: 10.1029/2006GL026024.

[106] Jöckel, P., Kuhlmann, R. von, Lawrence, M., G., Steil, B., Brenninkmeijer, C., A., M., Crutzen, P., J., Rasch, P., J., Eaton, B., 2001. On a fundamental problem in implementing flux-form advection schemes for tracer transport in 3-dimensional general circulation and chemistry transport models. Q. J. R. Meteorol. Soc., 127, 1035-1052.

[107] Jöckel, P., Sander, R., Kerkweg, A., Tost, H., Lelieveld, J., 2005. The Modular Earth Submodel System (MESSy) - a new approach towards Earth System Modeling Technical Note, Atmos. Chem. Phys., 5, 433-444.

[108] Jung, G., Hedgecock, I., 2008. Modeling global atmospheric mercury dynamics with ECHMERIT model. Joint International Conference of the UNEP Global Partnership on Atmospheric Mercury Transport and Fate Research and Task Force on Hemispheric Transport of Air Pollution of the UNECE-LRTAP Convention: CNR-Institute for Atmospheric Pollution, 7-11 April 2008, Rome, Italy, (http://www.htap.org/meetings/2008/2008_04/agenda.htm).

[109] Kaas, E., 2008: A simple and efficient locally mass conserving semi-Lagrangian transport scheme. Tellus, 60A, 305-320.

[110] Kain J. S., Fritsch, J. M., 1990. A One-Dimensional Entraining/Detraining Plume Model and Its Application in Convective Parameterizations. J. Atm. Sci., 47, 2784-2802.

[111] Kaminski, J., Neary, L., Struzewska, J., McConnell, J. C., Lupu, A., Jarosz, J., Toyota, K., Gong, S. L., Cote, J., liu, X., Chance, K., Richter, A., 2008. GEM-AQ, an on-line global multiscale chemical weather modelling system: model description and evaluation of gas phase chemistry processes. Atmos. Chem. Phys., 8, 3255-3281.

[112] Karl, M., Gross, A., Leck, C. and Pirjola, L., 2007. Intercomparison of Dimethylsulfide Oxidation Mechanisms for the Marine Boundary Layer: Gaseous and particulate sulfur constituents. Journal of Geophysical Research, 112, D15304, doi:10.1029/2006JD00914.

[113] Kim, B., Schwartz, S., Miller, M., Min, Q., 2003. Effective radius of cloud droplets by ground-based remote sensing: Relationship to aerosol. J. Geophys. Res., 108, doi: 10.1029/2003JD003721.

[114] Kim, D., Stockwell, W., R., 2007. An online coupled meteorological and air quality modeling study of the effect of complex terrain on the regional transport and transformation of air pollutants over Western United States. Atmospheric Environment, 41, 2319-2334.

[115] Kim, Y., Cess, R., D., 1993. Effect of anthropogenic sulfate aerosols on low-level cloud albedo over oceans. J. Geophys. Res., 98, 14883-14885.

[116] King, M., D., Radke, L., F., Hobbs, P., V., 1993. Optical properties of marine stratocumulus clouds modified by ships. J. Geophys. Res., 98, 2729-2739.

[117] Kleinman, l., I., Daum, P., H., Lee, Y., N., Senum, G., I., Springston, S., R., Wang, J., Berkowitz, C., Hubbe, J., Zaveri, R., A., Brechtel, F., J., Jayne, J., Onasch, T., B., Worsnop, D., 2007. Aircraft observations of aerosol composition and ageing in New England and mid-Atlantic States during the summer 2002 New England Air Quality Study field campaign. J. Geophys. Res., 112, D09310, doi: 10.1029/2006JD007786.

[118] Klug, W., Graziani, G., Grippa, G., Pierce, D., Tassone, C., 1992. Evaluation Of Long Range Atmospheric Transport Models Using Environmental Radioactivity Data From The Chernobyl Accident, The ATMES Report. Elsevier Applied Science, London and New York.

[119] Korsholm, U., S., Baklanov, A., Sørensen, J., H., 2008a. Status and Evaluation of Enviro-HIRLAM: Differences between On-line and Off-line Models. Proceedings of the COST728 workshop: Integrated systemes of meso-meteorological and chemical transport models, Copenhagen, Denmark 21-23 May 2007; Eds. Baklanov, A., Mahura, A., Sokhi, R.

[120] Korsholm, U., S., Baklanov, A., Gross, A., Sørensen, J., H., 2008b. On the importance of the meteorological coupling interval in dispersion modeling during ETEX-1. Accepted for publication in Atm. Env.

[121] Korsholm, U. S., Baklanov, A., Gross, A., Mahura, A., Sass, B. H., Kaas, E., 2008. Online coupled chemical weather forecasting based on HIRLAM– overview and prospective of Enviro-HIRLAM. HIRLAM Newsletter, 54 (www.HIRLAM.org).

[122] Korsholm, U., S., Mahura, A., Baklanov, A., Gross, A., Petersen, C., Beekmann, M., 2008d. Sulfate aerosol-meteorology feedbacks on short timescales in a convective case. Submitted to Atm. Env.

[123] Kulmala, M., Laaksonen, A., Korhonen, P., Vesala, T., Ahonen, T., 1993. The effect of atmospheric nitric acid on cloud condensation nucleus activation. J. Geophys. Rev., 98, 22949-22958.

[124] Kulmala, M., Vehkamaki, H., Petaja, T., Del Maso, M., Lauri, A., Kerminen, V.-M., Birmili, W., McMurry, P., H., 2004. Formation and growth rates of ultra fine atmospheric particles: a review of observations. Journal of Aerosol Science, 35(2), 143-176.

[125] Kuo, H. L., 1965. On the formation and intensification of tropical cyclones through latent heat release by cumulus convection. J. Atmos. Sci., 22, 40-63.

[126] Laaksonen, A., Korhonen, P., Kulmala, M., Charlson, R., 1998. Modification of the Köhler equation to include soluble trace gasses and slightly soluble substances. J. Atmos. Sci., 55, 853-862.

[127] Landgraf, J., Crutzen, P. J., 1998. An efficient methof for online calculations of photolysis and heating rates. J. Atmos. Sci., 55, 863-878.

[128] Lauritzen, P., H., Kaas, E., Machenhauer, B., Lindberg, K., 2008. A Mass-Conservative Version of the Semi-Implicit Semi-Lagrangian HIRLAM. Quart. J. Roy. Meteor. Soc., 134, 1583-1595.

[129] Leaitch, W., R., Isaac, G., A., Strapp, J., W., Banic, C., M., Wiebe, H., A., 1992. The relationship between cloud droplet number concentrations and anthropogenic pollution: Observations and climatic implications. J. Geophys. Rev., 97, 2463-2472.

[130] Lee, S., M., Yoon, S., -C., Byun, D., W., 2004. The Effect of Mass Inconsistency of Meteorological Field Generated by a Meteorological Model on Air Quality Modeling. Atm. Env., 38, 2917-2926.

[131] Lemonsu, A., Masson, V., Pigeon, G., Moppert, C., 2006. Sea-Town Interactions over Marseille: 3d, Urban Boundary Layer and Thermodynamical Field near the Surface. Theoretical and Applied Climatology, 84, 171-178.

[132] Li, Z., Leighton, H., 1993. Global Climatologies of Solar Radiation Budgets at the Surface and in the Atmosphere From 5 Years of ERBE Data. J. Geophys. Res., 98, 4919-4939.

[133] Lin J. C., Matsui, T., Pielke Sr., R., A., Kummerow, C., 2006. Effects of biomass-burning-derived aerosols on precipitation and clouds in the Amazon Basin: a satellite-based empirical study, J. Geophys. Res., 111, doi:10.1029/2005JD006884.

[134] Lin, S., J., Rood, R., B., 1996. Multidimensional flux-form semi-Lagrangian transport schemes. Mon. Wea. Rev., 124, 2046-2070.

[135] Lohmann, U., stier, P., Hoose, C., Ferrachat, S., Kloster, S., Roekner, E., Zhang, J., 2007. Cloud microphysics and aerosol indirect effectsin the global climate model ECHAM5-HAM. Atmos. Chem. Phys., 7, 3425-3446.

[136] Louis, J. F., 1976. A parametric model of vertical eddy fluxes in the atmosphere. Bound.-Layer Met., 17, 187-202.

[137] Lu, M., -L., Seinfeld, J., H., 2005. Study of the aerosol indirect effect by large-eddy simulation of marine stratocumulus. J. Atmos. Sci., 62, 3909-3932.

[138] Lurmann, F. W., Lloyd, A. C., Atkinson, R., 1986. A chemical mechanism for use in long-range transport/acid deposition computer modelling. J. Geophys. Res., 91, 10905-10936.

[139] Lynch, P., McGrath, R., McDonald, A., 1999. Digital Filter Initialization for HIRLAM. HIRLAM Technical Report, 42 (www.HIRLAM.org).

[140] Madronich, S., 1987. Photodissociation in the atmosphere, 1, actinic flux and the effects of ground reflections and clouds. J. Geophys. Res., 92, 9740-9752.

[141] Majewski, D., Liermann, D., Prohl, P., Ritter, B., Buchhold, M., Hanisch, T., Paul, G., Wergen, W., Baumgardner, J., 2002. The operational global icosahedral-hexagonal grid point model GME: Description and high resolution tests. Monthly Weather Review, 130, 319 - 338.

[144] Martin, G., M., Johnson, D., W., Spice, A., 1994. The measurement abd parameterization of effective radius of droplets in warm stratocumulus clouds. J. Atm. Sci., 51, 1823-1842.

[145] Maryon, H., Ryall, B., 1996, Developments to the UK nuclear accident response model (NAME), Department of Environment, UK Met. Office, DoE report: DOE/RAS/96.011.

[146] Masson, V., 2006.Urban surface modelling and the mesoscale impact of cities. Theoretical and Applied Climatology, 84, 35-45.

[147] May, W., 2008. Potential future changes in the characteristics of daily precipitation in Europe simulated by the HIRHAM regional climate model. Clim.Dyn.(2008) 30:581-603, DOI 10.1007/s00382-007-0309-y.

[148] McDonald, 1995. The HIRLAM two time level, three dimensional semi-Lagranian, semi-implicit, limited area, grid point model of the primitive equations. HIRLAM technical report, 17 (www.hirlam.org).

[149] McNider, R. T., Moran, M. D. and Pielke Sr., A. R ., 1996. Influence of diurnal and inertial boundary layer oscillations on long-range dispersion. Atmospheric Environment, 22, 2445-2462.

[150] McRae, G., J., Goodin, W., R., Seinfeld, J., H., 1982. Numerical solution of the atmospheric diffusion equation for chemically reacting flows. J. Comp. Phys., 45, 1-42.

[151] Mellor, G. L., Yamada, T., 1974. A hierachy of turbulence closure models for planetary boundary layers. J. Atmos. Sci., 31, 1791-1806.

[152] Mellor, G. L., Yamada, T., 1982. Development of a turbulence closure model for geophysical fluid problems. Rev. Geophys. Sapce Phys., 20, 851-875.

[153] Meng, Z., Seinfeld, J., H., 1996. Time scales to achieve atmospheric gas-aerosol equilibrium for volatile species. Atm. Env., 30, 2889-2900.

[154] Menon, S., Del Genio, a. D., Koch, D., Tselioudis, G., 2002. GCM simulations of the Aerosol Indirect Effect: Sensitivity to Cloud Parameterization and Aerosol Burden. J. Atmos. Sci., 59, 692-713.

[155] Michalakes, J., J. Dudhia, D. Gill, T. Henderson, J. Klemp, W. Skamarock, and W. Wang, 2004. The Weather Reseach and Forecast Model: Software Architecture and Performance. Proceedings of the 11th ECMWF Workshop on the Use of High Performance Computing In Meteorology, 25-29 October 2004, Reading U.K. Ed. George Mozdzynski (http://www.wrf-model.org/wrfadmin/publications.php)

[156] Molders, N., Olson, M., A., 2004. impact of urban effects on precipitation in high latitudes. J. Hydrometeor., 5, 409-429.

[157] Moran, M. D. and Pielke Sr., A., R., 1996. Evaluation of a mesoscale atmospheric dispersion modeling system with observations from the 1980 Great Planes mesoscale tracer field experiment. Part II: dispersion simulations. Journal of Applied Meteorology, 35, 308-329.

[158] Mosca, S., Bianconi, R., Graziani, G. and Klug, W., 1998: ATMES II: Evaluation of Long-Range Dispersion Models Using Data of the 1st ETEX release. EUR 17756 EN. Office for official publications of the European Communities, Luxembourg. ISBN 92-828-3657-X.

[159] Moussiopoulos, N., Sahm P., Kunz, R., Vögele, T., Schneider, C. and Kessler, C., 1997. High resolution simulations of the wind flow and the ozone formation during the Heilbronn ozone Experiment. Atmos. Environ. 31, 3177-3186.

[160] Nair, R., D., Machenhauer, B., 2002. The mass-conservative cell-integrated semi-L agrangian advection scheme on the sphere. Mon. Wea. Rev., 130, 649-667.

[161] Nastrom, J. S. and Pace, J., C., 1998. Evaluation of the effect of meteorological data resolution on lagrangian particle dispersion simulations using the etex experiment. Atmospheric Environment, 32 (24), 4187-4194.

[162] Näslund, E., Thaning, L., 1991, On the settling velocity in a nonstationary atmosphere, Aerosol Science and Technology, 14, 247-256.

[163] Nenes, A., Ghan, S., Hayder, A., Chuang, P. Y., Seinfeld, H., 2001. Kinetic limitations on cloud droplet formation and impact on cloud albedo. Tellus, 53B, 133-149.

[164] Nicholls, S., 1984. The dynamics of stratocumulus: Aircraft observations and comparisons with a mixed layer model. Q. J. R. Meteorol. Soc, 110, 783-820.

[165] Nodop, K., Connolly, R. and Girardi, F., 1998. The Field Campaigns of the European Tracer Experiment (ETEX): Overview and results. Atmospheric Environment, 32 (24), 4095-4108.

[166] Noh, Y., Cheon, W. G., hong, S. Y., Raasch, S., 2003. Improvement of the K-profile for the planetary boundary layer based on large eddy simulation data. Bound.-Layer Meteor., 107, 401-427.

[167] Ohmura, A., Gilgen, H., Hegner, H., Müller, G., Wild, M., Dutton, E., G., Forgan, B., Fröhlich, C., Philipona, R., Heimo, A., König-Langlo, G., McArthur, B., Pinker, R., Whitlock, C., H., Dehne, K., 1998. Baseline Surface Radiation Network (BSRN/WCRP): New Precision Radiometry for Climate Research. Bull. Amer. Meteor. Soc., 79, 2115-2136.

[168] Oke, T., R., 1987. Boundary Layer Climates. Methuen, London and New York, 435.

[169] Ou, ,S. -C., Liou, K., N., 1995. Ice microphysics and climatic temperature feedback. Atm. Res., 35, 127-138.

[170] Ovtchinnikov, M., Ghan, S., J., 2005. Parallel simulations of aerosol influence on clouds using cloud-resolving and single-column models. J. Geophys. Res., 110, doi: 10.1029/2004JD005088.

[171] Paluch, I., R., Lenschow, D., H., 1991. Stratiform cloud formation in the marine boundary layer. J. Atm. Sci., 48, 2141-2158.

[172] Peckham, S., E., Grell, G., A., Fast, J., Gustafson, W., I., Ghan, S., J., Zaveri, R., Easter, R., C., Barnard, J., Chapman, E., Schmitz, R., Salzmann, M., 2008. WRF/Chem version3.0 users guide (http://ruc.fsl.noaa.gov/wrf/WG11/).

[173] Penner, J., E., Andreae, M., Annegarn, H., Barrie, L., Feichter, J., Hegg, D., Jayaraman, A., Leaitch, R., Murphy, D., Nganga, J., Pitari G., Ackerman, A., Adams, P., Austin, P., Boers, R, Boucher, O., Chin, M., Chuang, C., Collins, B., Cooke, W., DeMott, P., Feng, Y., Fischer, H., Fung, I., Ghan, S., Ginoux, P., Gong, S., -L., Guenther, A., Herzog, M., Higurashi, A., Kaufman, Y., Kettle, A., Kiehl, J., Koch, D., Lammel, G., Land, C., Lohmann, U., Madronich, S., Mancini, E., Mishchenko, M., Nakajima, T., Quinn, P., Rasch, P., Roberts, D., L., Savoie, D., Schwartz, S., Seinfeld, J., Soden, B., Tanré, D., Taylor, K., Tegen, I., Tie, X., Vali, G., Dingenen, R., Van., Weele, M., Van., Zhang, Y., 2001. *In: Climate Change 2001: The Scientific Basis. Contribution of Working Group I to the Third Assessment Report of the Intergovernmental Panel on Climate Change (IPCC)*[Houghton, J., ,T., Ding, Y., Griggs, D., J., Noguer, M., Linden, P., J., van der., Xiaosu, D. (eds.)]. Cambridge University Press, Cambridge, United Kingdom and New York, NY, USA.

[174] Penner, J., Dong, X., Chen, Y., 2004. Observational evidence of a change in radiative forcing due to the indirect aerosol effect. Nature, 427, 231-234.

[175] Persson, C., Rodhe, H., De Geer, L. E., 1986. The Chernobyl Accident - A meteorological analysis of how radionuclides reached Sweden, SMHI/RM Report No. 55.

[176] Pielke Sr., A., R., 2002a. Mesoscale Meteorological Modeling. Second edition, international Geophysics Series 78, Academic Press, p. 493.

[177] Pielke Sr., A., R., 2002b. Mesoscale Meteorological Modeling. Second edition, international Geophysics Series 78, Academic Press, p. 513.

[178] Pielke Sr., A., R., 2002c. Mesoscale Meteorological Modeling. Second edition, international Geophysics Series 78, Academic Press, p. 512.

[179] Pielke Sr., A., R., 2002d. Mesoscale Meteorological Modeling. Second edition, international Geophysics Series 78, Academic Press, p. 504.

[180] Platnick, S., Durkee, P., A., Nielsen, K., Taylor, J., P., Tsay, S., -C., King, M., D., Ferek, R., J., Hobbs, P., V., Rottman, j., W., 2000. The role of background cloud microphysics in the radiative formation of shiptracks. J. Atmos. Sci., 57, 2607-2624.

[181] Pöschl, U., von Kuhlmann, R., Poisson, N., Crutzen, P., J., 2000. Development and intercomparison of condensed isoprene oxidation mechanisms for global atmospheric modeling. J. Atm. Chem., 37, 29-52.

[182] Poppe, D., Andersson-Sköld, Y., Baart, A., Builtjes, P., J., H., Das, M., Fiedler, F, Hov, Ø, Kirchner, F., Kuhn, M., Makar, P., A., Milford, J., B., Roemer, M., G., M., Ruhnke, R., Simpson, D., Stockwell, W., R., Strand, A., Vogel, B., Vogel, H., 1996. Gas-Phase Reactions in

Atmospheric Chemistry and Transport Models: a model Intercomparison. EUROTRAC a EUREKA Environmental Project. EUROTRAC International Scientific Secretariat, Garmisch-Partenkirchen.

[183] Prather, M., McElroy, M., Russel, G., Rind, D., 1987. Chemistry of the Global Troposphere: Fluorocarbons as Tracers of Air Motion. J. Geophys., Res., 92, D6, 6579-6613.

[184] Priestly A, 1993. A quasi-conservative version of the semi-Lagrangian advection scheme. Mon. Wea. Rev., 121, 621-632

[185] Radke, L., F., Coakley, J., A., Jr., King, m., D., 1989. Direct and remote sensing observations of the effects of ships on clouds. Science, 246, 1146-1149.

[186] Ramanathan, V., Crutzen, P., J., Kiehl, J., T., Rosenfeld, D., 2001. Science, 294, 2119 - 2124.

[187] Rasch, P, Williamson, D-, L., 1990. Computational aspects of moisture transport in global models of the atmosphere. Q. J. R., Meteorol. Soc., 116, 1071-1090.

[188] Rasch, P., Kristjansson, J., 1998, A comparison of the CCM3 Model Climate using diagnosed and predicted condensate parameterizations, J. Climate, 11, 1587-1614.

[189] Robert, A., 1981. A stable numerical integration scheme for the primitive meteorological equations. Atmos. Ocean, 19, 35-46.

[190] Robert, A., 1982. A semi-Lagrangian semi-implicit numerical integration scheme for the primitive meteorological equations. J. Meteor. Soc. Japan, 60, 319-324.

[191] Roger, J., C., Guinot, B., Cachier, H., 2008. Submitted to GRL.

[192] Rogers, R., R., 1979. A short course in cloud physics. 2nd Ed. Pergamon Press, Oxford, New York, Toronto, Sydney, Paris, Frankfurt.

[193] Rosenfeld, D., 2000. Suppression of Rain and Snow by Urban and Industrial Air Pollution. Science, 287, 1793-1796.

[194] Rosenfeld, D., Lohmann, U., Raga, G., B., O'Dowd, C., Kulmala, M., Fuzzi, S., Reissell, A., Andrae, M., O., 2008. Science, 321, 1309-1313.

[195] Rotach, M. W., Vogt, D., Bernhofer, E., Batchvarova, A., Christen, A., Clappier, A., Feddersen, B., Gryning, S. E., Martucci, G., Mayer, H., Mitev, V., Oke, T. R., Parlow, H., Richner, M., Roth, Y. A., Roulet, D., Ruffieux, H., Salmond, J. A., Schatzman, M, Voogt, J. A., 2005. BUBBLE – an Urban Boundary Layer Meteorology Project, Theoretical and Applied Climatology, 81, 231-261.

[196] Rotman, D., A., Atherton, C., S., Bergmann, D., J., Cameron-Smith, P., J., Chuang, ,C., C., Connell, P, S., Dignon, J., E., Franz, A., Grant, K., E., Kinnison, D., E., Molenkamp, C., R., Proctor, D., D., Tannahill, J., R., 2004. IMPACT the LLNL 3-D global troposphere-stratosphere chemical transport model: A model description. J. Geophys. Res., 109, D04303, doi:10.1029/2002JD003155.

[197] Rotstayn, L., D., Penner, J., E., 2001. Indirect aerosol forcing, quasi forcing, and climate response. J. Clim., 14, 2969-2975.

[198] Sass, B., 2002, A research version of the STRACO cloud scheme, Danish Meteorological Institute, Technical report no 02-10 (http://www.dmi.dk/dmi/index/viden/dmi-publikationer/videnskabeligerapporter.htm).

[199] Satheesh, S., K., Moorthy, K., K., 2005. Radiative effects of natural aerosols: A review. Atm. Env., 39, 2089-2110.

[200] Savijärvi, H., 1990. Fast radiation parameterization schemes for mesoscale and short-range forecast models. J. Appl. Meteor., 29, 437-447.

[201] Schell B., Ackermann, I.J., Hass, H., Binkowski, F.S., and Ebel, A., 2001. Modeling the formation of secondary organic aerosol within a comprehensive air quality model system, Journal of Geophysical research, 106, 28275-28293

[202] Schlünzen K.H., Hinneburg D., Knoth O., Lambrecht M., Leitl B., Lopez S., Lüpkes C., Panskus H., Renner E., Schatzmann M., Schoenemeyer T., Trepte S. and Wolke R., 2003. Flow and transport in the obstacle layer - First results of the microscale model MITRAS. J. Atmos. Chem., 44, 113-130.

[203] Scott, B., C., 1978. Parameterization of sulfate removal by precipitation. J. Appl. Meteor., 17, 1375-1389.

[204] Sehmel, A., 1980, Particle and gas deposition, a review, Atm. Env., 14, 983-1011.

[205] Seinfeld, J, H., Pandis, S., N., 1998. Atmospheric Chemistry and Physics, 2nd Ed., John wiley and Sons, Inc., Hoboken.

[206] Shepherd, J., M., 2005. A Review of Current Investigations of Urban-Induced Rainfall and Recommendations for the Future. Earth Interactions, 9, 1-27.

[207] Smolarkiewicz, P., Grabowski, W. W., 1990. The multidimensional positive definite advection transport algorithm: nonoscillatory option. J. Comp. Phys., 86, 355-375.

[208] Sokol, Z, 1999. Comparison of several numerical schemes applied to advection equations. Q. J. R. Meteorol. Soc., 125, 213-224.

[209] Staniforth, A., N., Côté, J., 1991. Semi-Lagrangian integration schemesfor atmospheric models–A review. Mon. Wea. Rev., 119, 2206-2223.

[210] Stevens, B., G., Cotton, W., R., Feingold, G., Moeng, C., -H., 1998. Large-eddy simulations of strongly precipitating shallow stratocumulus-topped boundary layers. J. Atmos. Sci., 55, 3616-3638.

[211] Stier, P., Feichter, J., Kinne, S., Kloster, S., Vignati, E., Wilson, J., Ganzeveld, L., Tegen, I., Werner, M., Balkanski, Y., Schulz, M., Bourcher O., Minikin, A., Petzold, A., 2005. The aerosol-climate model ECHAM5-HAM. Atmos. Chem. Phys., 5, 1125-1156.

[212] Stockwell, W., Middeltonn, P., Chang, J., Tang, X., 1990. The second generation Regional Acid Deposition Model - chemical Mechanism for Regional Air Quality Modelling. J. Geophys. Res., 95, 16343.

[213] Stockwell, W., Kirchner, F., Kuhn, M., Seefeld, S., 1997. A new mechanism for regional atmospheric chemistry modelling. J. Geophys. Res., 102, 847-879.

[214] Stokes, G., M., Schwartz, S., E., 1994. The Atmospheric Radiation Measurement (ARM) Program: Programmatic Background and Design of the Cloud and Radiation Test Bed. Bull. Amer. Meteor. Soc., 75, 1201-1221.

[215] Stull, R. B., 1988. An Introduction to Boundary Layer Meteorology. Kluwer Academic Publishers, Dordrecht/Boston/London.

[216] Sundqvist, H. 1988, Parameterization of condensation and associated clouds in models for weather prediction and general circulation simulation, Kluwer Academic, 1, 433-461.

[217] Sundqvist, H., Berge, E., Kristjánsson", J., 1989, Condensation and Cloud Parameterization Studies with a Mesoscale Numerical Weather Prediction Model, Mon. Wea. Rev., 117, 1641-1657.

[218] Sundqvist, H., 1993, Inclusion of Ice Phase of Hydrometeors in Cloud Parameterization for Mesoscale and Largescale Models, Beitr. Phys. Atmosph./Contrib. Atmos. Phys., 66, 137-147.

[219] Sørensen, J. H., Rasmussen, A., Ellermann, T. and Lyck, E., 1998. Mesoscale influence on long-range transport -evidence from ETEX modelling and observations. Atmospheric Environment, 32 (24), 4207-4217.

[220] Theloke, J. and Friedrich, R., 2007. Compilation of a database on the composition of anthropogenic VOC emissions for atmospheric modeling in Europe. Atm. Env., 41, 4148-4160.

[221] Tiedtke, M., 1989. A comprehensive mass flux scheme for cumulus parameterization in large-scale models. Mon. Wea. Rev, 117, 1779-1800.

[222] Toro, E. F., 1989. A weighted average flux method for hyperbolic conservation laws. Proc. Roy. Soc. Lond. A, 423, 401-418.

[223] Tulet, P. V., Crassier, F., Cousin, K., Suhre, K., Rosset, R., 2005. ORILAM, a three-moment lognormal aerosol scheme for mesoscale atmospheric model: online coupling into the Meso-NH-C model and validation on the Escompte Campaign. J. Geophys. Res., 110, D18201, doi: 10.1029/2004JD005716.

[224] Twohy, C., H., Petters, M., D., Snider, J., R., Stevends, B., Tahnk, W., Wetzel, M., Russel, L., Burnet, F., 2005. Evaluation of the aerosol indirect effect in marine stratocumulus clouds: Droplet number, size, liquid water path and radiative impact. J. Geophys. res., 110, doi: 10.1029/2004JD005116.

[225] Twomey, S., 1974. Pollution and the Planetary Albedo. Atm. Env., 8, 1251-1256.

[226] Undén, P., Rontu, L., Järvinen, H., Lynch, P., Calvo, J., Cats, G., Cuhart, J., Eerola, K. *et al.*, 2002. HIRLAM-5 Scientific Documentation. December 2002, HIRLAM-5 project report, SMHI, Norrköping, Sweden.

[227] United Nations, 2006. United Nations World Urbanization Prospects: The 2005 Revision. United Nations, New York (http://www.un.org/esa/population/publications/WUP2005/2005wup.htm).

[228] Valcke, S., Redler, R., 2006. OASIS4 User Guide (OASIS4_0_2), PRISM Support Initiative Report No 4 (https:oasistrac.cerfacs.fr)

[229] Venkatram, A., Karamchandani, P., Pai, P., Goldstein, R., 1994. The development and application of a simplified ozone modelling system. Atm. Env., 28, 3665-3678.

[230] Vignati, E., Wilson, J., Stier, P., 2004. M7: An efficient size-resolved aerosol microphysics module for large-scale aerosol transport models. J. Geophys. Res., 109, D22202, doi:10.1029/2003JD004485.

[231] Visschedijk, A., Zandveld, P., Denier van der Gon, H., 2007. A high resolution gridded European emission database for the EU integrated project GEMS. TNO report, 2007-A-R0233/B.

[232] Vogel, H., Bäumer, D., Bangert, M., Lundgren, K., Rinke, R., Stanelle, T., Vogel, B., 2007. COSMO-ART - Aerosols and Reactive Trace Gases within the COSMO model. Proceedings of the COST728 workshop: Integrated systemes of meso-meteorological and chemical transport models, Copenhagen, Denmark 21-23 May.

[233] Wallace, M., J., Hobbs, V., P., 2000. Atmospheric Science, An Introductory Survey, Academic Press, 84.

[234] Warner, J., Twomey, S., 1967. The production of cloud nuclei by cane fires and the effect on cloud droplet concentration. J. Atmos. Sci., 24, 704-706.

[235] Warner, J., 1968. A reduction in rainfall associated with smoke from sugar-cane fires-An inadvertent weather modification ? J. Appl. Meteor., 7, 247-251.

[236] Wesely L., M., 1989, Parameterization of surface resistances to gaseous dry deposition in regional-scale numerical models, Atmospheric Environment, 23, 1293-1304.

[237] Wetzel, M., A., Stowe, L., L., 1999. Satelitte-observed patterns in stratus microphysics, aerosol optical thickness and shortwave radiative forcing. J. Geophys. Res., 104, 31287-31299.

[238] Whitby, E.R., McMurry, P.H., 1997, Modal aerosol dynamics modeling. Aerosol Sci. and Technol. 27, 673-688.

[239] Wilck, M., 1999, Model modelling of multicomponent aerosols. Verlag für Wissenschaft und Forschung Gmbh, Postfach 304051 Berlin.

[240] Williams, E., Rosenfeld, D., Madden, N., Gerlach, J., Gears, N., Atkinson, L., Dunnemann, N., Frostrom, G., Antonio, M., Biazon, B., Camargo, R., Franca, H., Gomes, A., Lima, M., Machado, R., Manhaes, S., Nachtigall, L., Piva, h., Quintiliano, W, Machado, L., Artaxo, P., Roberts, G., Renno, N., Blakeslee, R., Bailey, J., Boccippio, D., Betts, A., Wolff, D., Roy, B., Halverson, J., Rickenbach, T., Fuentes, J., Avelino, E., 2002. Contrasting convective regimes over the Amazon: Implications for cloud electrification J. Geophys. Res., 107, doi:10.1029/2001JD000380.

[241] Wong, K., K., Dirks, R., A., 1978. Mesoscale Perturbations on Airflow in the Urban Mixing Layer, Americal Meteorological Society, 677-688.

[242] Wortmann, S., Vilhena, M., T., Moreira, D., M., Buske, D., 2005. A new analytical approach to simulate the pollutant dispersion in the PBL. Atm. Env., 39, 2171-2178.

[243] Wyser, K., Rontu, L., Savijärvi, H., 1999. Introducing the Effective Radius into a Fast Radiation Scheme of a Mesoscale Model. Contr. Atmos. Phys., 72, 205-218.

[244] Xue, H., Feingold, G., 2006. large-Eddy Simulations of Trade Wind Cumuli: Investigation of Aerosol Indirect Effects. J. Atm. Sci., 63, 1605-1622.

[245] Xue, H., Feingold, G., Stevens, B., 2008. Aerosol Effects on Clouds, Precipitation, and the Organization of Shallow Cumulus Convection. J. Atm. Sci., 65, 392-406.

[246] Yang, R. J., Xia, A. G., Michelangeli, D. V., Plummer, D. A., Neary, L., Kaminski, J. W., McConnell, J.C., 2003. Evaluationg a Canadian regional air quality model using ground-based observations in north-eastern Canada and United States. J. Environ. Monit., 40-46.

[247] Yuskiewicz, B., Stratmann, F., Wiedensohler, A., 1997. The effects of on-cloud sulfate production on light scattering in the atmosphere. J. Aer. Sci., 28, supp. 1, 697-698(2).

[248] Zanetti, P., 1990, Air Pollution Modeling-Theories, Computational Methods and Available Software, Southampton: Computational Mechanics and New York.

[249] Zaveri, R. A., Peters, L. K., 1999. A new lumped structure photochemical mechanism for large-scale applications. J. Geophys. Res., 104, 387 -415.

[250] Zaveri, R. A., Easter, R. C., Fast, J. D., Peters, L. K., 2008. Model for Simulating Aerosol Interactions and Chemistry (MOSAIC). J. Geophys. Res., doi: 10.1029/2007jd008782.

[251] Zhang, Y., Seigneur, C., Seinfeld, J. H., Jacobson, M. Z., Binkowski, F. S., 1999. Simulation of aerosol dynamics: A comparative review of algorithms used in air quality models. Aerosol Sci. Tech., 31, 487-514.

[252] Zhang, Y., Pun, B., Vijayaraghavan, K., Wu, S.-Y., Seigneur, C., Pandis, S., Jacobson, M., Nenes, A., Seinfeld, J. H., 2004. Development and application of the model for aerosol dynamics, reaction, ionization and dissolution (MADRID). J. Geophys. Res., 109, D01202, doi: 10.1029/2003JD003501.

[253] Zhang, Y., 2008. Online-coupled meteorology and chemistry models: history, current status and outlook. Atmos. Chem. Phys., 8, 2895-2932.

Appendix 1: Vertical coordinates

This appendix displays the coefficients used in the definition of the vertical η coordinates:

Full level $(k)^a$	A	B
1	1003.0288086	0.0000000
2	3001.4104004	0.0000000
3	4960.2226562	0.0003962
4	6836.0625000	0.0019211
5	8594.7812500	0.0051903
6	10209.9921875	0.0107089
7	11661.8281250	0.0188780
8	12935.8710937	0.0300004
9	14022.3007812	0.0442874
10	14915.1914062	0.0618649
11	15611.9296875	0.0827797
12	16112.7851562	0.1070057
13	16420.5507812	0.1344501
14	16540.2812500	0.1649603
15	16479.0976562	0.1983290
16	16246.0195312	0.2343019
17	15851.8515625	0.2725827
18	15309.0937500	0.3128400
19	14631.8203125	0.3547139
20	13835.6132812	0.3978215
21	12937.4218750	0.4417636
22	11955.4335937	0.4861313
23	10908.9218750	0.5305114
24	9817.9960937	0.5744935
25	8703.3828125	0.6176761
26	7586.1132812	0.6596724
27	6487.1289062	0.7001174
28	5426.9101562	0.7386733
29	4424.9843750	0.7750363
30	3499.3583984	0.8089430
31	2665.9750977	0.8401762
32	1938.0393066	0.8685716
33	1325.3183594	0.8940237
34	833.3806152	0.9164925
35	462.8203125	0.9360095
36	208.4135284	0.9526840
37	58.2347870	0.9667096
38	3.6336498	0.9783701
39	0.0000000	0.9880459
40	0.0000000	0.9962208

^{a}The levels are labeled from top to bottom

Appendix 2: b-parameters

Parameters for the radiation parameterization adhering to equation 5.6 [243].

Absorption parameters	Transmission parameter
b_{10a} $1.55 \cdot 10^{-4}$	b_{13a} 7.00
b_{10b} $8.18 \cdot 10^{-3}$	b_{13b} -4.75
b_{11} 1.29	b_{14} $8.30 \cdot 10^{-2}$
b_{12} 0.545	

Appendix 3: Enviro-HIRLAM call tree

A partial call tree of Enviro-HIRLAM displaying names of the major subroutines which have been modified or added and a short description of the processes described in the routines.

```
GEMINI
│
├── DFI (initilization)
│
├── SL2TIM
│        │
│        ├── INITRACE (initilization and background values)
│        ├── HDIFF4 (horizontal diffusion)
│        ├── ADVBOTT (advection)
│        ├── ITRACER (emissions)
│        ├── PHYS
│        │       │
│        │       ├── RADIA (first indirect effect)
│        │       ├── VCBR ──── DRYDEP (vertical diffusion and dry deposition)
│        │       ├── CONDS (STRACO convection and condensation)
│        │       │       │
│        │       │       ├── PREVAP (second indirect effect)
│        │       │       └── WETDEP (wet deposition)
│        │
│        ├── CHEM_SIMPLE (chemical driver)
│                │
│                ├── CHEMT_SIMP (gas-phase chemistry)
│                ├── NUCRATE (nucleation rate)
│                ├── THERM_EQ (thermodynamic equilibrium in aerosols)
│                └── AEROSOL (aerosol dynamics)
```

Appendix 4: Zero-dimensional testing of NWP-Chem

A box model version of NWP-Chem has previously been tested at DMI as part of the development of the scheme [79]. The results are not published yet and therefore an overview is given here. The test is based on the urban plume case defined in a EUROTRAC sub-project [182]. The set-up considers a clear sky case on 1 July 1985 at local noon in the point ($45°$ N, $0°$ E). The solar declination is $23°$ and the ground albedo is assumed to be 0.1. The model was integrated forward 120 hours using surface conditions. The initial temperature was 288.15 K, the pressure was 1013.25 hPa, the specific humidity was 1 % and the table shows the initial conditions of the species. All other species fields were initially set to 0. All aerosol options as well as dry and wet deposition was switched of, so that only gas-phase chemistry was considered. Emissions were taken from [182] and corresponds to $1.1 \cdot 10^6$ cm^{-3}s^{-1} NO, $2.2 \cdot 10^5$ cm^{-3}s^{-1} SO$_2$ and $2.4 \cdot 10^6$ cm^{-3}s^{-1} CO (other species such as VOC's may be found in the reference).

The test case was repeated three times using the RACM scheme with a GEAR solver (green lines in the figure), NWP-Chem with a GEAR solver (blue line in figure) and NWP-Chem with the QSSA solver (green line in figure). The figure displays the temporal development of NO, NO$_2$, O$_3$, SO$_2$ and H$_2$SO$_4$ for the three executions. All the schemes reproduced the diurnal cycles of NO and NO$_2$ and O$_3$. NWP-Chem has a tendency to overestimate the daytime peaks in NO as compared to the RACM scheme and the afternoon to evening level of constant concentration is less pronounced. Likewise, for NO$_2$ the overall structure of the peaks compares well with RACM but the fine scale structure is not reproduced. NO acts as a sink for O$_3$, but the larger concentration of NO$_2$ during daytime and the comparable concentration during nighttime exerts a strong forcing on O$_3$ leading to a general

Specie	Initial mixing ratio
NO	37.5 ppbV
NO_2	12.5 ppbV
O_3	50.0 ppbV
SO_2	8.66 ppbV
CO	94.5 ppbV
VOC	0.5 ppmC
HNO_3	0.10 ppbV
H_2	500 ppbV
H_2O_2	2.0 ppbV
HCHO	1.0 ppbV
CH_4	1700 ppbV

increase.

The diurnal cycles of SO_2 and H_2SO_4 are in phase with the RACM simulation. In both NWP-Chem and RACM the balance be tween SO_2 and H_2SO_4 is controlled by the HO concentration (see chapter 3.11). The main difference between RACM and NWP-Chem is the simplifications in the NWP-Chem organic chemistry. The organic reactions have great influence on the HO concentrations in RACM. The simplifications in NWP-Chem leads to an overestimation of HO and, thereby, to a general underestimation of SO_2 and an overestimation of H_2SO_4.
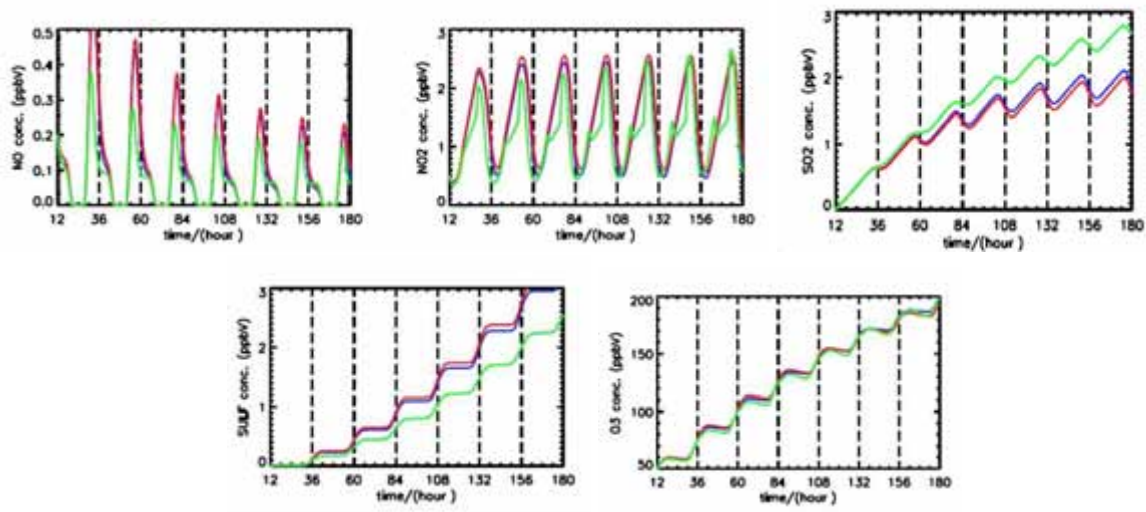
In general the simple NWP-Chem scheme compares well with RACM and reproduces most features of the concentration evolution for the species considered here. Overestimations of SO_2 and underestimations of H_2SO_4 are induced by the simplified treatment of organic chemistry in NWP-Chem.

Previous reports

Previous reports from the Danish Meteorological Institute can be found on:
http://www.dmi.dk/dmi/dmi-publikationer.htm